CIAMTIS

U.S. DOT Region 3 University Transportation Center

Design of Crack-Arrest Holes for Distortion-Induced Fatigue Cracking in Steel Bridges

May 2023

Prepared by:

Y. Chen, J. Saunders, I. Hodgson, R. Sause,
Lehigh University

r3utc.psu.edu

PennState College of Engineering | LARSON TRANSPORTATION INSTITUTE

DISCLAIMER

Technical Report Documentation Page

1. Report No.	2. Government Accession No.	3. Recipient's Catalog No.
CIAM-UTC-REG8		

4. Title and Subtitle	5. Report Date
Design of Crack-Arrest Holes for Distortion-Induced Fatigue Cracking in Steel Bridges	May 8, 2023
	6. Performing Organization Code

7. Author(s)	8. Performing Organization Report No.
Yixin Chen - 0000-0001-7262-1031 Joseph Saunders - 0000-0001-8698-3471 Ian Hodgson - 0009-0005-2309-0197 Richard Sause - 0000-0002-6143-4385	

9. Performing Organization Name and Address	10. Work Unit No. (TRAIS)
ATLSS Center, Lehigh University 117 ATLSS Drive Bethlehem, PA 18015	**11. Contract or Grant No.** 69A3551847103

12. Sponsoring Agency Name and Address	13. Type of Report and Period Covered
U.S. Department of Transportation Research and Innovative Technology Administration 3rd Fl, East Bldg E33-461 1200 New Jersey Ave, SE Washington, DC 20590	Draft Final Report 02/11/2019 – 03/31/2021
	14. Sponsoring Agency Code

15. Supplementary Notes

Work funded through The Pennsylvania State University through the University Transportation Center Grant Agreement, Grant No. 69A3551847103

16. Abstract

Distortion-induced fatigue cracking in the web gap region near a transverse member connection plate is relatively common for steel girder bridges constructed in the 1960's and 1970's. Retrofit of a distortion-induced fatigue crack that runs along a connection plate-to-web weld with a CAH is also relatively common, however fatigue cracking beyond the CAH, after the retrofit has been observed. This research has considered two reasons why a fatigue crack may appear to reinitiate: (1) the CAH was not properly designed, or (2) the original fatigue crack geometry was not properly identified, so that the CAH did not intercept the tip of the crack. This report specifically addresses the first reason. A CAH design approach and recommended CAH dimensions are presented. In the design approach, the local structural stress (LSS) range at a critical connection plate-to-web weld toe location and the maximum magnitude principal stress range (MMPS) on the CAH edge are used to assess the fatigue performance of a CAH design. In this fatigue performance assessment, these stress results obtained from finite element analysis are compared with standard fatigue resistance from (AASHTO, 2018). Fatigue tests of 16 small-size test specimens with full-scale welds, simulated cracks, and CAHs were performed to validate the fatigue performance assessment used in the CAH design approach. Stresses from FEA and measured stresses are used to assess the potential for fatigue cracking in the test specimens. The stress-life data from the tests consistently exceeded the design S-N curve and typically exceeded the mean S-N curve for AASHTO Fatigue Category C; therefore, AASHTO Fatigue Category C is a reasonable and conservative fatigue resistance for assessing the potential for new weld toe fatigue cracking after a CAH retrofit is installed.

17. Key Words	18. Distribution Statement
Distortion-Induced Fatigue Cracking, Crack-Arrest-Hole (CAH) Retrofit, Fatigue Crack Reinitiating, CAH Design Approach, FEA, Fatigue Test, LSS Range	No restrictions. This document is available from the National Technical Information Service, Springfield, VA 22161

19. Security Classif. (of this report)	20. Security Classif. (of this page)	21. No. of Pages	22. Price
Unclassified	Unclassified	83	

Form DOT F 1700.7 (8-72) Reproduction of completed page authorized

TABLE OF CONTENTS

1. CHAPTER 1 1

Background 1

Project Objective 5

Research Approach 5

2. CHAPTER 2 6

Finite Element Models 6
Modeling Technique 6
Global Model 6
Sub Models 7
Material Properties 8
Loading 8
Finite Element Meshes and Stress Analysis 9

3. CHAPTER 3 13

FEA Stresses in Web Gap Region from Out-of-Plane Deformation of Girder Web 13

FEA Stress Results for Fatigue-Damaged Web gap region retrofit with CAHs 15
Stress at Edge of CAH 16
Variation of Stress Normal to Connection Plate-to-Web Weld with Distance along Weld 16
Variation of Stress Normal to Connection Plate-to-Web Weld with Distance in Perpendicular Direction from Weld 17
Variation of Stress Normal to Connection Plate-to-Web Weld through Girder Web Thickness 18

Crack Length and CAH Size Effects 19

Study of Mesh Characeristics 23
Levels of Mesh Refinement 23
Mesh Configuration 24

4. CHAPTER 4 27

FEA of Test Specimens 27
Overview of FEA Model 27

Boundary and Loading Conditions 29
Element Type and Mesh 30
Comparison of Results with Sub Model B 30

Cyclic Loading Fatigue Tests 32
Test Specimens 32
Test Setup 35
Control System and Loading Protocol 38
Inspection Protocol and Data Acquisition System 40
Instrumentation 42
Measurement of Strain and Estimation of Stress Ranges 45

5. CHAPTER 5 46

Estimated Stress Ranges 46

Linearly extrapolated LSS Ranges 54

Inspection Findings 63

Assessment of Fatigue Performance 66

6. CHAPTER 6 71

Details of CAH Design Approach 71

Application of CAH Design Approach 73

7. CHAPTER 7 75

Conclusions from FEA Results 76

Conclusions from Fatigue Tests 77

Recommendations 77

Future Work 78

8. REFERENCES 79

LIST OF FIGURES

Figure 1. Exaggerated deformation of two-girder bridge under vehicular live load, localized out-of-plane reverse-curvature bending deformation, and resulting stresses in web gap when connection plates are not welded to girder flanges..... 2
Figure 2. Distortion-induced fatigue cracking in girder web gap region at web-to-flange and end of connection plate-to-web weld toes produced by transverse member end rotation. 3
Figure 3. Fatigue crack appearing to reinitiate after installation of crack-arrest hole..... 4
Figure 4. Exploded view of Global Model, Sub Model A, and Sub Model B and locations of Sub Model A and Sub Model B. 7
Figure 5. Sub Model B geometry and locations of crack and CAH. 8
Figure 6. Sub Model B Uniform Mesh 1 through 4 shown with 2.0 inch diameter CAHs. 10
Figure 7. Extrapolation methods and reference points for different uniform mesh types (adapted from (Hobbacher, 2016): (a) linear extrapolation method for relatively coarse mesh (Uniform Mesh 1); (b) linear extrapolation method for relatively fine mesh (Uniform Mesh 3); and (c) quadratic extrapolation method for relatively fine mesh (Uniform Mesh 3). 11
Figure 8. Uniform Mesh 1 and 3 and Skewed Mesh 1 and 3 with 2.0 inch diameter CAHs. 12
Figure 9. Contour plots of normal stress (S11) on inside web face from different Sub Model B using Skewed Mesh 3. (Note: Stress contours are presented with limit from -20 ksi to 20 ksi). 15
Figure 10. Maximum magnitude principal stress along edge of northeast CAH at inside and outside faces of girder web from Sub Model B4 using Skewed Mesh 3. 16
Figure 11. Linearly extrapolated LSS, single-point LSS, and 0.4t and 1.0t FEA (S11) stresses normal to connection plate-to-web weld on inside web face from Sub Model B4 using Skewed Mesh 3.....17
Figure 12. Stress normal to connection plate-to-web weld (S11) along select paths on inside web face from Sub Model B4 using Skewed Mesh 3 (circled stresses are used in LSS extrapolation).....18
Figure 13. Stress normal to connection plate-to-web weld (S11) through girder web thickness from Sub Model B4 using Skewed Mesh 3.....19
Figure 14. Contour plots of normal stress (S11) for select original fatigue crack lengths and CAH diameters on inside web face from Sub Model B4 using Skewed Mesh 3. (Note: Stress contours are presented with limits from -10 ksi to 10 ksi). 20
Figure 15. Largest maximum magnitude principal stresses on edge of CAH for various original fatigue crack lengths and CAH diameters from Sub Model B4 using Skewed Mesh 3. 22
Figure 16. Largest LSS normal to connection plate-to-web weld on inside web face for various original fatigue crack lengths and CAH diameters from Sub Model B4 using Skewed Mesh 3. 22
Figure 17. Location of largest LSS normal to connection plate-to-web weld measured from intersection point, d_{max}, for various original fatigue crack lengths and CAH diameters from Sub Model B4 using Skewed Mesh 3. 23
Figure 18. Largest FEA stress, linearly extrapolated LSS, quadratic extrapolated LSS, and single-point LSS at fillet weld toe as Sub Model B4 mesh is refined from Uniform Mesh 1 through 4 with 2.0 inch crack and 2.0 inch diameter CAHs. 24
Figure 19. FEA model of 11.75 inch wide test specimen with 2.0 inch long crack-like features and with 2.5 inch diameter CAHs. 28
Figure 20. Test specimen FEA model highlighting seams to model crack-like features. 29

Figure 21. Elevation of FEA model with boundary conditions. 30
Figure 22. Test specimen FEA model with Uniform Mesh 3 with 4.0 inch long crack-like features and 2.5 inch diameter CAHs. 30
Figure 23. Variation of linearly extrapolated LSS normal to weld toe as a function of distance along weld toe from edge of CAH for test specimen with 2.0 inch long crack-like feature and 2.5 inch diameter CAH from FEA of test specimen with Uniform Mesh 3. 31
Figure 24. Fatigue test specimen (a) elevation view; (b) section view. 34
Figure 25. Photo of (a) Test Specimen; (b) Spare Specimen. 35
Figure 26. Overview of test setup used for fatigue tests near southwest corner of Multi-Directional Experimental Laboratory strong floor. 36
Figure 27. Test setup with specimens for cyclic loading laboratory fatigue tests. 37
Figure 28. Photo of test setup during fatigue tests. 38
Figure 29. MTS FlexTest control system. 39
Figure 30. Inspection tools. 41
Figure 31. Campbell Scientific CR9000 data acquisition systems. 41
Figure 32. (a) Strain gage names; (b) Section view with LSS gage dimensions. 43
Figure 33. Edge of east CAH with edge gage installed for specimen SAW-12-25-4-2-N. 44
Figure 34. Comparison of FEA (red) to estimated stress range perpendicular to weld toe versus distance from weld toe with LSS linear extrapolation (dashed) for specimens SAW-12-25-2-2.5-N and SAW-12-25-2-2.5-S at (a) $L_{Max\text{-}LSS}$ from CAH edge, and (b) $L_{Max\text{-}LSS}$ +1.0 inch from CAH edge. 55
Figure 35. Comparison of FEA (red) to estimated stress range perpendicular to weld toe versus distance from weld toe with LSS linear extrapolation (dashed) for specimens SAW-12-25-4-2.5-N and SAW-12-25-4-2.5-S at (a) $L_{Max\text{-}LSS}$ from CAH edge, and (b) $L_{Max\text{-}LSS}$ +1.0 inch from CAH edge. 56
Figure 36. Comparison of FEA (red) to estimated stress range perpendicular to weld toe versus distance from weld toe with LSS linear extrapolation (dashed) for specimens SAW-12-25-2-2-N and SAW-12-25-2-2-S at (a) $L_{Max\text{-}LSS}$ from CAH edge, and (b) $L_{Max\text{-}LSS}$ +1.0 inch from CAH edge. 57
Figure 37. Comparison of FEA (red) to estimated stress range perpendicular to weld toe versus distance from weld toe with LSS linear extrapolation (dashed) for specimens SAW-12-25-4-2-N and SAW-12-25-4-2-S at (a) $L_{Max\text{-}LSS}$ from CAH edge, and (b) $L_{Max\text{-}LSS}$ +1.0 inch from CAH edge. 58
Figure 38. Comparison of FEA (red) to estimated stress range perpendicular to weld toe versus distance from weld toe with LSS linear extrapolation (dashed) for specimens SAW-12-30-2-2.5-N and SAW-12-30-2-2.5-S at (a) $L_{Max\text{-}LSS}$ from CAH edge, and (b) $L_{Max\text{-}LSS}$ +1.0 inch from CAH edge. 59
Figure 39. Comparison of FEA (red) to estimated stress range perpendicular to weld toe versus distance from weld toe with LSS linear extrapolation (dashed) for specimens SAW-12-30-4-2-N and SAW-12-30-4-2-S at (a) $L_{Max\text{-}LSS}$ from CAH edge, and (b) $L_{Max\text{-}LSS}$ +1.0 inch from CAH edge. 60
Figure 40. Comparison of FEA (red) to estimated stress range perpendicular to weld toe versus distance from weld toe with LSS linear extrapolation (dashed) for specimens SAW-12-40-2-2-N and SAW-12-40-2-2-S at (a) $L_{Max\text{-}LSS}$ from CAH edge, and (b) $L_{Max\text{-}LSS}$ +1.0 inch from CAH edge. 61
Figure 41. Comparison of FEA (red) to estimated stress range perpendicular to weld toe versus distance from weld toe with LSS linear extrapolation (dashed) for specimens SAW-12-40-4-2.5-N and SAW-12-40-4-2.5-S at (a) $L_{Max\text{-}LSS}$ from CAH edge, and (b) $L_{Max\text{-}LSS}$ +1.0 inch from CAH edge. 62

Figure 42. Variation of estimated stress range for LSS gage at 0.4t, $L_{Max\text{-}LSS}$ +1.0 inch from CAH edge for west fillet weld of specimen SAW-12-25-4-2-S. 64
Figure 43. Comparison between FEA linear extrapolated LSS along weld toe (top), dye penetration test result (center), and FEA contour of stress normal to weld toe (bottom) for specimen SAW-12-25-2-2-S, west weld at 521,000 cycles after 20% decrease in estimated stress range for LSS gage at 0.4t, $L_{Max\text{-}LSS}$ from CAH edge.....65
Figure 44. Photo of dye penetration result for specimen SAW-12-25-2-2.5-S east weld after 1,333,000 cycles of cyclic loading fatigue testing. 66
Figure 45. S-N data for test specimens and design, mean, and upper bound S-N curves for AASHTO Fatigue Category C. 69
Figure 46. S-N data for test specimens, design and mean S-N curves for AASHTO Fatigue Category C, and mean S-N curves for ECCS SAW test data and ECCS SMAW test data. 70

LIST OF TABLES

Table 1. Linearly extrapolated LSS results normal to connection plate-to-web fillet weld toe on web surface from different Sub Model B using Skewed Mesh 3. 15
Table 2. Largest linearly extrapolated weld toe LSS from Sub Model B4 with Uniform Mesh and Skewed Mesh using Mesh 1 (1.0t x 1.0t) for 2.0 inch long crack. 25
Table 3. Largest linearly extrapolated weld toe LSS from Sub Model B4 with Uniform Mesh and Skewed Mesh using Mesh 3 (0.4t x 0.4t) for 2.0 inch long crack. 25
Table 4. Largest quadratic extrapolated weld toe LSS from Sub Model B4 with Uniform Mesh and Skewed Mesh using Mesh 3 (0.4t x 0.4t) for 2.0 inch long crack. 26
Table 5. Largest maximum magnitude principal stress at edge of CAH from Sub Model B4 with Uniform Mesh and Skewed Mesh using Mesh 1 (1.0t x 1.0t) for 2.0 inch long crack. 26
Table 6. Largest maximum magnitude principal stress at edge of CAH from Sub Model B4 with Uniform Mesh and Skewed Mesh using Mesh 3 (0.4t x 0.4t) for 2.0 inch long crack. 26
Table 7. Comparison of $L_{Max\text{-}LSS}$ and $L_{95\%}$ for test specimen and Sub Model B, for various test specimen widths, crack lengths, and CAH diameters from FEA with Uniform Mesh 3. 32
Table 8. Cyclic loading laboratory fatigue test matrix. 33
Table 9. Cyclic loading protocol used for laboratory fatigue tests. 39
Table 10. Nominal gage locations for gages LSS1, LSS2, LSS5, and LSS6. 44
Table 11. Measured edge gage locations for various specimens. 45
Table 12. Comparison of FEA stress range to estimated stress range at gages G1-G4 for specimens SAW-12-25-2-2.5-N and SAW-12-25-2-2.5-S. 47
Table 13. Comparison of FEA stress range to estimated stress range at gages G1-G4 for specimens SAW-12-25-4-2.5-N and SAW-12-25-4-2.5-S. 47
Table 14. Comparison of FEA stress range to estimated stress range at gages G1-G4 for specimens SAW-12-25-2-2-N and SAW-12-25-2-2-S. 48
Table 15. Comparison of FEA stress range to estimated stress range at gages G1-G4 for specimens SAW-12-25-4-2-N and SAW-12-25-4-2-S. 48
Table 16. Comparison of FEA stress range to estimated stress range at gages G1-G4 for specimens SAW-12-30-2-2.5-N and SAW-12-30-2-2.5-S. 48
Table 17. Comparison of FEA stress range to estimated stress range at gages G1-G4 for specimens SAW-12-30-4-2-N and SAW-12-30-4-2-S. 48
Table 18. Comparison of FEA stress range to estimated stress range at gages G1-G4 for specimens SAW-12-40-2-2-N and SAW-12-40-2-2-S. 49
Table 19. Comparison of FEA stress range to estimated stress range at gages G1-G4 for specimens SAW-12-40-4-2.5-N and SAW-12-40-4-2.5-S. 49
Table 20. Comparison of FEA stress range to estimated stress range at gages LSS1-LSS8 for specimens SAW-12-25-2-2.5-N and specimens SAW-12-25-2-2.5-S. 49
Table 21. Comparison of FEA stress range to estimated stress range at gages LSS1-LSS8 for specimens SAW-12-25-4-2.5-N and SAW-12-25-4-2.5-S 50
Table 22. Comparison of FEA stress range to estimated stress range at gages LSS1-LSS8 for specimens SAW-12-25-2-2-N and SAW-12-25-2-2-S. 50
Table 23. Comparison of FEA stress range to estimated stress range at gages LSS1-LSS8 for specimens SAW-12-25-4-2-N. and SAW-12-25-4-2-S. 51
Table 24. Comparison of FEA stress range to estimated stress range at gages LSS1-LSS8 for specimens SAW-12-30-2-2.5-N and specimens SAW-12-30-2-2.5-S. 51
Table 25. Comparison of FEA stress range to estimated stress range at gages LSS1-LSS8 for specimens SAW-12-30-4-2-N and SAW-12-30-4-2-S 52

Table 26. Comparison of FEA stress range to estimated stress range at gages LSS1-LSS8 for specimens SAW-12-40-2-2-N and SAW-12-40-2-2-S. 52
Table 27. Comparison of FEA stress range to estimated stress range at gages LSS1-LSS8 for specimens SAW-12-25-4-2-N. and SAW-12-25-4-2-S. 53
Table 28. Comparison of FEA stress range to estimated stress range at gages Edge1 and Edge2 for selected specimens. 53
Table 29. S-N data from test specimen fillet welds 67

CHAPTER 1

Introduction

BACKGROUND

Tens of thousands of steel bridges constructed in the 1960's and 1970's (and earlier) are still critical components of transportation systems. Many of these older steel bridges have welded steel details that are likely to develop fatigue cracks during their service life. If not effectively repaired, many such fatigue cracks have the potential to lead to brittle fracture and bridge collapse. Large fatigue cracks often require a bridge to be fully or partially closed while expensive emergency repairs are made, leading to extensive owner costs and disruption of traffic.

The AASHTO LRFD bridge design specifications (BDS) (AASHTO, 2018) characterizes fatigue cracks as being either load-induced or distortion-induced. Load-induced fatigue cracking of bridge members (e.g., girders, floor beams, stringers, etc.) is caused by bending and/or axial response of the member. Distortion-induced fatigue cracking, on the other hand, is caused by secondary stresses that develop from differential deformations within the system of bridge members that are not always considered in design. The majority of fatigue cracks in bridges are distortion-induced (Bowman, et al., 2012) and distortion-induced cracking affects many types of steel bridges (Demers & Fisher, 1989). Distortion-induced fatigue cracking often occurs in the webs of longitudinal steel bridge members (e.g., girders) adjacent to the connection plates for the transverse members of the bridge (e.g., floor beams, cross-frames, or diaphragms) and is a result of cyclic out-of-plane distortion of the webs of these longitudinal bridge members (Fisher, et al., 1990).

Individual longitudinal steel bridge members are often analyzed as pin-supported line elements during bridge design. However, the actual behavior of a steel bridge system of longitudinal members with transverse members is more accurately represented as a three-dimensional grillage with semi-rigid connections between members. In a typical older two-girder bridge with a deck supported by floor beams and stringers, the traffic loads atop the bridge deck produce flexural deformations in the floor beam as it spans between the longitudinal I-shaped girders, as shown in Figure 1. These flexural deformations include end rotations of the floor beams, which are attached to connection plates that are welded to the webs of the girders. If the connection plates are not welded to the flanges of the girders (see Figure 1), the floor beam end rotations will result in compatible out-of-plane bending deformation of the girder webs, which requires a concentrated out-of-plane reverse-curvature bending deformation in the small unwelded portion of the girder web adjacent to the flanges (denoted the "web gap"). This concentrated reverse-curvature bending of the web gap, produces vertical tensile and compressive weld toe stresses on opposite faces of the webs (Figure 1). Under traffic loading, cyclic stresses can lead to fatigue cracking along the girder web-to-flange weld toe and the connection plate-to-web weld toe as shown in Figure 2. The region near the web gap, where this distortion-induced fatigue cracking may occur, is of interest for this study, and is denoted the "web gap region". Fatigue cracks that occur in the web gap region often propagate into the girder web, and have the potential to lead to brittle fracture in the girder web.

The out-of-plane bending stresses in the girder web caused by the floor beam end rotations are influenced by torsional restraint of the girders. For example, increased out-of-plane bending stresses can develop where the bottom flange of the girder is restrained from lateral deformation, such as at the location of the girder bearings, as suggested by the schematic deformation pattern of Figure 1. As noted above, similar distortion-

induced fatigue cracking can occur in other bridge types such as commonly-used multi-girder bridges, when the diaphragm connection plates are not welded to the girder flanges.

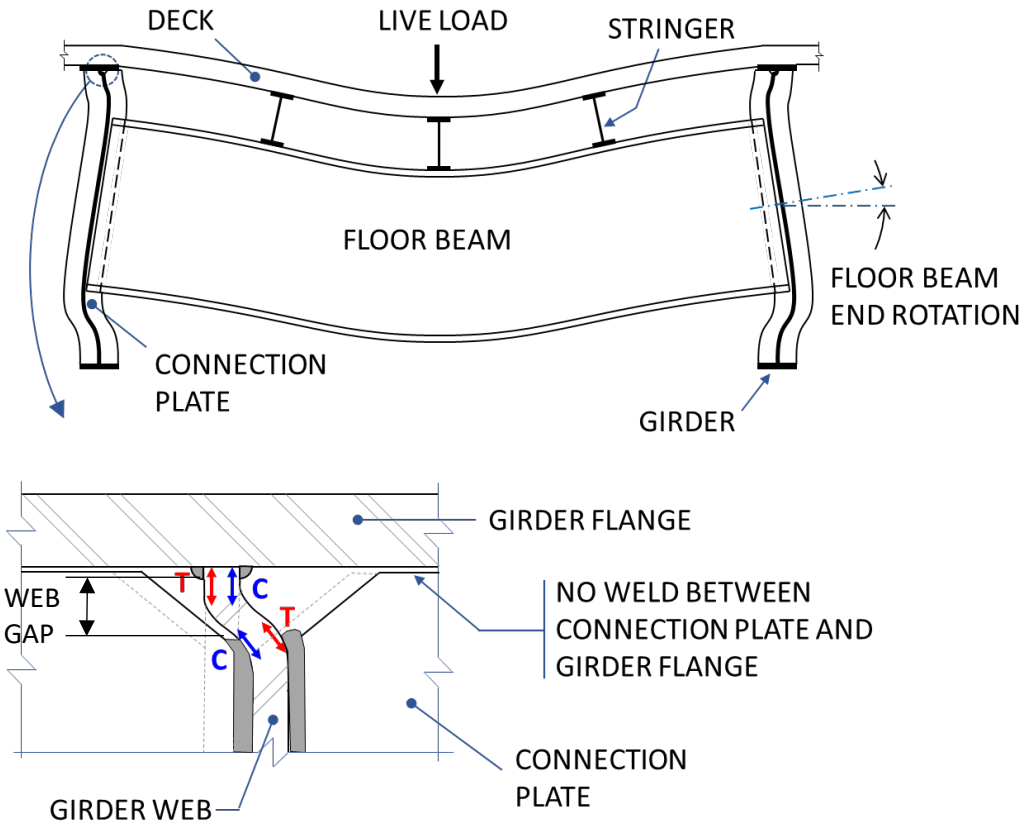

Figure 1. Exaggerated deformation of older two-girder bridge under vehicular live load, localized out-of-plane reverse-curvature bending deformation, and resulting stresses in web gap when connection plates are not welded to flanges.

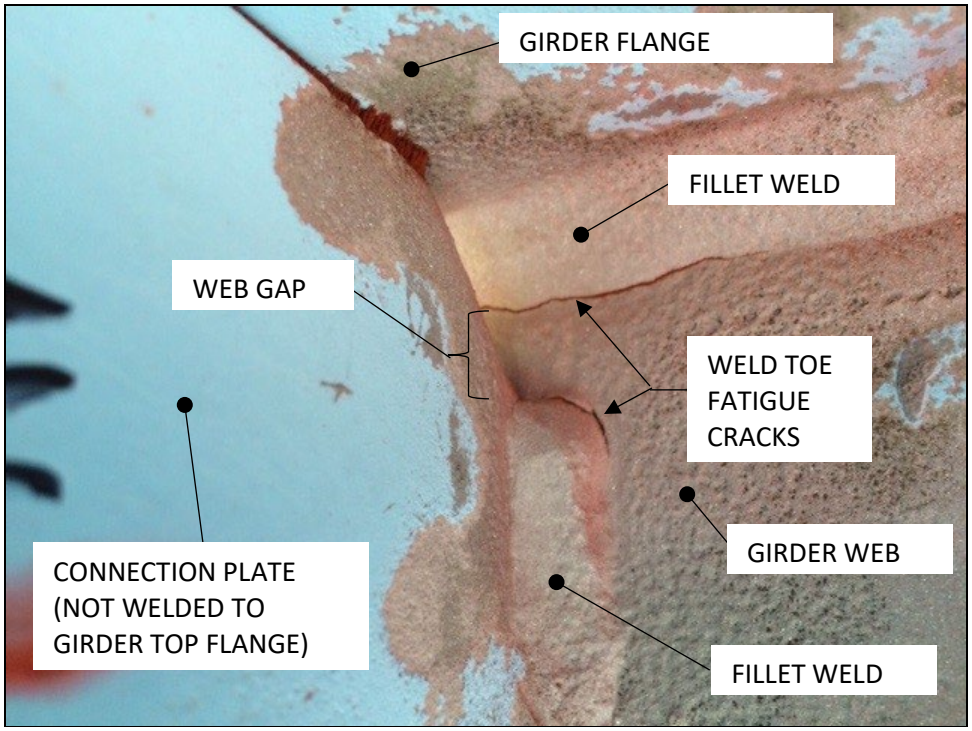

Figure 2. Distortion-induced fatigue cracking in girder web gap region at web-to-flange and end of connection plate-to-web weld toes produced by transverse member end rotation.

The concentrated reverse-curvature bending of the web gap is sensitive to the configuration of the connections between the transverse member (floor beam) connection plate and the longitudinal bridge member (girder), in particular whether the connection plate was welded or bolted to the girder flange and the length of the web gap. (Fisher, et al., 1990) studied distortion-induced fatigue in web gap regions and found that assessing the potential for distortion-induced fatigue cracking in the web gap is complex, requiring detailed finite element analysis (FEA), and is not practical for typical bridge design. Rather, control of distortion-induced web gap fatigue cracking is achieved in design by using proper connection details (AASHTO, 2018).

Prior to the introduction of modern fatigue design provisions, welding of connection plates to the tension flanges of steel bridge girders (with a stress demand of more than 75% of their design capacity) was not permitted (AASHO, 1949), due to concerns about fatigue at welds on tension flanges. As a result, many older steel bridges were constructed without welds between the connection plates and tension flange, so distortion-induced web gap fatigue cracking is relatively common for steel bridges constructed in the 1960s and 1970s (or earlier). Later research showed that the fatigue resistance of welds on tension flanges can be easily considered in design (Fisher, et al., 1974). Thus, a welded (or bolted) connection between a connection plate and girder tension flange is now required. Welding or bolting the connection plate to the tension flange prevents distortion-induced fatigue cracking in the web gap from occurring.

Retrofit of older steel bridges by welding transverse member connection plates to the girder flanges is not always feasible due to concerns with field weld quality and potential impacts on bridge traffic. Also, bolting connection plates to the top flanges of girders is often impractical since the bridge deck limits access to the top flange. Additionally, the elements needed to connect the connection plate to the flange (e.g., steel tees or angles) are difficult to design with sufficient stiffness to reduce out-of-plane deformation of the web gap. Retrofit by using crack-arrest holes (CAHs) to stop the growth of fatigue cracks is most often used to address distortion-induced fatigue cracking (Dexter & Ocel, 2013) due to their demonstrated effectiveness

and ease of installation. A properly designed and installed CAH blunts the crack tip (by removing the crack tip) reducing the stress intensity and reducing the potential for further crack growth. However, in some cases, fatigue cracking appears to reinitiate. Figure 3 shows an example of distortion-induced fatigue cracking in the web of a bridge girder in which a fatigue crack appears to reinitiate after a CAH was installed. The photo shows a fatigue crack below (i.e., beyond) the CAH that was installed to control the original fatigue crack in the web gap region.

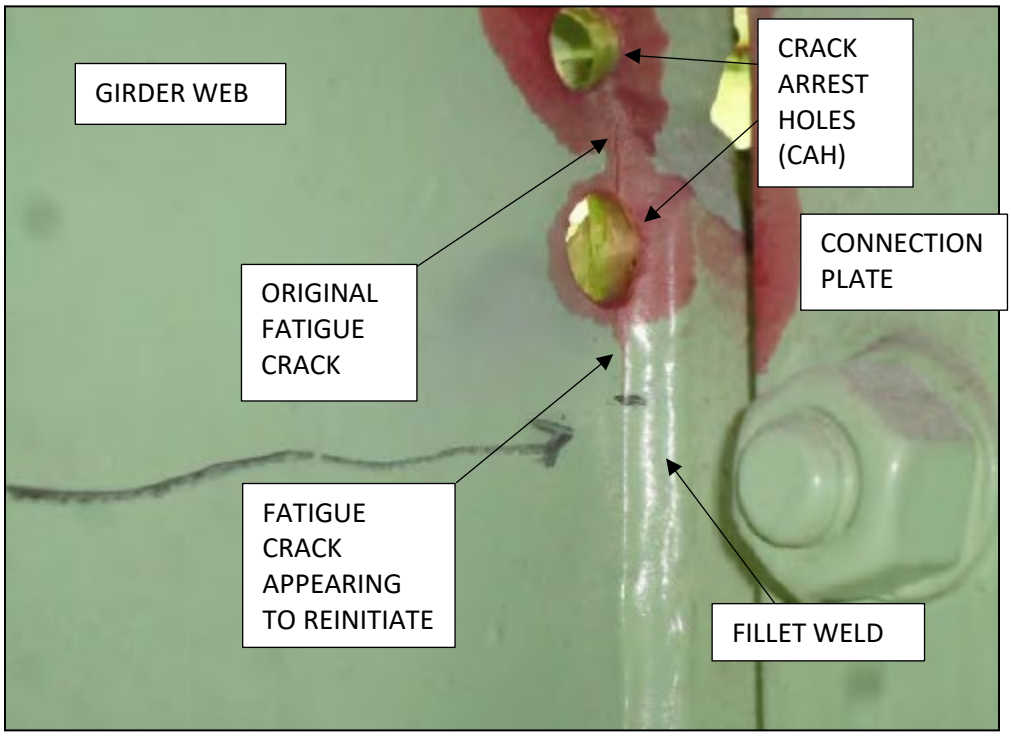

Figure 3. Fatigue crack appearing to reinitiate after installation of crack-arrest hole (CAH).

This work considers two reasons why a fatigue crack may appear to reinitiate: (1) the CAH was not properly designed, or (2) the original fatigue crack geometry was not properly identified, so that the CAH did not intercept the tip of the crack. Referring to the crack shown in Figure 3, this crack may "reinitiate" because the size and location of the lower CAH in the photo, in combination with the weld toe, has created a stress condition that causes a fatigue crack to initiate from the weld toe near the CAH, that is, the CAH was not properly designed. Alternately, this fatigue crack may "reinitiate" because the original crack, which was growing downward along the weld toe (visible above the lower CAH in the figure), was not properly identified and the CAH did not intercept the crack tip enabling the crack to continue to grow. Since the original fatigue crack was growing along the weld toe, both reasons are plausible, because: (1) the weld toe creates a stress concentration which makes the CAH difficult to design and may cause a crack to initiate near the CAH, and (2) the weld toe makes it difficult to properly identify the crack geometry (especially, the crack tip), which makes it difficult to reliably intercept the crack tip and may allow the original crack to continue to grow.

(Liu, et al., 2018) studied the first reason for apparent reinitiation of such weld toe fatigue cracking. In this work, the effectiveness of a CAH retrofit for distortion-induced fatigue cracking at a connection plate-to-web weld was investigated using parametric FEA studies and full-scale fatigue testing. The study considered constant amplitude cyclic loading of the connection plate in the out-of-plane direction of the girder web. Since the force amplitude of the cyclic loading was constant, the FEA results indicated that an

increasing crack length resulted in increased local stresses in the web gap region. The results showed that a CAH with a diameter of at least 25 mm (1 inch) significantly reduces the stress intensity at the adjacent connection plate-to-web weld (when the crack tip is removed), but the presence of the CAH results in a stress concentration at the connection plate-to-web weld toe at a location beyond the CAH and a fatigue crack may initiate at this location (Liu, et al., 2018). The location of the largest stress concentration at the weld toe is a short distance from the CAH, not at the intersection of the CAH and the weld toe. This finding from FEA was confirmed by laboratory fatigue testing of a girder test specimen (Liu, et al., 2018).

The present report addresses the first of the two reasons why a fatigue crack may appear to reinitiate, that the CAH was not properly designed. The second reason, that the original fatigue crack geometry was not properly identified, is a subject for future research. This report presents research on the stresses that are associated with distortion-induced fatigue cracking in the web gap region, and presents an approach to design CAHs to control an original fatigue crack in the web gap region. Stresses in the web gap region, and the potential for fatigue cracking after a CAH is installed are studied, and tests on small-size specimens are used to verify the design approach for avoiding fatigue cracking after the CAH is installed.

PROJECT OBJECTIVE

This project addresses the need to extend the life of older, fatigue-damaged steel bridges. Given that distortion-induced web gap fatigue cracking is relatively common for steel bridges constructed in the 1960s and 1970s (and earlier), and that CAHs are often used to retrofit distortion-induced fatigue cracks that run along transverse member connection plate-to-web welds in steel girder bridges, the objective of this research is to present an approach to design an effective CAH to retrofit a distortion-induced fatigue crack that initiates in a web gap and propagates along a transverse member connection plate-to-web weld.

Initiation of a fatigue crack along the connection plate-to-web weld toe after the CAH is installed would indicate that that the CAH is ineffective (i.e., improperly designed), therefore, this research focuses on the stress conditions that could cause a fatigue crack to initiate at the connection plate-to-web weld toe after the CAH is installed. The original fatigue crack, propagating from the web gap along the connection plate-to-web weld toe, is assumed to have been properly identified and the CAH is assumed to have intercepted the tip of the original fatigue crack. The research investigates the potential for a fatigue crack to initiate and the location where a crack might initiate after the CAH is installed. Various original fatigue crack lengths and CAH diameters are studied to determine the influence of these parameters. A CAH design approach and recommended CAH dimensions are presented.

RESEARCH APPROACH

Detailed three-dimensional (3D) finite element analyses (FEA) of a typical two-girder bridge, with the deck supported by floor beams and stringers, constructed in the late 1960s, are used to study distortion-induced fatigue behavior in the web gap region of the bridge girders. The local structural stress (LSS) at the weld toe is evaluated from FEA results using standard extrapolation methods and is used to assess the potential for fatigue cracking. Other stress results from FEA are also used. Using FEA and LSS methods, the influences of the original fatigue crack length and CAH diameter on stresses in the web gap region are studied.

A CAH design approach and recommended CAH dimensions are presented, which are expected to provide good fatigue performance, by avoiding fatigue cracking after CAHs are installed. The design approach compares stress results from FEA and LSS methods with standard fatigue resistance from (AASHTO, 2018).

Fatigue tests of small-size test specimens with full-scale welds, simulated cracks, and CAHs are performed to validate the fatigue performance assessment used in the CAH design approach. Stresses from FEA and LSS methods, and measured stresses are used to assess the potential for fatigue cracking.

CHAPTER 2

Finite Element Modeling Approach

This study used three-dimensional linear elastic finite element analyses (FEA) of a typical two-girder bridge, with the deck supported by floor beams and stringers, to determine web gap region stresses where the floor beam connection plates are attached to the girder webs. This typical two-girder bridge was constructed in the late 1960s and has a history of distortion-induced fatigue cracking at the floor beam connection plate-to-web fillet welds. The FEA was conducted using ABAQUS, a commercially available software produced by Dassault Systèmes. A sub-modeling technique was used to study the local behavior of the web gap region.

Parametric FEA studies, in which the length of the original fatigue crack along the connection plate-to-web weld and the diameter of the CAH are varied, were performed using the FEA sub models. In addition, the characteristics of the finite element sub-models were studied, and stress results from four different levels of mesh refinement and two mesh configurations adapted from (Hobbacher, 2016) were compared. Finally, several standard methods of determining the local structural stress (LSS) at the weld toe were compared. The various weld toe LSS results were used to assess the potential for fatigue cracking. Detailed 3D FEA was also used to design the test specimens for the laboratory fatigue tests.

FINITE ELEMENT MODELS

Modeling Technique

The FEA used a global model of the bridge along with a node-based sub-modeling technique, which interpolates nodal displacement results from a global model to determine the boundary displacements of a sub model (Dassault Systemes Simulia Corp., 2016). The FEA displacement results from a global model of the typical two-girder bridge were used as the input boundary displacements for a smaller, more refined sub model (Sub Model A) of the region surrounding the web gap. A second level sub model (Sub Model B) of a smaller region surrounding the web gap, with a more refined mesh was created, and FEA displacement results from Sub Model A were used as the input boundary displacements for Sub Model B. Fillet welds, an original crack (i.e., the distortion-induced fatigue crack before installation of the CAH), along the floor beam connection plate-to-web weld toe, and CAHs are included in Sub Model B. The use of this sub-modeling technique reduced the effort needed to create a refined mesh of the web gap region and facilitated the parametric study of the original fatigue crack length and CAH diameter using Sub Model B.

Global Model

The Global Model is based on a two-girder steel highway bridge with a history of distortion-induced fatigue cracking at the floor beam connection plate-to-web fillet welds. Constructed in the late 1960s, this bridge has a total length of more than 3400 feet, carries two lanes of traffic, and is comprised of a concrete deck and parapet supported by rolled steel stringers, welded-steel-plate floor beams with lateral bracing, and two welded-steel-plate girders. The girders are continuous over three piers and have pin-and-hanger assemblies

separating the bridge into three-span units. The floor beam connection plates are fillet welded to the girder webs but are not welded to the girder tension flanges. The Global Model (see Figure 4) represents one three-span unit of the bridge, and includes the concrete deck with parapets, steel stingers, steel floor beams with lateral bracing, and steel girders. At each end of the Global Model, vertical springs represent the stiffness of the bridge spans beyond the pin-and-hanger assemblies (in-plane girder rotations are unrestrained). The stiffness of these springs was estimated using an FEA model of the adjacent part of the bridge. The bridge piers and bearings were modeled simply as pin supports, with displacements at the bearing locations restrained in the vertical and transverse directions (and free for the other four degrees of freedom).

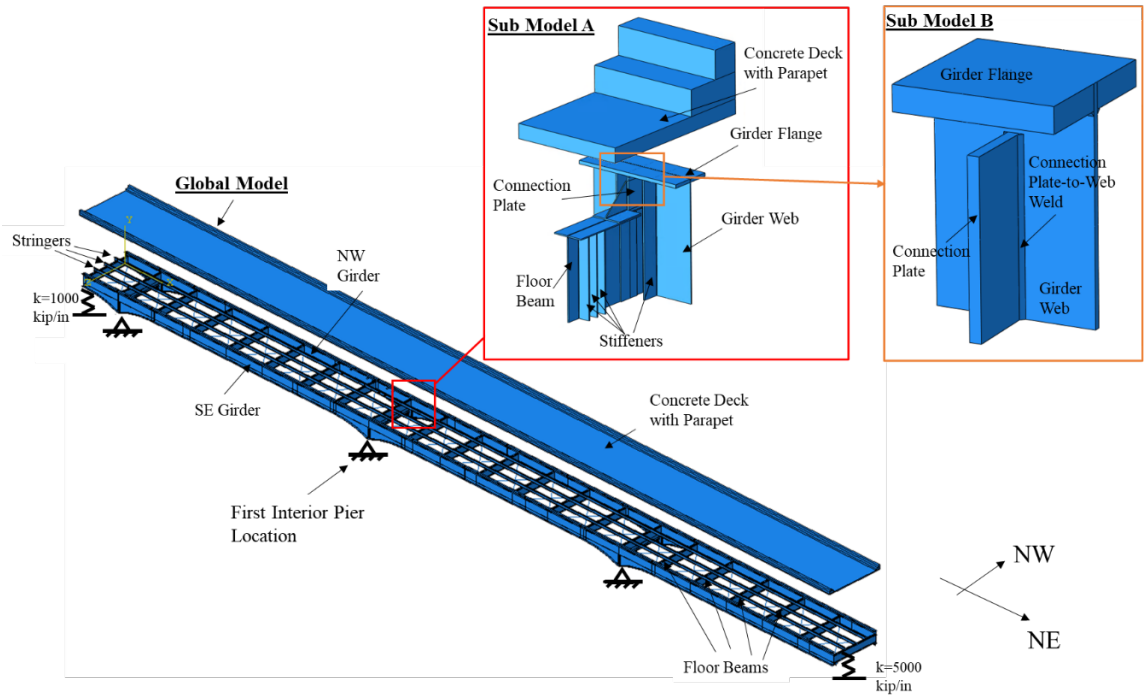

Figure 4. Exploded view of Global Model, Sub Model A, and Sub Model B and locations of Sub Model A and Sub Model B.

Sub Models

The two levels of sub models (i.e., Sub Model A and Sub Model B) were used to investigate the stresses in the web gap region of the northwest girder at the first interior pier of the Global Model as shown in Figure 4. Sub Model A represents a portion of the Global Model, including portions of the concrete deck with parapet, steel girder, steel floor beam, connection plate, stiffeners, and fillet welds between each component. Sub Model B represents a portion of Sub Model A, including portions of the steel girder web and top flange, connection plate, stiffener on the outside face of girder web which is aligned with the connection plate, and fillet welds between each component.

Sub Model B was used for parametric study of the original fatigue crack length and the CAH diameter, and to study the effects of mesh refinement and mesh configuration. Sub Model B includes a model of the original fatigue crack and the CAH (Figure 5). The original fatigue crack is modeled by assigning a plane of mesh discontinuity (termed a "seam") along the connection plate-to-web weld toe and through the girder web thickness. Coincident, duplicate nodes are included in the finite element mesh along the seam which allows the seam to open, simulating a fatigue crack. The original fatigue crack along the connection plate-to-web fillet weld toe was modeled as a continuous seam across the top edge of the connection plate, and along each weld toe on each side of the connection plate as shown by the red line in Figure 5. One CAH is

positioned on each side of the connection plate at the end of the seam that models the original fatigue crack. The CAH is located so that it penetrates the fillet weld by 1/8 inch, as shown in Figure 5. Each CAH is assumed to be centered on the tip of the original fatigue crack, so the original fatigue crack length is defined to be from the top edge of the connection plate to the center of the CAH. The web gap between the web-to-flange weld toe and top edge of the connection plate is assumed to be 2.0 inches. The girder flange is 2.0 inches thick; the connection plate is 7/8 inch thick; and the girder web is 1/2 inch thick. The connection plate-to-web fillet weld and web-to-flange fillet weld were modeled with a simple geometry, with a 5/16 inch leg and a zero-radius notch at each weld toe. The unfused strip and the fit-up gap at the fillet weld root were not modeled. The connection plate-to-web fillet weld was assumed to stop at the top of the connection plate without wrapping around the top edge of the connection plate.

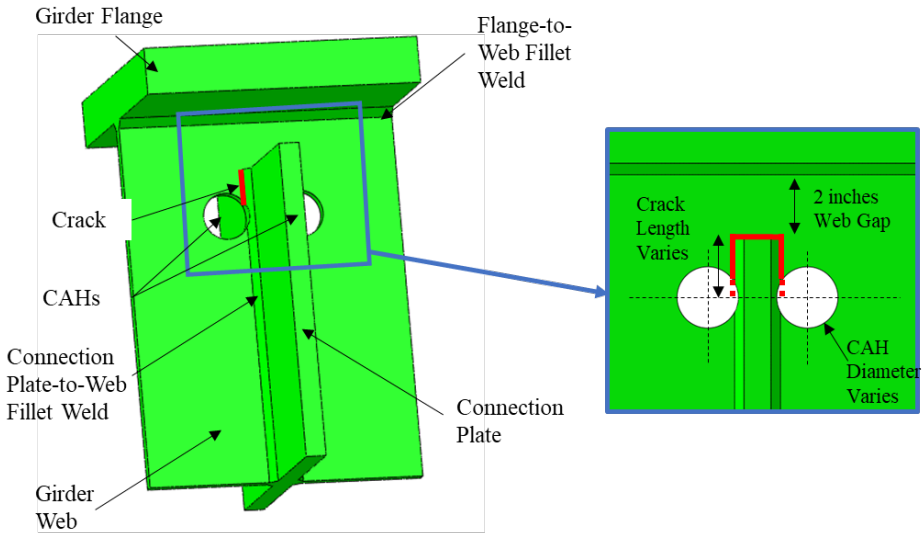

Figure 5. Sub Model B geometry and locations of crack and CAH.

Material Properties

General linear elastic material properties for steel and concrete were used in the FEA models. The modulus of elasticity and Poisson's ratio for steel were assumed to be 29,000 ksi and 0.3, respectively. The modulus of elasticity and Poisson's ratio for concrete were assumed to be 3,000 ksi and 0.2, respectively.

Loading

The Global Model was loaded with a three-axle truck, which included one 20.2 kip front axle and one 52.2 kip rear tandem axle spaced 20 feet apart. The truck was transversely centered in the lane closest to the northwest girder (see Figure 4) and positioned longitudinally with the rear tandem axle centered above the floor beam at the first interior pier. The load used in the FEA was the gross vehicle weight of the three-axle truck with an additional 15% impact factor, resulting in 20.2 kips x 1.15 = 23.2 kips for the front axle load and 52.2 kips x 1.15 = 60.0 kips for the rear tandem axle load.

The total rear tandem axle load used in the FEA (60.0 kips) exceeds the factored AASHTO tandem axle load for the Fatigue I (i.e., infinite fatigue life) limit state from the 7th edition of the AASHTO LRFD BDS (AASHTO, 2016) which, using the Fatigue I load factor (1.5) and 15% impact factor, is 32 kips x 1.5 x 1.15 = 55.2 kips. However, the rear tandem axle load used in the FEA (60.0 kips) is less than the factored AASHTO tandem axle load for the Fatigue I limit state from the 8th Edition of AASHTO LRFD BDS

(AASHTO, 2018), where the load factor was increased to 1.75, resulting in a factored rear tandem load of 32 kips x 1.75 x 1.15 = 64.4 kips.

When the stress range at a location in a steel bridge element corresponding to the factored tandem axle load for the Fatigue I limit state is less than the corresponding AASHTO fatigue category constant amplitude fatigue limit (CAFL), infinite fatigue life is expected at that location (AASHTO, 2018). For the Fatigue II (i.e., finite fatigue life) limit state, the fatigue load specified for design is 45% of the fatigue load specified for the Fatigue I (i.e., infinite fatigue life) limit state (AASHTO, 2018). Therefore, the stress range from an analysis that uses the Fatigue I limit state load should be divided by a factor of 2.2 before it is compared to the standard finite-life fatigue resistance from (AASHTO, 2018). Note that dead load stresses and residual stresses are not directly included in the fatigue assessments described herein since the assessments are based on fatigue stress ranges.

Finite Element Meshes and Stress Analysis

Three-dimensional meshes for the FEA models were generated using the ABAQUS structured meshing algorithm (Dassault Systemes Simulia Corp., 2016) with a defined target element size. Reduced integration elements were used. The Global Model has 8-node quadratic shell elements with an average size of approximately 20.0 inches over most of the model. In the region within 30 feet before and after the first interior pier, the Global Model has 20-node solid quadratic hexahedral elements with an average size of approximately 2.0 inches. At the transitions, shell-to-solid coupling constraints in ABAQUS (Dassault Systemes Simulia Corp., 2016) were used to constrain the displacement and rotation of each shell element node to the average displacement and rotation of the surface of the solid elements in the vicinity of the shell node. Sub Model A and Sub Model B have 20-node solid quadratic hexahedral elements only. Sub Model A has an average element size of approximately 1.0 inch. A mesh refinement study was performed using Sub Model B. Four levels of mesh refinement with average element size ranging from 0.5 inch to 0.1 inch were used in the study, denoted Mesh 1 through Mesh 4.

The various Sub Model B element meshes were developed to quantify the connection plate-to-web weld toe stresses using a local structural stress (LSS) approach, as follows. To assess the potential for fatigue cracking at a weld toe, where nominal stresses are poorly defined, the International Institute of Welding (IIW) (Hobbacher, 2016) and AASHTO LRFD BDS (AASHTO, 2018) specifies the use of an LSS approach in which the weld toe LSS is determined by extrapolation of surface stresses at reference points with defined distances from the weld toe. (AASHTO, 2018) suggests comparing the weld toe LSS with the nominal fatigue resistance (design S-N curve) of AASHTO Fatigue Category C. Past research has demonstrated that comparing the weld toe LSS with AASHTO Fatigue Category C provides a reliable assessment of weld toe fatigue cracking. Note, the terminology for the LSS approach is slightly different in different specification documents (e.g., “LSS” is used in AASHTO LRFD BDS; while “Hot Spot Stress” is used in IIW and Eurocode). Two mesh sizes are specified in (Hobbacher, 2016): (1) a relatively coarse mesh with the element length equal to 1.0t in the direction normal to the weld toe, where t is the thickness of the part where the surface stress is being determined; and (2) a relatively fine mesh with element length no more than 0.4t in the direction normal to the weld toe. Note that the LSS at the connection plate-to-web weld toe is determined by extrapolation of surface stresses on the girder web, therefore, t is the girder web thickness of 1/2 inch. In creating the element mesh, constraints on the mesh geometry can be specified to ensure that nodal stress results are available at the specified reference points.

The maximum magnitude principal stress (MMPS) on the CAH edge were evaluated. The MMPS is the nodal FEA principal stress with the largest magnitude on the CAH edge. (AASHTO, 2018) recommends AASHTO Fatigue Category A for a radiused opening with a flame cut edge having a "smooth" finish (within an orthotropic steel bridge deck). The stress at the cut edge that should be compared with the AASHTO Fatigue Category A resistance is not fully specified in AASHTO; however, (Saunders, 2021) found that comparing a stress similar to the MMPS with AASHTO Fatigue Category A is conservative for

assessing fatigue cracking on a smooth cut edge. Therefore, to assess the potential for fatigue cracking at the edge of the CAH, the MMPS on the CAH edge is compared with the nominal fatigue resistance of AASHTO Fatigue Category A.

In Sub Model B, as shown in Figure 6, the element dimensions of 1.0t x 1.0t (0.5 inch x 0.5 inch) in Mesh 1 are based on the relatively coarse mesh specified in (Hobbacher, 2016); the element dimensions of 0.4t x 1.0t (0.2 inch x 0.5 inch) in Mesh 2 are based on the relatively fine mesh specified in (Hobbacher, 2016); Mesh 3 has a finer mesh size than Mesh 2, with typical element dimensions of 0.4t by 0.4t (0.2 inch x 0.2 inch); Mesh 4 has a more refined mesh than Mesh 3, with typical element dimensions of 0.2t by 0.2t (0.1 inch x 0.1 inch). The Mesh 3 dimensions meet the requirements for a relatively fine mesh (Hobbacher, 2016), and, the elements used in Mesh 3 have equal edge lengths, which can be automatically generated by ABAQUS without additional mesh constraints. Compared to Mesh 2, Mesh 3 requires more computation time, but less modeling effort. The more refined mesh in Mesh 4 was used to ensure that the FEA stress results have converged. Note that Mesh 1 and Mesh 2 have 2 elements through the thickness of the girder web, Mesh 3 has 3 elements through the web thickness and Mesh 4 has 5 elements through the web thickness.

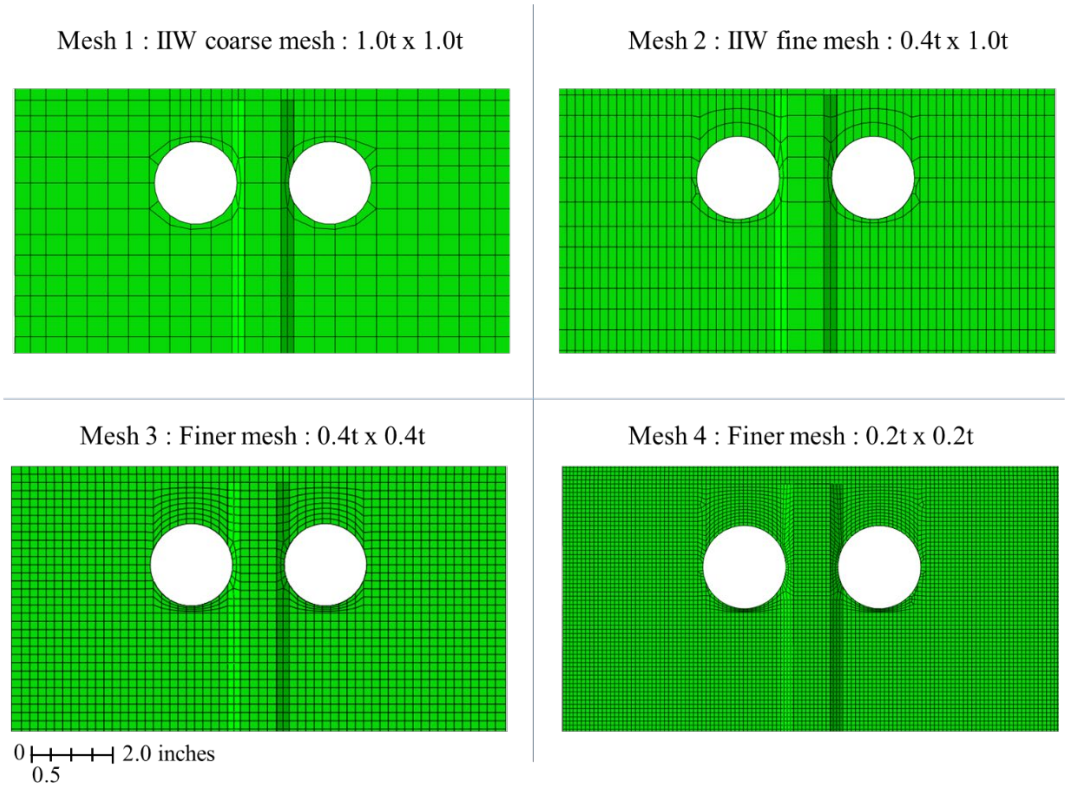

Figure 6. Sub Model B Uniform Mesh 1 through 4 shown with 2.0 inch diameter CAHs.

The LSS at the connection plate-to-web weld toe was determined by extrapolation of surface stresses at reference points with defined distances from the weld toe (Hobbacher, 2016). Linear extrapolation using the relatively coarse mesh requires stresses at reference points located 0.5t and 1.5t from the weld toe. Using the relatively fine mesh, stresses at reference points located 0.4t and 1.0t from the weld toe are required for linear extrapolation; stresses at reference points located 0.4t, 0.9t and 1.4t from the weld toe are required for quadratic extrapolation (Hobbacher, 2016). Note, the quadratic extrapolation is recommended for stress conditions with pronounced non-linear stress increase towards the weld toe (Hobbacher, 2016). These

extrapolation methods with their respective reference points for different mesh types are shown schematically in Figure 7.

In addition to these extrapolation methods, an alternative method that determines the LSS from the surface stress at a single reference point, specified in (DNV, 2011) was also considered, and termed the "single-point method" in this study. The 1.0t x 1.0t element size (Mesh 1) is recommended for the single-point method, and the single-point LSS at the weld toe is taken as the stress at a reference point located 0.5t from the weld toe, multiplied by a factor of 1.12 (DNV, 2011).

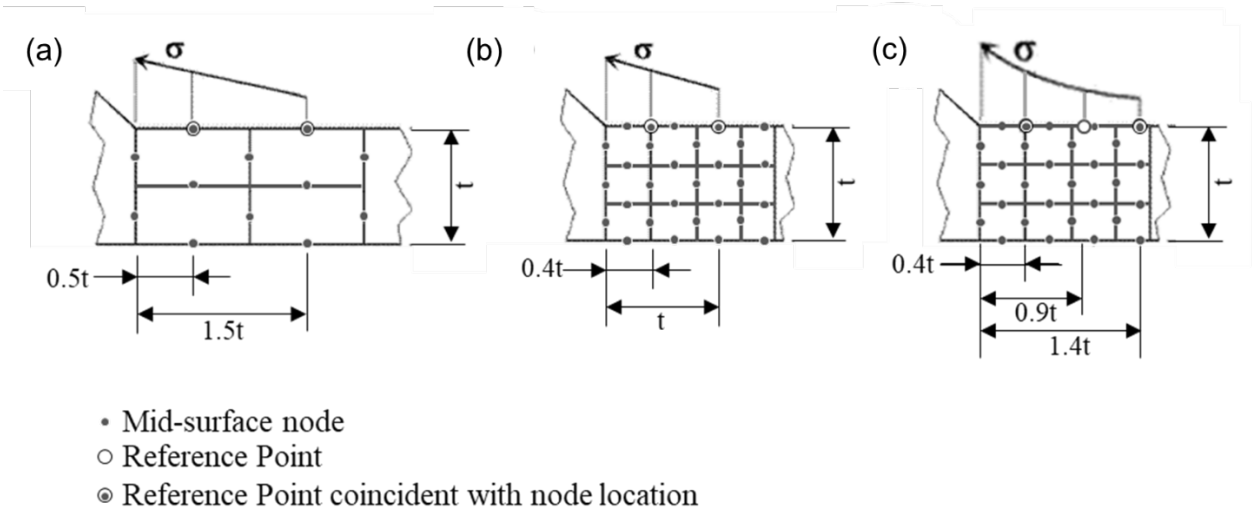

Figure 7. Extrapolation methods and reference points for different uniform mesh types (adapted from (Hobbacher, 2016): (a) linear extrapolation method for relatively coarse mesh (Uniform Mesh 1); (b) linear extrapolation method for relatively fine mesh (Uniform Mesh 3); and (c) quadratic extrapolation method for relatively fine mesh (Uniform Mesh 3).

Adjacent to a typical fillet weld (without the presence of a CAH), the elements with the required size can be generated uniformly near the fillet weld toe in the FEA model, and the reference points for LSS extrapolation are usually at the element corner node or mid-surface node locations (see Figure 7). However, in a web gap region with a CAH retrofit, the geometry is more complex due to the presence of the CAH, and the elements that are near the fillet weld toe may be skewed (see Figure 8). For a mesh with a skewed configuration, the reference points may not coincide with the element nodes. To compute the stress/strain values at a point of interest that do not coincide with nodal locations, ABAQUS will interpolate results from the nodes near the point of interest using the geometric approximation of the element shape (Dassault Systemes Simulia Corp., 2016). With this capability, stress results can be determined for a reference point not coincident with an element node. Thus, the reference points do not need to be coincident with the node locations, and the elements can be generated automatically by setting a target mesh size in ABAQUS, which simplifies the FEA modeling process.

To study the accuracy of the interpolated results from a skewed mesh configuration, and the sensitivity of the weld toe LSS results to the reference point locations with respect to the node locations, two mesh configurations were studied using Sub Model B, denoted "Uniform Mesh" and "Skewed Mesh" as shown in Figure 8. In a Uniform Mesh, cuboid elements are maintained near the connection plate-to-web fillet weld toes by defining vertical and horizontal partition lines in the FEA model. Around the CAHs, a few trapezohedral elements are generated to create compatibility with the CAH circumference. In a Skewed Mesh, trapezohedral elements are generated over a larger region automatically by ABAQUS, the cuboid elements are not maintained near the connection plate-to-web fillet weld toes. The Uniform Mesh allows

the reference points for extrapolating the weld toe LSS to be coincident with the node locations. The Skewed Mesh requires less modeling effort; however, the node locations are not coincident with the weld toe LSS extrapolation reference points. The two mesh configurations are studied using the Mesh 1 and Mesh 3 levels of refinement. Later in this report, the LSS extrapolated from reference point stress results that are interpolated within the trapezohedral elements of the Skewed Mesh model are compared with the LSS extrapolated from reference point stress results that are extracted at the element node locations in the Uniform Mesh model.

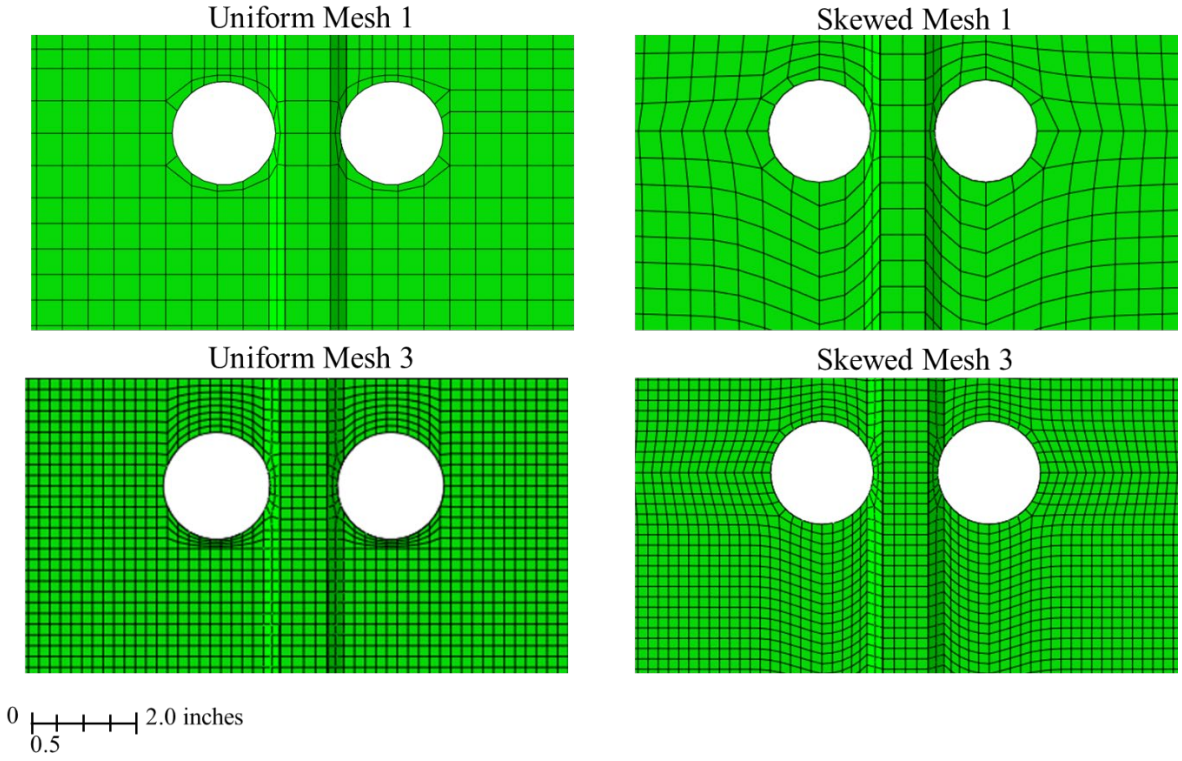

Figure 8. Uniform Mesh 1 and 3 and Skewed Mesh 1 and 3 with 2.0 inch diameter CAHs.

CHAPTER 3

Finite Element Analysis Parametric Studies

The FEA stress results for the web gap region generated using Sub Model B are presented in this chapter. The FEA stress results were used to understand the stress condition created by an original fillet weld toe fatigue crack combined with CAHs at the fillet weld toe. Understanding and quantifying this stress condition enables the potential for fatigue cracking to be assessed, leading to recommendations for the design of CAHs to prevent fatigue cracks from developing in the web gap region after the CAHs are installed.

Parametric FEA studies were performed in which the LSS at the weld toe and the MMPS at the edge of the CAH were evaluated for three different original crack lengths (i.e., 2.0 inches, 4.0 inches and 6.0 inches) and seven different CAH diameters ranging from 0.5 inch to 3.5 inches. In addition, the effect of the finite element mesh characteristics was studied, using the four different levels of mesh refinement and the two mesh configurations.

FEA STRESSES IN WEB GAP REGION FROM OUT-OF-PLANE DEFORMATION OF GIRDER WEB

As discussed previously, in a typical two-girder bridge with the deck supported by floor beams and stringers, when the connection plate for the floor beam is welded to the girder web but is not connected to the flange, out-of-plane bending deformation of the girder web due to the end rotation of the floor beam can produce large web plate bending stresses within the web gap region, which may lead to fatigue cracking. An original fatigue crack that is initially horizontal at the weld toe at the end of the floor beam connection plate-to-web weld, often turns to become vertically oriented, propagating downwards along the connection plate-to-web weld toe away from the web gap as shown in Figure 2 and Figure 3.

Before the potential for fatigue cracking along the connection plate-to-web weld toe after a CAH retrofit was studied, the development of the original fatigue crack and the effectiveness of a CAH retrofit were investigated by an FEA parametric study. The stress responses due to the out-of-plane bending deformation of the girder web in the web gap region, before and after the original fatigue crack develops, and with and without a CAH retrofit, were studied using Sub Model B with different configurations (see Figure 9), including: (1) the as-built condition with no fatigue crack (Sub Model B1); (2) the condition with the original fatigue crack and without CAHs installed (Sub Model B2); (3) the condition without a fatigue crack and with CAHs installed (Sub Model B3); and (4) the condition with the original fatigue crack and with CAHs installed (Sub Model B4). In this study, the original fatigue crack is located along the connection plate-to-web weld toe with a length of 2.0 inches, and the CAH diameter is 2.0 inches. The FEA were performed using Skewed Mesh 3 (see Figure 8).

Figure 9 shows contour plots of the normal stress (S11) in the horizontal direction normal (i.e., perpendicular) to the connection plate-to-web fillet weld on the face of the girder web from Sub Model B1 through B4. The corresponding largest LSS (in tension from linear extrapolation) and with its location along the connection plate-to-web weld is shown in Table 1. Note that due to the asymmetry of the three-span unit of the bridge represented by the Global Model in the longitudinal direction of the bridge (see Figure

4), the stresses are slightly larger at the northeast (NE) side of the connection plate and these slightly larger FEA stress results from the northeast side are reported.

FEA results for Sub Model B1 (representing the initial uncracked condition of the web gap region) show that the out-of-plane bending of the girder web produces large stresses in the web gap region. The largest LSS normal to the weld toe (i.e., horizontal) is 13.1 ksi at the top end of the connection plate. When the original fatigue crack is included in Sub Model B2, the largest LSS is 10.6 ksi near the tip of the crack. The reduction in LSS from including the fatigue crack is attributed to increased flexibility of the girder web gap region from the presence of the crack, as deformations with the same amplitude from Sub Model A are applied to both Sub Model B1 and Sub Model B2. Although the LSS from linear extrapolation near the crack tip is large in magnitude, the actual local stress at the crack tip is expected to be much larger (infinite in theory), and continued crack growth would occur without a retrofit. Sub Model B3 shows that installing CAHs in an uncracked web gap region increases the stress. The largest LSS from Sub Model B3 normal to the weld toe (i.e., horizontal) is 16.0 ksi at the weld toe at the top end of the connection plate, compared to 13.1 ksi for Sub Model B1 without the CAHs.

Sub Model B4 provides web gap region stresses with the presence of the original fillet weld toe fatigue crack and with CAHs installed. In addition to eliminating the large local stress near the crack tip (as in Sub Model B2), the results from Sub Model B4 demonstrate that properly designed CAHs installed at the tips of an original fatigue crack that runs along the connection plate-to-web weld toe will reduce the LSS normal to the weld toe. For instance, with a 2.0 inch long original fatigue crack retrofit with 2.0 inch diameter CAHs, the largest LSS from Sub Model B4 is 6.2 ksi, significantly less than the constant amplitude fatigue limit (CAFL) of 10 ksi for AASHTO Fatigue Category C. Comparing the LSS from Sub Model B4 with the LSS from Sub Model B1 shows that the CAHs move the location of the largest LSS from the top end of the connection plate to a location below the CAHs along the connection plate-to-web weld. This location of largest LSS is not at the intersection between the edge of the CAH and the fillet weld toe (i.e., the *intersection point*), but is 0.9 inch below this intersection point. This finding that the location of the largest LSS is a short distance away from the intersection point is consistent with FEA results from (Liu, et al., 2018).

At the largest LSS location in Sub Model B4 (0.9 inch from the intersection point), the LSS was determined for each type of Sub Model B. The results are presented in the last column in Table 1. At this location, the LSS from the other Sub Model B are smaller. The increase in the LSS at this location in Sub Model B4 is due to the stress concentration effects of the CAHs. This finding indicates that to determine the remaining fatigue life at this location of largest LSS after the CAH retrofit, the fatigue damage at this location accumulated before the development of a fatigue crack or the installation of the CAH retrofit can be neglected.

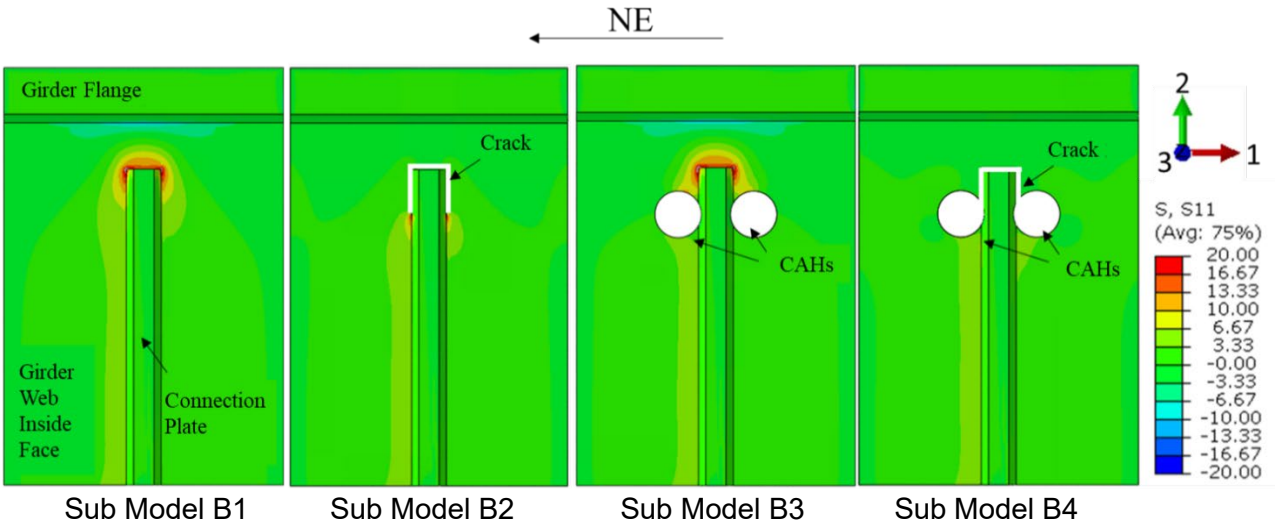

Figure 9. Contour plots of normal stress (S11) on inside web face from different Sub Model B using Skewed Mesh 3. (Note: Stress contours are presented with limit from -20 ksi to 20 ksi).

Table 1. Linearly extrapolated LSS results normal to connection plate-to-web fillet weld toe on web surface from different Sub Model B using Skewed Mesh 3.

	CAH Diameter (inches)	Original Crack Length (inches)	Largest LSS (ksi)	Location of Largest LSS	LSS at 0.9 inch from Intersection Point (ksi)
Sub Model B1	N/A	N/A	13.1	End of connection plate	4.2
Sub Model B2	N/A	2.0	10.6	Near crack tip	5.3
Sub Model B3	2.0	N/A	16.0	End of connection plate	3.8
Sub Model B4	2.0	2.0	6.2	0.9 inch from intersection point	6.2

FEA STRESS RESULTS FOR FATIGUE-DAMAGED WEB GAP REGION RETROFIT WITH CAHS

Using Sub Model B4 for the web-gap region with an original fatigue crack and with CAHs installed, the stresses in the web gap region were thoroughly studied. Initially, the condition with a 2.0 inch long original fatigue crack along the connection plate-to-web weld toe retrofit with 2.0 inch diameter CAHs was studied. Then a further parametric study with various original fatigue crack lengths and CAH diameters was completed, which is presented later. Skewed Mesh 3 was used to determine these stress results.

Stress at Edge of CAH

A plot of the MMPS around the circumference of the northeast (NE) CAH versus the angular measure from the bottom of the CAH on both the inside face (attached to the floor beam connection plate) and outside face of the girder web is shown in Figure 10. As the figure indicates, the largest MMPS of 5.0 ksi in tension occurs at an angle of 11 degrees at the edge of the inside web face (i.e., at the corner where the edge of the CAH meets the inside web face) and -8.3 ksi in compression occurs at an angle of 338 degrees at the edge of the outside web face. The CAH intersects the connection plate-to-web weld toe at 300 degrees with -2.0 ksi at the edge of the inside face and -3.5 ksi at the edge of the outside face. The locations of largest MMPS are not at the intersection of the edge of the CAH with the fillet weld toe (i.e., the *intersection point*). As shown in Figure 10, the MMPS near the bottom of the CAH from approximately 313 degrees to 107 degrees (passes through 360/0 degrees) at the edge of the inside web face is tensile, and at the edge of the outside web face is compressive, indicating out-of-plane bending response of the girder web (as the connection plate and web are pulled inward by the floor beam end rotation). The MMPS on the edge of the CAH is approximately 20% of the 24 ksi CAFL for AASHTO Fatigue Category A, the expected fatigue resistance of drilled holes with surface treated edges (e.g., grinding), so fatigue cracking is not expected at the edge of the CAH. Note that the fatigue resistance for the surface treated edge of the CAH is significantly larger than the fatigue resistance for the fillet weld toe (i.e., AASHTO Fatigue Category C).

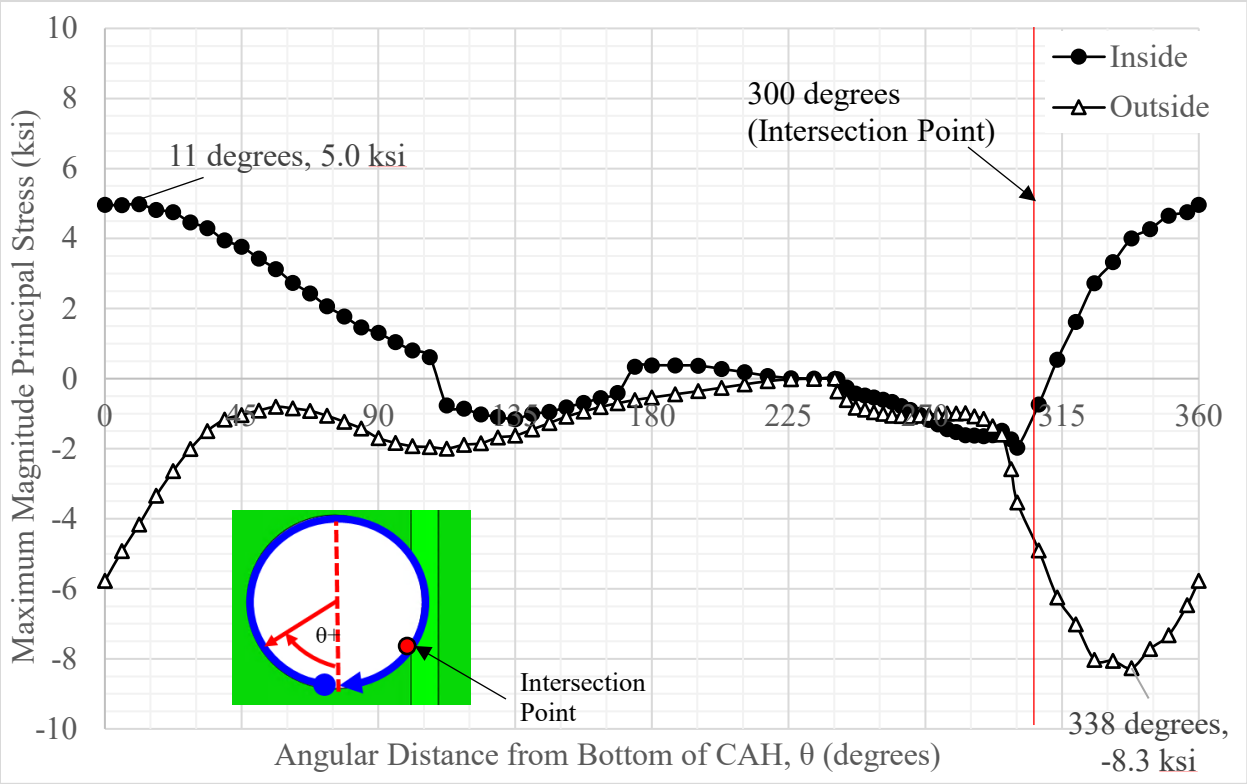

Figure 10. Maximum magnitude principal stress along edge of northeast CAH at inside and outside faces of girder web from Sub Model B4 using Skewed Mesh 3.

Variation of Stress Normal to Connection Plate-to-Web Weld with Distance along Weld

The variation with the distance along the weld of the stress normal to the connection plate-to-web weld toe (i.e., horizontal) on the inside face of the girder web was studied. The linearly extrapolated LSS, the single-point LSS, and FEA stress normal to the weld toe at distances of 0.4t and 1.0t from the weld toe versus the

distance along the connection plate-to-web weld measured from the intersection of the CAH edge with the fillet weld toe (i.e., the *intersection point*) are shown in Figure 11. Note, the distances of 0.4t and 1.0t away from the weld toe are the reference points for the linear extrapolation method using a relatively fine mesh (Hobbacher, 2016).

As shown in Figure 11, the linearly extrapolated LSS, single-point LSS, and FEA stresses vary similarly along the connection plate-to-web weld, with the largest stress at a short distance away from the intersection point which is approximately equal to 0.9 inch for a 2.0 inch long original fatigue crack with 2.0 inch diameter CAHs. FEA results presented later show that the distance to the location of largest stress from the intersection point increases with increasing CAH diameter. The magnitude of the linearly extrapolated LSS is close to the magnitude of the single-point LSS, indicating that the two methods provide comparable results. Note that stresses normal to the weld toe along the stiffener-to-web weld on the outside girder web face are in compression from out-of-plane bending of the web (as the connection plate and web move inward due to the floor beam end rotation).

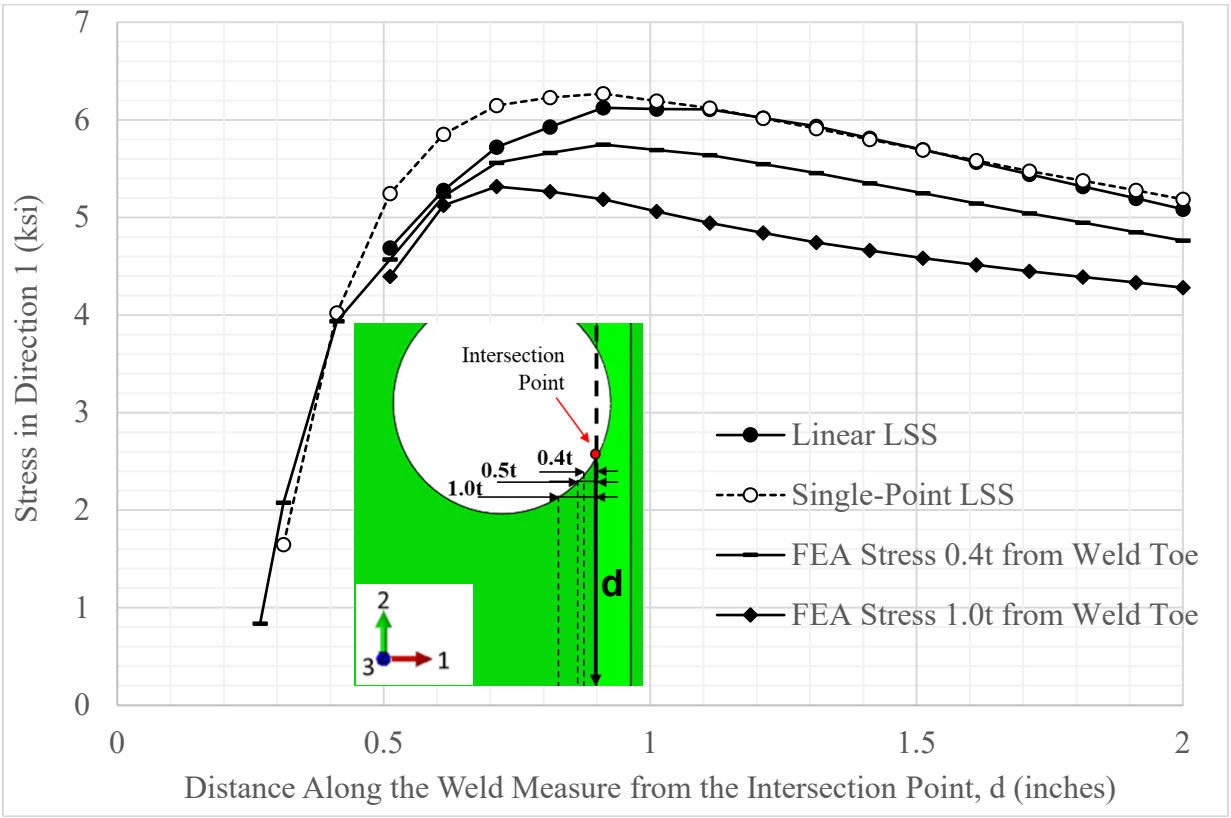

Figure 11. Linearly extrapolated LSS, single-point LSS, and 0.4t and 1.0t FEA (S11) stresses normal to connection plate-to-web weld on inside web face from Sub Model B4 using Skewed Mesh 3.

Variation of Stress Normal to Connection Plate-to-Web Weld with Distance in Perpendicular Direction from Weld

The variation of stress normal to the connection plate-to-web weld toe (i.e., horizontal) on the inside girder web face with the distance in the direction perpendicular to the weld was studied. The normal stresses were determined every 0.1 inch along a series of 1.5 inch long paths, with each path oriented perpendicular to the weld toe. The first path is located at the bottom edge of the CAH, which is 0.5 inch from the intersection point for the crack length of 2.0 inches and CAH diameter of 2.0 inches. Figure 12 shows the normal stresses

along Path 2 and Path 5, and the corresponding linear extrapolation of the LSS along each path. The largest linearly extrapolated LSS of 6.1 ksi occurs on Path 5 which is 0.4 inch away from the bottom of the CAH (approximately 0.9 inch from the intersection point). An observation from Figure 12 is that the stress gradient tends to be gradual near the weld toe, suggesting that the linear extrapolation method (Hobbacher, 2016) is suitable to determine the connection plate-to-web weld toe LSS, and that the quadratic extrapolation method (Hobbacher, 2016) is unnecessary.

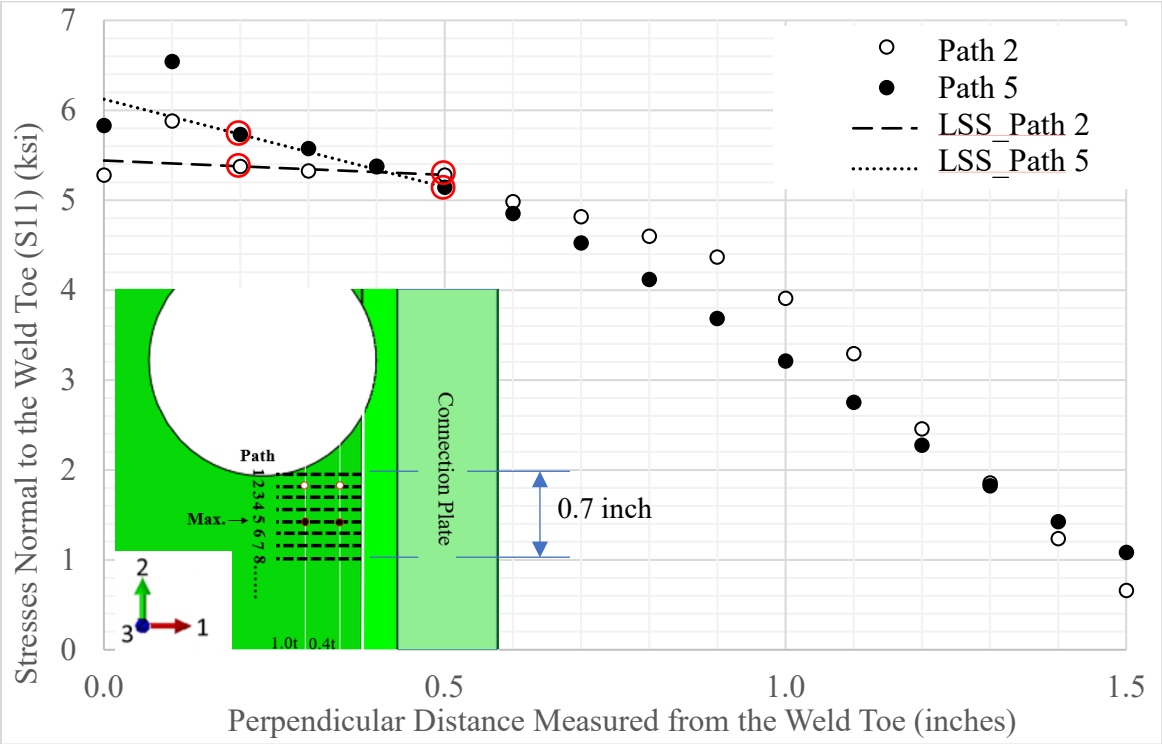

Figure 12. Stress normal to connection plate-to-web weld (S11) along select paths on inside web face from Sub Model B4 using Skewed Mesh 3 (circled stresses are used in LSS extrapolation).

Variation of Stress Normal to Connection Plate-to-Web Weld through Girder Web Thickness

Figure 13 shows the variation of stress normal to the weld (i.e., horizontal) through the thickness of the girder web at a (perpendicular) distance of 0.4t (i.e., 0.2 inch) away from the weld toe and at a distance 0.9 inch along the weld from the intersection point, the location of the largest linearly extrapolated LSS. As shown, the stress decreases linearly through the web thickness from 5.7 ksi in tension at the inside face of the girder web to -6.6 ksi in compression at the outside surface. The stress at the mid-thickness of the girder web plate is -0.4 ksi in compression. The stresses at the inside and outside faces of the web are similar in magnitude and opposite in sign, and the mid-thickness stress that develops is small in magnitude, demonstrating that the fatigue stress in the web gap region is dominated by out-of-plane bending of the girder web, and the stress due to primary (in-plane) bending of the girder web is insignificant.

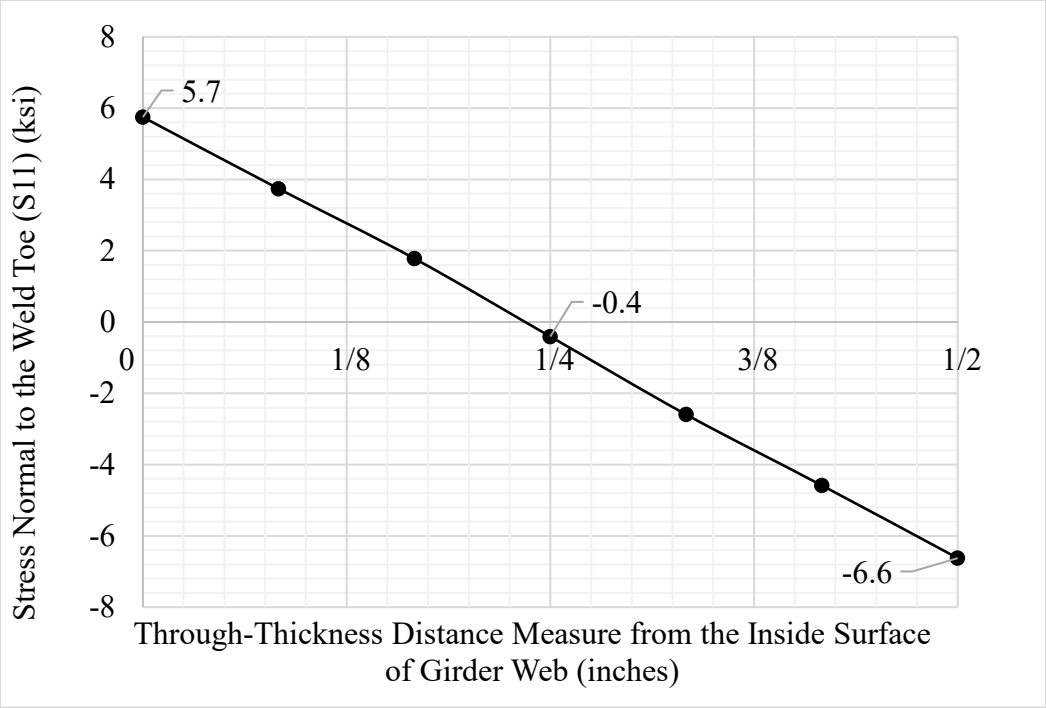

Figure 13. Stress normal to connection plate-to-web weld (S11) through girder web thickness from Sub Model B4 using Skewed Mesh 3.

Crack Length and CAH Size Effects

This section presents the parametric FEA studies in which the stress normal to the connection plate-to-web weld toe and the maximum magnitude principal stress at the edge of the CAH were evaluated for three different original crack lengths (i.e., 2.0 inches, 4.0 inches and 6.0 inches) and seven different CAH diameters ranging from 0.5 inch to 3.5 inches.

Figure 14 shows contour plots of the normal stress (S11) in the direction perpendicular to the weld (i.e., horizontal) on the inside face of the girder web from FEA for original fatigue crack lengths of 2.0 inches and 6.0 inches and CAH diameters of 0.5 inch, 1.0 inch, 2.0 inches and 3.0 inches. A comparison of the contour plots shows that for all four CAH diameters, the normal stress decreases as the crack length increases from 2.0 inches to 6.0 inches. Similarly, a comparison of the contour plots shows that increasing the CAH diameter results in decreases in the normal stress near the intersection of the CAH edge with the fillet weld toe.

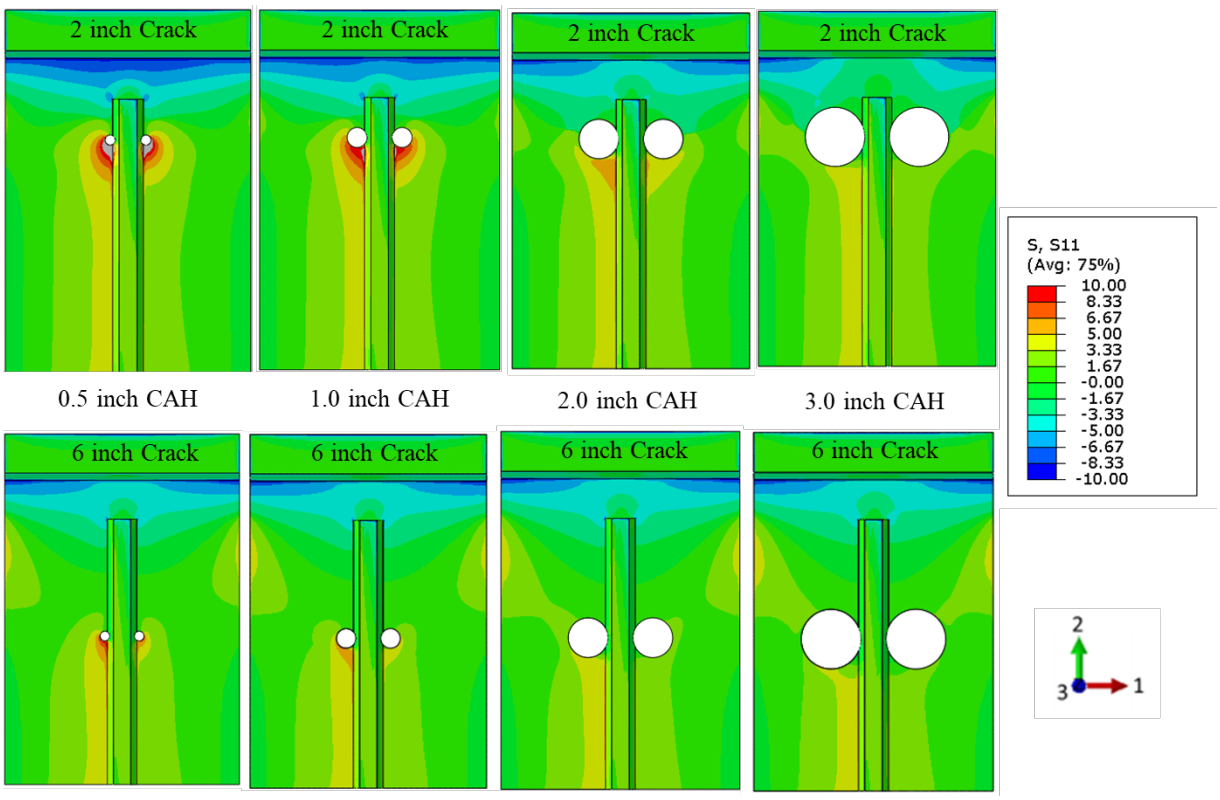

Figure 14. Contour plots of normal stress (S11) for select original fatigue crack lengths and CAH diameters on inside web face from Sub Model B4 using Skewed Mesh 3. (Note: Stress contours are presented with limits from -10 ksi to 10 ksi).

Figure 15 shows the variation of the largest MMPS at the edge of the CAH for various original fatigue crack lengths and CAH diameters. The largest MMPS is greatest for a 0.5 inch diameter CAH and a 2 inch original crack length, but is less than the 24 ksi CAFL for AASHTO Fatigue Category A for all the cases that were studied, therefore, fatigue cracks are not expected to initiate from the edge of the CAHs. Figure 16 shows the variation of the largest LSS (from the linear extrapolation method) along the connection plate-to-web weld for various original fatigue crack lengths and CAH diameters. The location of the largest LSS along the connection plate-to-web weld measured from the intersection point for various original fatigue crack lengths and CAH diameters is shown in Figure 17. These stress results are obtained from FEA of Sub Model B4 using Skewed Mesh 3.

Figure 15 and Figure 16 show that as the original fatigue crack length increases, both the largest MMPS on the CAH edge and the largest LSS at the weld toe decrease in magnitude. With a 2.0 inch long crack and a 1.0 inch diameter CAH, the largest MMPS and the largest LSS are 9.8 ksi and 11.2 ksi, respectively. With a 6.0 inch long crack and a 1.0 inch diameter CAH, the largest MMPS on the CAH edge and the largest LSS at the weld toe are 8.1 ksi and 6.0 ksi, respectively. These trends are inconsistent with the observation by (Liu, et al., 2018) that a longer original fatigue crack increases the stresses in the web gap region, and this inconsistency is explained as follows.

The stresses presented by (Liu, et al., 2018) were determined from FEA in which *constant amplitude forces* were applied to models of the web gap region as the original fatigue crack length and/or the CAH diameter were varied. The stresses presented in this report were determined from FEA in which *constant amplitude deformations*, determined from Sub Model A, were applied to detailed Sub Model B of the web gap region as the original fatigue crack length and/or the CAH diameter are varied. The *constant amplitude force*

approach of (Liu, et al., 2018) simulates an assumed condition in a typical two-girder bridge with floor beams and stringers, where the moment transferred between the end of the floor beam and the girder web (i.e., through the floor beam connection plate) does not change as the original local distortion-induced fatigue crack grows or when CAHs are installed. In this assumed condition, the increased flexibility of the web gap region from original fatigue crack growth or CAH installation does not decrease the moment at the end of the floor beam, which implies that the rotation of the end of the floor beam increases as the local flexibility increases. The *constant amplitude deformation* approach used here simulates an assumed condition in a typical two-girder bridge where the relative rotation between the end of the floor beam and the plane of the girder web does not change as the original local distortion-induced fatigue crack grows or when CAHs are installed. In this assumed condition, the increased flexibility of the web gap region from original fatigue crack growth or CAH installation does not increase the rotation at the end of the floor beam, which implies that the moment transferred between the end of the floor beam and the girder web decreases as the local flexibility increases. The *constant amplitude force* approach provides an upper bound and the *constant amplitude deformation* approach provides a lower bound to the web gap region stresses. When the amplitude of the floor beam end rotation is controlled by the flexural characteristics of the floor beam (i.e., the floor beam span and flexural stiffness), rather than the rotational restraint provided by the out-of-plane bending stiffness of the girder web, the *constant amplitude deformation* approach provides results that are close to the actual condition. In this work, we assume that the amplitude of the floor beam end rotation is controlled by the flexural characteristics of the floor beam, so the *constant amplitude deformation* approach is used herein.

Figure 15 and Figure 16 show that increasing the CAH diameter reduces the largest MMPS on the CAH edge and the largest LSS at the weld, regardless of original fatigue crack length. As the CAH diameter increases from 0.5 inch to 2.0 inches, the rate of decrease of the largest MMPS and the LSS is more pronounced than the rate of decrease as the CAH diameter increases from 2.0 inches to 3.5 inches. In addition, increasing the CAH diameter moves the location of the largest LSS farther from the intersection point, as shown in Figure 17. The figure shows that a CAH diameter in the range from 2.0 inches to 3.0 inches is effective in reducing stresses for various original fatigue crack lengths, and this CAH diameter range is recommended. This recommend CAH diameter range is within the recommended CAH diameter range of 2.0 to 4.0 inches by (Dexter & Ocel, 2013).

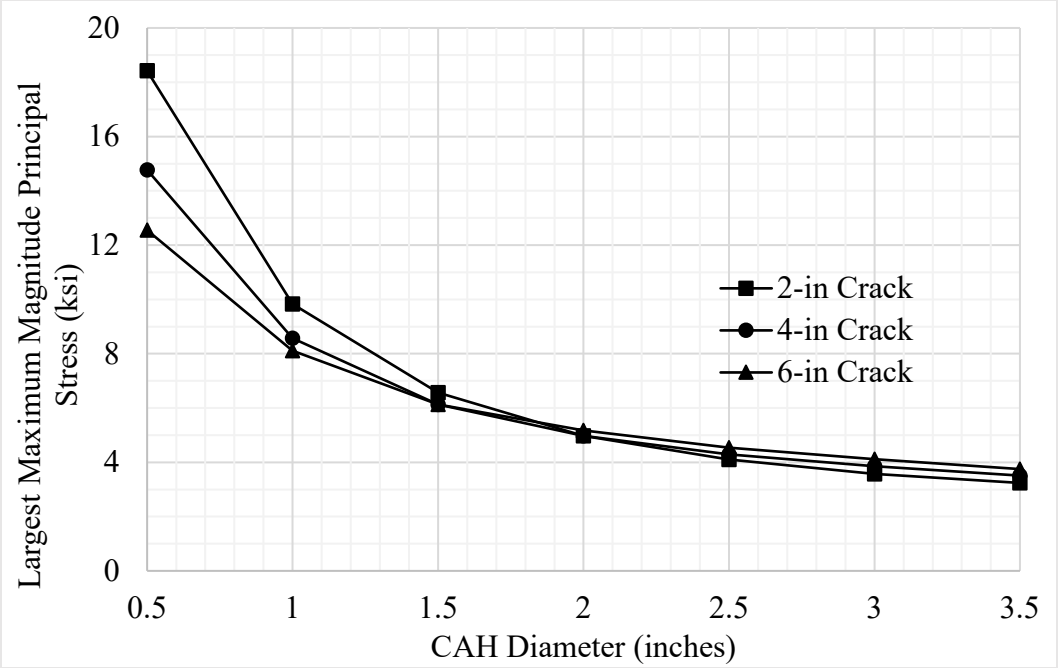

Figure 15. Largest maximum magnitude principal stresses on edge of CAH for various original fatigue crack lengths and CAH diameters from Sub Model B4 using Skewed Mesh 3.

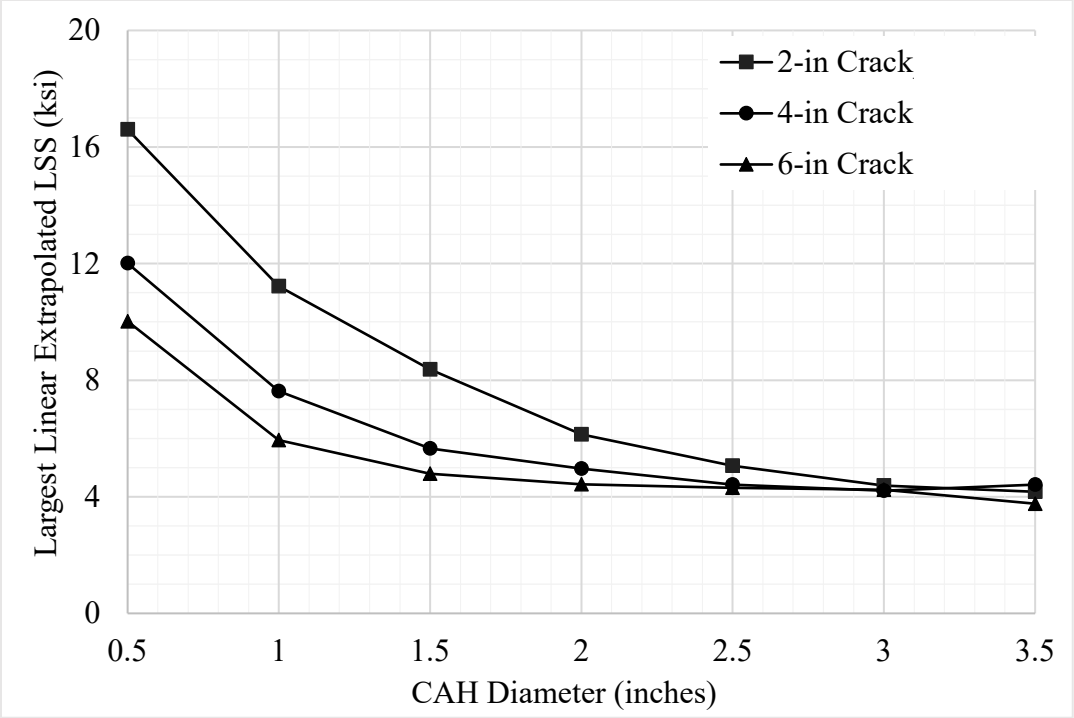

Figure 16. Largest LSS normal to connection plate-to-web weld on inside web face for various original fatigue crack lengths and CAH diameters from Sub Model B4 using Skewed Mesh 3.

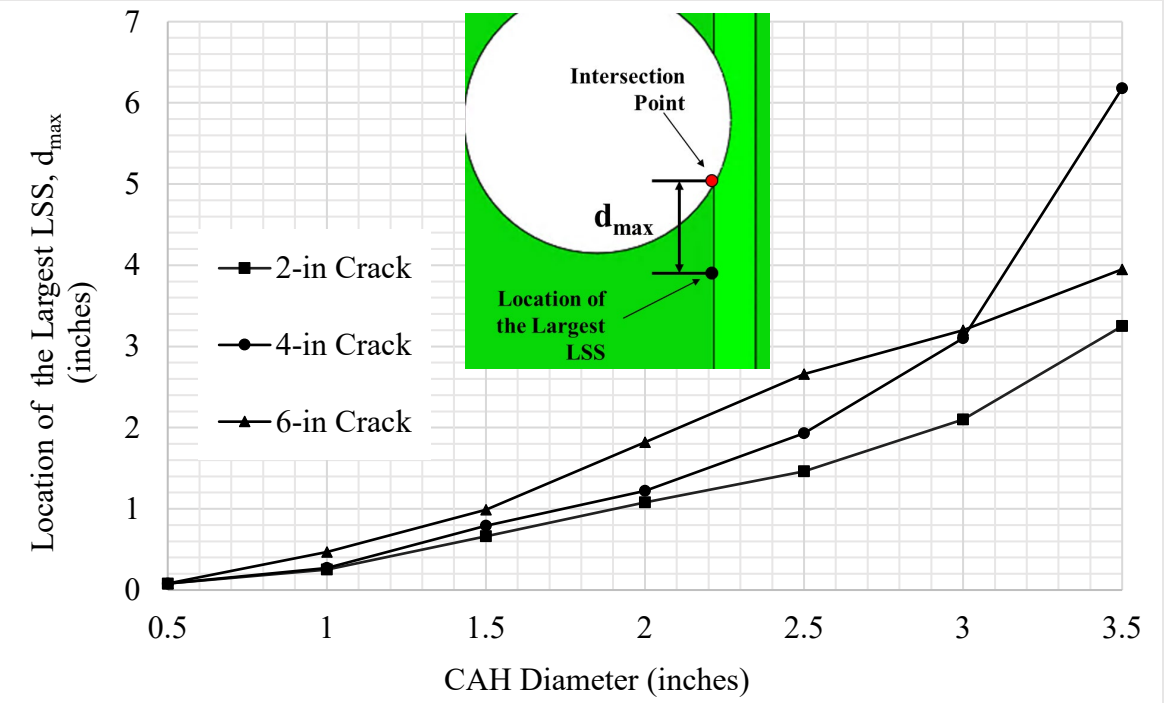

Figure 17. Location of largest LSS normal to connection plate-to-web weld measured from intersection point, d_{max}, for various original fatigue crack lengths and CAH diameters from Sub Model B4 using Skewed Mesh 3.

STUDY OF MESH CHARACERISTICS

A study of the effects of mesh refinement and mesh configuration on the FEA stress results for a fatigue-damaged web gap region with CAHs was performed using Sub Model B4. Four different levels of mesh refinement and two mesh configurations were studied. The largest MMPS at the edge of the CAH, and the weld toe LSS, determined by linear extrapolation and by quadratic extrapolation, as well as the single-point weld toe LSS were compared.

Levels of Mesh Refinement

FEA using Sub Model B4 with four different levels of mesh refinement and a uniform mesh configuration was used to study the effect of mesh refinement on the stresses at the connection plate-to-web weld toe. The largest nodal FEA stress at the weld toe, the largest linearly extrapolated LSS, the largest quadratic extrapolated LSS, and the largest single-point LSS obtained using Uniform Mesh 1 through 4 are plotted against a normalized mesh size in Figure 18. The normalized mesh size parameter is introduced to quantify the different mesh sizes considered in the mesh refinement study. The normalized mesh size is calculated for elements near the weld toe, and is the product of the two adjacent element edge lengths divided by the element thickness squared. For example, for Mesh 3, the normalized mesh size equals 0.4t times 0.4t divided by t^2, which is 0.16. In Figure 18 the normalized mesh size is plotted on a reversed log scale on the horizontal axis.

As shown in Figure 18, as the mesh is refined, the largest nodal FEA stress at the weld toe increases without convergence as a result of a zero-radius notch at the weld toe. The linearly extrapolated LSS converges using Mesh 3 with a magnitude of 6.1 ksi. The linearly extrapolated LSS is 6.5 ksi and 6.6 ksi using Mesh 1 and Mesh 2, respectively, slightly larger than the converged value of 6.1 ksi. The quadratic extrapolated LSS decreases as the mesh is refined from Mesh 2 to Mesh 3, and then increases from Mesh 3 to Mesh 4.

As discussed previously, the stress gradient near the weld toe is gradual (see Figure 12), therefore, the quadratic extrapolation method is not necessary for evaluating the fillet weld toe stress. The single-point LSS converges using Mesh 3, with a magnitude of 6.3 ksi. The single-point LSS is 6.6 ksi and 6.2 ksi using Mesh 1 and Mesh 2, respectively. The converged linearly extrapolated LSS and the single-point LSS are within 3.2% of each other, suggesting that either method may be appropriate for assessing the fillet weld toe fatigue performance. Although a relatively coarse mesh, corresponding to Uniform Mesh 1 (1.0t x 1.0t) and a fine mesh corresponding to Uniform Mesh 2 (0.4t x 1.0t) are recommended in (Hobbacher, 2016), Uniform Mesh 3 (0.4t x 0.4t), which meets the requirements for a relatively fine mesh (Hobbacher, 2016) was widely used in the present study since refinement to the level of Mesh 3 produces converged linear extrapolated LSS and requires less modeling effort.

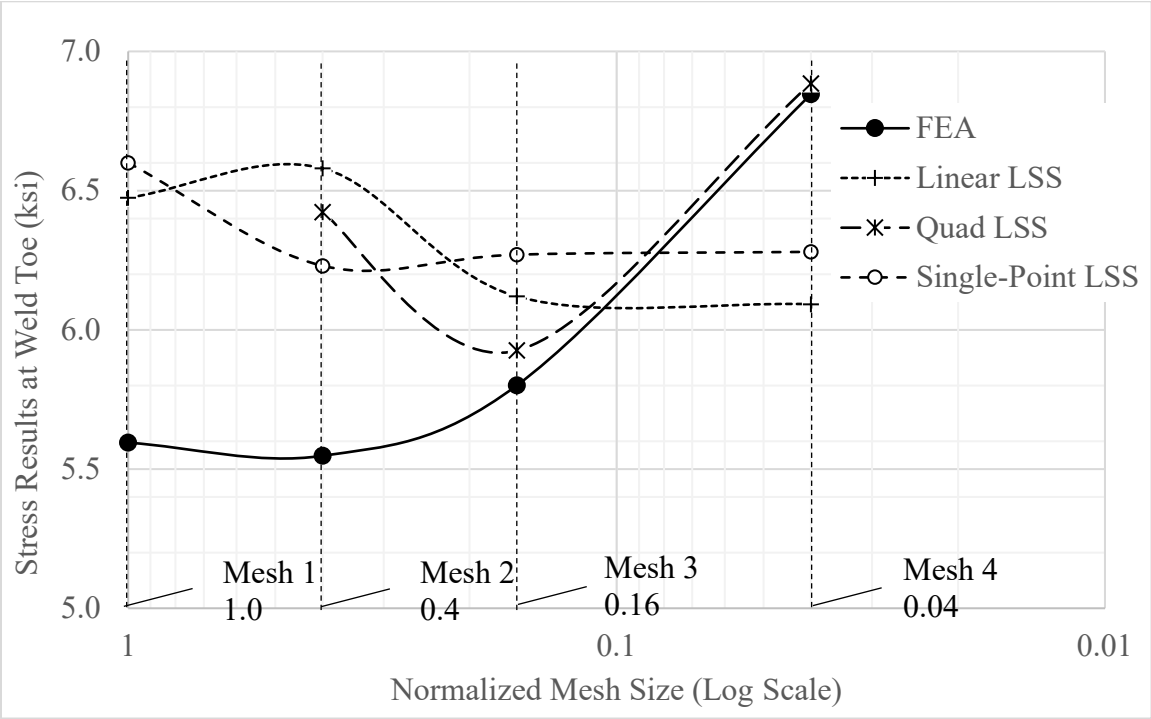

Figure 18. Largest FEA stress, linearly extrapolated LSS, quadratic extrapolated LSS, and single-point LSS at fillet weld toe as Sub Model B4 mesh is refined from Uniform Mesh 1 through 4 with 2.0 inch crack and 2.0 inch diameter CAHs.

Mesh Configuration

FEA using Sub Model B4 with two different mesh configurations, a Uniform Mesh and Skewed Mesh, were used to study the effect of the mesh configuration on the stresses. The models included a 2.0 inch long original fatigue crack, and three CAH diameters, 1.0, 2.0, and 3.0 inches were considered. As discussed in Chapter 2, the Uniform Mesh elements near the connection plate-to-web fillet weld are cuboid in shape, while a Skewed Mesh has some elements near the weld toe that are trapezohedral or skewed, with corner angles that vary from 90 degrees, due to the presence of the CAHs. In a Uniform Mesh, the reference points used to extrapolate the LSS at the weld toe coincide with nodes in the mesh, so the stresses used to extrapolate the LSS are nodal stresses. In a Skewed Mesh, the reference points may not coincide with the nodes, so the reference point stresses are interpolated from the nodal stresses from adjacent nodes using the shape factor for the specified element by ABAQUS (Dassault Systemes Simulia Corp., 2016). Note that the nodal stresses themselves are calculated in ABAQUS by extrapolating from analytically exact stresses at the integration points.

The largest linearly extrapolated LSS at the weld toe from Uniform and Skewed Mesh 1 and from Uniform and Skewed Mesh 3 is summarized in Table 2 and Table 3, respectively. The largest quadratic extrapolated LSS at the weld toe from Uniform and Skewed Mesh 3 is summarized in Table 4. The largest MMPS at the edge of the CAH from Uniform and Skewed Mesh 1 and from Uniform and Skewed Mesh 3 is summarized in Table 5 and Table 6, respectively. This minimum element skew angle for each Skewed Mesh is shown in the tables. The minimum element skew angle is the minimum angle between two adjacent faces in an element used for extrapolation of the LSS, which ranges from 0 to 90 degrees. A smaller minimum element skew angle indicates the elements are more distorted (or less cuboid). As the CAH diameter increases, the minimum element skew angle in the Skewed Mesh decreases, resulting in more distorted elements near the connection plate-to-web weld. The minimum skew angle for the elements used for extrapolation of the LSS in the Uniform Mesh is 90 degrees.

The difference between the FEA results from the Skewed Mesh and the Uniform Mesh is included in the tables, given as a percentage, where a negative sign indicates the result from the Skewed Mesh is smaller than result from the Uniform Mesh. For the Mesh 1 level of refinement, the average absolute difference in the largest linearly extrapolated LSS from Table 2 is 5.2%, and the average absolute difference in the largest MMPS at the edge of the CAH from Table 5 is 6.4%.

Using Mesh 3, the average absolute difference in the largest linearly extrapolated LSS, the largest quadratic extrapolated LSS, and the largest MMPS on the CAH edge is 0.6%, 1.0%, and 1.0%, from Table 3, Table 4, Table 6, respectively. These results indicate that at the Mesh 3 level of mesh refinement, the distortion of the elements in a Skewed Mesh has inconsequential effect on the stresses.

In summary, the mesh refinement and mesh configuration studies indicate that for an FEA model with a sufficiently-refined mesh, such as Mesh 3, the differences in the largest linearly extrapolated LSS, the largest quadratic extrapolated LSS, and the largest MMPS on the CAH edge between the Uniform Mesh and Skewed Mesh are small. Therefore, either mesh configuration can be used in a sufficiently-refined mesh to determine these stresses.

Table 2. Largest linearly extrapolated weld toe LSS from Sub Model B4 with Uniform Mesh and Skewed Mesh using Mesh 1 (1.0t x 1.0t) for 2.0 inch long crack.

CAH Diameter (inches)	Minimum Element Skew Angle (degrees)	Largest LSS, Uniform Mesh (ksi)	Largest LSS, Skewed Mesh (ksi)	% Difference
1.0	81	11.70	11.28	-3.6%
2.0	47	6.54	7.18	9.8%
3.0	40	4.41	4.51	2.3%

Table 3. Largest linearly extrapolated weld toe LSS from Sub Model B4 with Uniform Mesh and Skewed Mesh using Mesh 3 (0.4t x 0.4t) for 2.0 inch long crack.

CAH Diameter (inches)	Minimum Element Skew Angle (degrees)	Largest LSS, Uniform Mesh (ksi)	Largest LSS, Skewed Mesh (ksi)	% Difference
1.0	68	11.25	11.23	-0.2%
2.0	40	6.12	6.14	0.3%
3.0	35	4.18	4.24	1.4%

Table 4. Largest quadratic extrapolated weld toe LSS from Sub Model B4 with Uniform Mesh and Skewed Mesh using Mesh 3 (0.4t x 0.4t) for 2.0 inch long crack.

CAH Diameter (inches)	Minimum Element Skew Angle (degrees)	Largest LSS, Uniform Mesh (ksi)	Largest LSS, Skewed Mesh (ksi)	% Difference
1.0	68	11.11	11.20	0.8%
2.0	40	5.93	5.96	0.5%
3.0	35	4.13	4.20	1.7%

Table 5. Largest maximum magnitude principal stress at edge of CAH from Sub Model B4 with Uniform Mesh and Skewed Mesh using Mesh 1 (1.0t x 1.0t) for 2.0 inch long crack.

CAH Diameter (inches)	Minimum Element Skew Angle (degrees)	Largest CAH edge MMPS, Uniform Mesh (ksi)	Largest CAH edge MMPS, Skewed Mesh (ksi)	% Difference
1.0	81	11.96	10.65	-11.0%
2.0	47	5.67	5.39	-4.9%
3.0	40	4.23	4.09	-3.3%

Table 6. Largest maximum magnitude principal stress at edge of CAH from Sub Model B4 with Uniform Mesh and Skewed Mesh using Mesh 3 (0.4t x 0.4t) for 2.0 inch long crack.

CAH Diameter (inches)	Minimum Element Skew Angle (degrees)	Largest CAH edge MMPS, Uniform Mesh (ksi)	Largest CAH edge MMPS, Skewed Mesh (ksi)	% Difference
1.0	68	10.00	9.83	-1.7%
2.0	40	5.00	4.98	-0.4%
3.0	35	4.15	4.11	-1.0%

CHAPTER 4

Fatigue Test Design and Analysis

Fillet-welded test specimens with crack-like features and CAHs were designed and fabricated, and subjected to cyclic loading laboratory fatigue tests. These test specimens were tested to validate the use of FEA and the linear extrapolation method for LSS, discussed in Chapter 2 and Chapter 3, to evaluate the potential for fatigue cracking of the floor beam connection plate-to-web weld toe after CAHs are installed. The test specimens are designed to simulate a condition where CAHs are installed to retrofit an original fatigue crack that initiated at the top edge of the floor beam connection plate-to-web weld and propagated vertically along the weld toe. The test specimens were subjected to plate bending to simulate the out-of-plane bending deformation of the girder web in the web gap region caused by floor beam end rotations in a typical two-girder bridge with the deck supported by floor beams and stringers.

Before conducting the fatigue tests, 3D linear-elastic FEA studies were performed to design the test specimens. The loading and boundary conditions were designed to replicate the stress conditions observed in the FEA studies of the web gap region with an original fatigue crack retrofit with CAHs, as described in Chapter 3. FEA stress results for the test specimens are compared to the estimated stress range results (calculated from the measured strains) from the fatigue tests. The linear extrapolation method for determining the LSS is used to assess the fatigue performance of the test specimens, using both the FEA and fatigue test results. The linear extrapolation method was selected used due to its widespread use, extensive documentation, and ease of implementation.

The test specimen properties were varied parametrically, with different crack-like features simulating different original crack lengths and different CAH diameters included in the set of test specimens. The fatigue performance of the test specimens was assessed by the potential for fatigue cracking at the fillet weld toe near the CAHs.

FEA OF TEST SPECIMENS

3D linear-elastic FEA was used to design the test specimens. The test specimen FEA results were compared to FEA results presented in Chapter 3 from the parametric study of the web gap region of the two-girder steel bridge with CAHs installed to retrofit an original fatigue crack propagating vertically along the floor beam connection plate-to-web fillet weld toe. The test specimens were designed so the position of the largest linearly extrapolated LSS along the weld toe, and the length of the weld toe with LSS equal to 95% (or more) of the largest LSS are similar to those from FEA of Sub Model B presented in Chapter 3.

Overview of FEA Model

The test specimens were designed to simulate a distortion-induced fatigue crack propagating vertically along a connection plate-to-web fillet weld toe, driven by out-of-plane bending deformation of the girder web and retrofit with CAHs. As shown in Figure 19, the test specimen includes two transverse stiffeners fillet welded a primary 1/2 inch thick, 24.0 inch long plate. Two test specimen widths (6.0 and 11.75 inches), two original crack lengths (2.0 and 4.0 inches), and two CAH diameters (2.0 and 2.5 inches) were

considered. In a study by (Campbell, et al., 2019), distortion-induced fatigue cracks with a length of 2.0 inches and 4.0 inches were detected by a random bridge inspector approximately 50% and 99% of the time, respectively. Considering these original crack lengths in the test program enables these crack lengths to be associated with a reasonable probability of detection during a bridge inspection. The two CAH diameters (2.0 and 2.5 inches) are within the recommended CAH diameter range of 2.0 to 4.0 inches (Dexter & Ocel, 2013). These CAH diameters are also within the recommended CAH diameter range of 2.0 to 3.0 inches to reduce the stress on the CAH edge and the LSS weld toe stress as determined from the FEA parametric study of Sub Model B presented in Chapter 3.

Similar to Sub Model B used in the FEA studies presented in Chapter 3, the fillet welds in the test specimens were modeled with a simple geometry, with a 5/16 inch leg and a zero-radius notch at each weld toe. The unfused strip and the fit-up gap at the fillet weld root were not modelled. One CAH was centered on each of the crack-like features in the test specimen and each CAH was located so that it penetrates the fillet weld by 1/8 inch. The crack-like feature along the weld toe is modeled as a seam in the FEA model, which lies in a plane perpendicular to the length of the test specimen as shown in Figure 20.

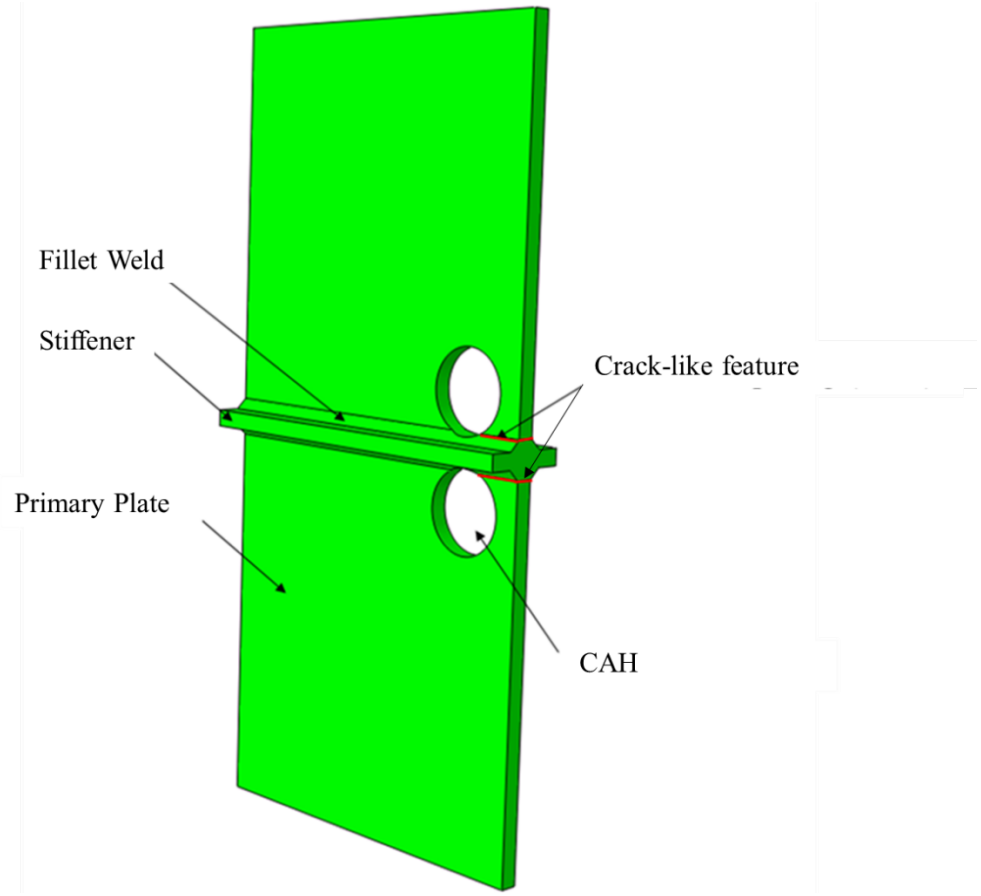

Figure 19. FEA model of 11.75 inch wide test specimen with 2.0 inch long crack-like features and with 2.5 inch diameter CAHs.

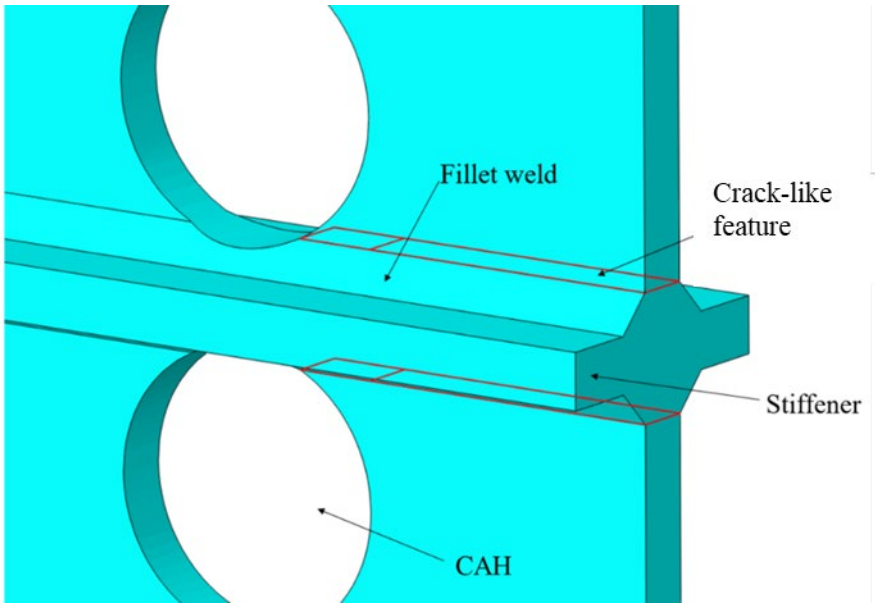

Figure 20. Test specimen FEA model highlighting seams to model crack-like features.

Boundary and Loading Conditions

Boundary and loading conditions for the test specimens were chosen to simulate the out-of-plane bending behavior of the girder web that will drive a distortion-induced fatigue crack propagating vertically along a connection plate-to-web fillet weld toe, as discussed in Chapter 3. The test specimens are simply supported with a span of 16.0 inches as shown in Figure 21. At the pin support, the three translational degrees of freedom are restrained. At the roller support, only the Z-direction translational degree of freedom is restrained. In the FEA model, the pin and roller supports are modeled by restraining a line of nodes across the full test specimen width. Downward pressure loads are applied at the center of the stiffener over a 1/2 inch by 3.0 inch area to produce bending in the test specimen. The loads are applied in two steps. During the first step, a minimum load is applied. During the second step, a load range is applied, simulating a sequence of loading that is used in the laboratory fatigue tests (as discussed later).

There is no reversal of stress under this loading sequence. Accordingly, near each fillet weld on the bottom face of the primary plate (see Figure 21), the loading condition produces a fully tensile stress range, and near each fillet weld on the top face of the primary plate, the loading condition produces a fully compressive stress range. Compression stress is considered to contribute to fatigue damage only if a net tension stress develops at the same location at some time during a loading cycle (AASHTO, 2018). Therefore, fatigue cracks are not expected near the fillet welds on top face of the primary plate during the fatigue tests since a fatigue crack which could develop at the fillet weld toe due to the effects of residual tensile stress from welding are not expected to propagate beyond the heat-affected zone under a fully compressive stress range (AASHTO, 2018).

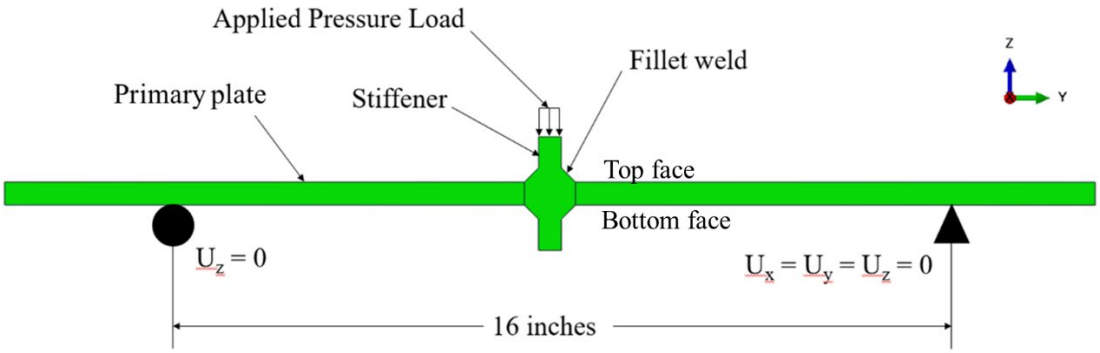

Figure 21. Elevation of FEA model with boundary conditions.

Element Type and Mesh

The test specimens were modeled using 20-node solid quadratic hexahedral elements with reduced integration. The FEA used Uniform Mesh 3 (see Chapter 2) with average element dimensions of 0.4t x 0.4t (where t is the thickness of the test specimen primary plate) was used. A representative test specimen FEA mesh is shown in Figure 22.

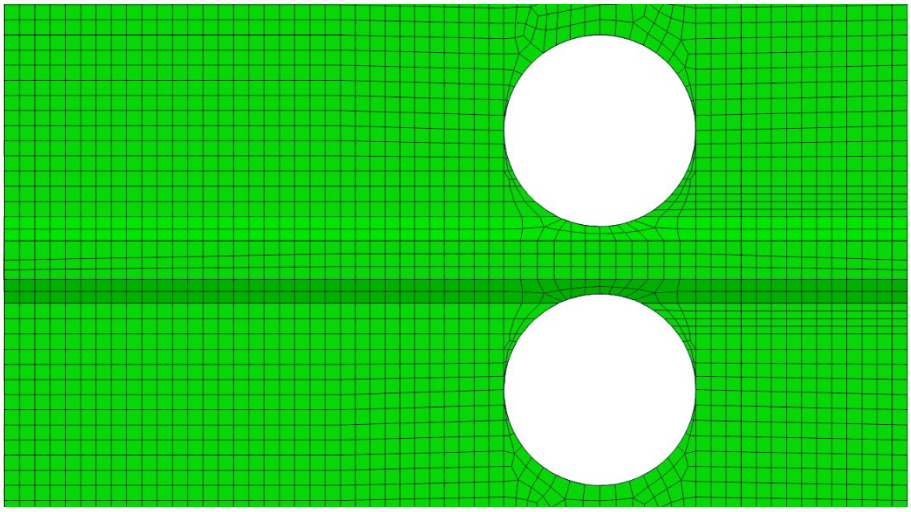

Figure 22. Test specimen FEA model with Uniform Mesh 3 with 4.0 inch long crack-like features and 2.5 inch diameter CAHs.

Comparison of Results with Sub Model B

Test specimen FEA results are compared with Sub Model B FEA results from Chapter 3, to assess the similarity of bending in the test specimen relative to out-of-plane bending of a girder web after CAH retrofit of a connection plate-to-web weld toe fatigue crack. To compare the FEA results from the two models, the linearly extrapolated LSS along the length of the weld toe, starting at the intersection of the CAH and fillet weld toe, was calculated from the results for the test specimen model. Since the loading amplitude in the FEA of the test specimen is arbitrary, the locations of the largest LSS and the length over which a large LSS (95% of the largest LSS) occurs are the results from FEA that are compared. The magnitudes of the largest LSS are not compared.

The location of the largest linearly extrapolated LSS along the weld toe, measured from the CAH edge, as shown in Figure 23, is denoted $L_{Max\text{-}LSS}$. The length of the weld toe with LSS greater than or equal to 95% of the largest LSS is denoted $L_{95\%}$, as shown in Figure 23. $L_{Max\text{-}LSS}$ and $L_{95\%}$ from the test specimen FEA are compared with these results from the Sub Model B FEA results. $L_{Max\text{-}LSS}$ represents a single approximate location where a fatigue crack is likely to initiate. Note in the Sub Model B FEA results presented previously in Figure 11, the location of the largest linearly extrapolated LSS was measured from the intersection of the weld toe and the CAH (i.e., from the *intersection point*). To be comparable with the results from FEA of the test specimens, values of $L_{Max\text{-}LSS}$ for Sub Model B are calculated from the edge of the CAH. $L_{95\%}$, provides an approximate weld toe length where fatigue cracking is expected to be initially observed. As $L_{95\%}$ increases, the likelihood that a crack-initiating weld toe discontinuity is contained within this length increases. Figure 23 shows a plot of the LSS at the weld toe as a function of the distance along the weld toe measured from the CAH edge from the test specimen FEA. The distances $L_{Max\text{-}LSS}$ and $L_{95\%}$ are shown in the figure.

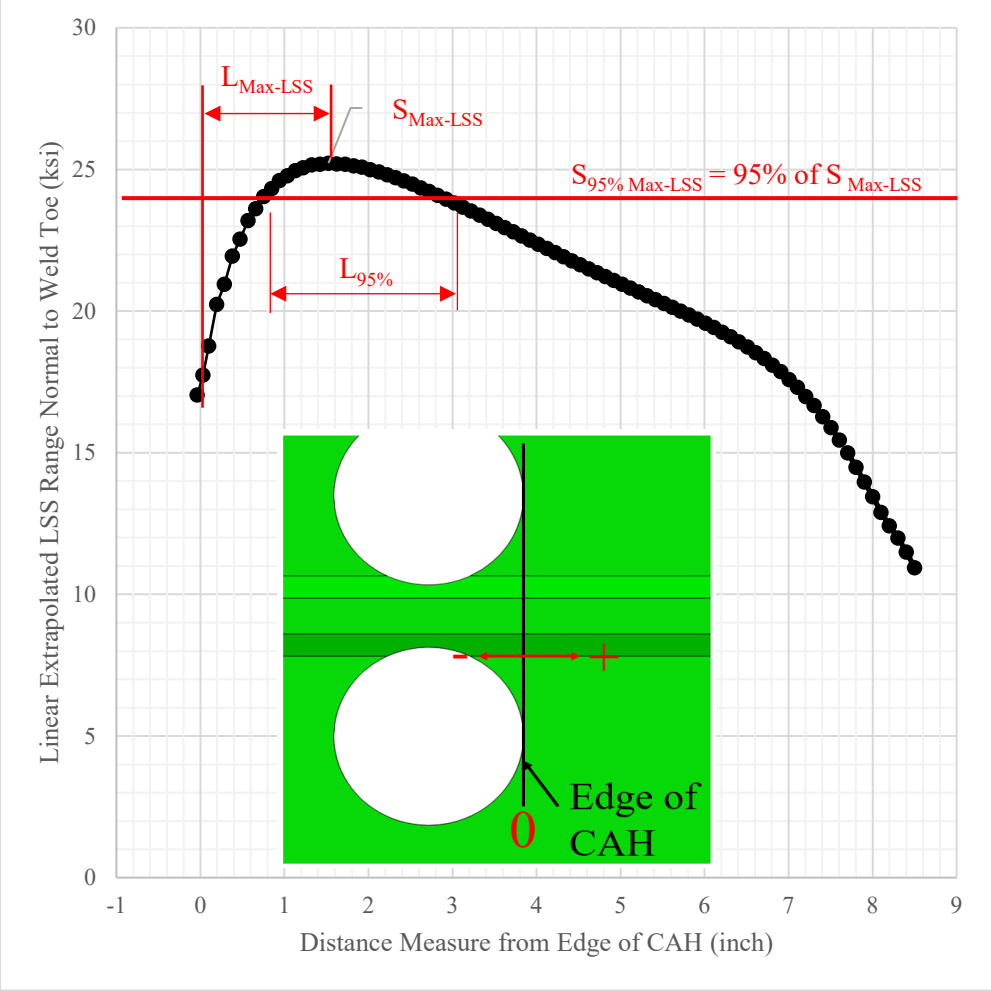

Figure 23. Variation of linearly extrapolated LSS normal to weld toe as a function of distance along weld toe from edge of CAH for test specimen with 2.0 inch long crack-like feature and 2.5 inch diameter CAH from FEA of test specimen with Uniform Mesh 3.

Table 7 summarizes $L_{Max\text{-}LSS}$ and $L_{95\%}$ for the test specimens and for Sub Model B with different original fatigue crack (i.e., crack-like feature) lengths and CAH diameters from FEA using Uniform Mesh 3.

Comparing the test specimen and Sub Model B results, the largest differences in $L_{Max\text{-}LSS}$ and $L_{95\%}$ are 0.88 inch and 1.50 inches, respectively. Generally, $L_{Max\text{-}LSS}$ and $L_{95\%}$ have similar magnitudes in the test specimen and Sub Model B FEA results (with the results for the test specimens as much as 206% larger than and 52% smaller than the results from Sub Model B). The results suggest that the bending of the test specimens is similar to the out-of-plane bending of a girder web after CAH retrofit of a connection plate-to-web weld toe fatigue crack, although for some combinations of original crack length and CAH diameter, $L_{95\%}$ is significantly different for the test specimens.

Table 7. Comparison of $L_{Max\text{-}LSS}$ and $L_{95\%}$ for test specimen and Sub Model B, for various test specimen widths, crack lengths, and CAH diameters from FEA with Uniform Mesh 3.

Fatigue Crack or Crack-like Feature Length (inch)	CAH Diameter (inch)	Test Specimen Width (inch)	$L_{Max\ LSS}$, Test Specimen (inch)	$L_{Max\ LSS}$, Sub Model B (inch)	$L_{95\%}$, Test Specimen (inch)	$L_{95\%}$, Sub Model B (inch)
2.0	2.0	6.0	0.94	0.50	1.03	0.65
2.0	2.5	6.0	0.83	0.75	1.02	1.05
2.0	2.0	11.75	1.38	0.50	1.99	0.65
2.0	2.5	11.75	1.53	0.75	2.18	1.05
4.0	2.0	11.75	0.99	0.70	1.29	1.15
4.0	2.5	11.75	0.97	1.35	1.35	2.85

CYCLIC LOADING FATIGUE TESTS

Based on FEA results for the test specimens, 11.75 inch wide specimens with 2.0 inch and 4.0 inch long crack-like features, and with 2.0 inch and 2.5 inch diameter CAHs were selected for the cyclic loading laboratory fatigue tests. A test setup with test fixtures, instrumentation, and a servo-hydraulic loading system was designed and assembled in the laboratory. The test specimens and test setup were regularly inspected during the fatigue tests to identify fatigue cracks or unexpected damage to the test fixtures.

Test Specimens

The test specimens shown in Figure 24 are comprised of a 1/2 inch thick (2 foot long) primary plate, with two fillet-welded (1/2 inch thick, 1 inch wide) transverse stiffeners (one on each side of the primary plate), with two crack-like features, and with two CAHs. To avoid having fillet weld starts and stops within the test specimens, fabrication of the specimens started by continuously welding two 20 foot long (1/2 inch thick, 1 inch wide) stiffeners to a 20 foot wide (1/2 inch thick, 2 foot long) primary plate, using the submerged-arc-welding (SAW) process. The primary plate was grade 50 steel plate. The fillet welds had nominal 5/16 inch legs. Multiple 11.75 inch wide test specimens (without weld starts or stops) were saw-cut from this 20 feet wide plate with welded stiffeners.

Each 11.75 inch wide test specimen had 2.0 inch or 4.0 inch long crack-like features that were saw-cut through the thickness of the primary plate using a band saw along the fillet weld toe on each side of the stiffeners. Then, 2.0 inch or 2.5 inch diameter CAHs were drilled using a carbide-tipped hole saw, centered on the tip of the crack-like feature and penetrating the fillet weld by 1/8 inch. One 9/16 inch pin hole was drilled at the location of each bearing, to maintain the position of the test specimen with respect to the bearings in the test setup. The cut edge of each CAH was surface finished with a 120 grit flapper wheel as commonly specified for CAH retrofits. The 120 grit is finer than the 80-100 grit recommended by (Dexter

& Ocel, 2013). This surface finishing of the CAH was performed to help avoid crack initiation from the edge of the CAHs.

The test matrix for the fatigue tests is in Table 8. The 16 test specimens include four specimens for each combination of crack-like feature length and CAH diameter. The test specimens were tested with three target stress ranges for the largest linearly extrapolated LSS equal to 25 ksi, 30 ksi, and 40 ksi. These target stress range values are within the range of constant amplitude cyclic stress ranges in previous fatigue tests used to develop the finite-life fatigue resistance for a transverse non-load carrying fillet weld (ECCS, TC6, 2018).

As shown in the table, the specimens have the following naming convention: Welding Process (WP) - Nominal Specimen Width (TT) - Target LSS Range (XX) - Crack-like Feature Length (VV) - CAH diameter (YY) - Specimen Identifier (Z). For example, a submerged-arc-welded (SAW) test specimen which has a width of 11.75 inches, a target LSS range of 25 ksi, 2.0 inch long crack-like features, and 2.0 inch diameter CAHs, and is tested on the north side of the test setup in the lab (as discussed later) is named SAW-12-25-2-2-N.

Two test specimens were tested simultaneously in the test setup. However, due to uncertainty or variability in the fatigue resistance, the two specimens were not expected to crack at the same number of cycles even when the applied stress range is the same for the two specimens. To ensure continuous operation of the cyclic loading fatigue tests in a test setup designed for two specimens, two spare specimens were fabricated. During the fatigue tests, if one test specimen cracked earlier than the other, a spare specimen was installed and tested together with remaining uncracked specimen. The spare specimens have the same overall dimensions as the test specimens (see Figure 25), but the crack-like features and CAHs were omitted, and a single stiffener was flux-core arc welded (FCAW) to the top of the primary plate to receive the applied load.

Table 8. Cyclic loading laboratory fatigue test matrix.

Test Specimen Name	No. of Specimens	Test Specimen Width (inch)	Target LSS Range (ksi)	Crack-like Feature Length (inch)	CAH Diameter (inch)
SAW-12-25-2-2.5-Z	2	11.75	25	2.0	2.5
SAW-12-25-4-2.5-Z	2	11.75	25	4.0	2.5
SAW-12-25-2-2-Z	2	11.75	25	2.0	2.0
SAW-12-25-4-2-Z	2	11.75	25	4.0	2.0
SAW-12-30-2-2.5-Z	2	11.75	30	2.0	2.5
SAW-12-30-4-2-Z	2	11.75	30	4.0	2.0
SAW-12-40-2-2-Z	2	11.75	40	2.0	2.0
SAW-12-40-4-2.5-Z	2	11.75	40	4.0	2.5

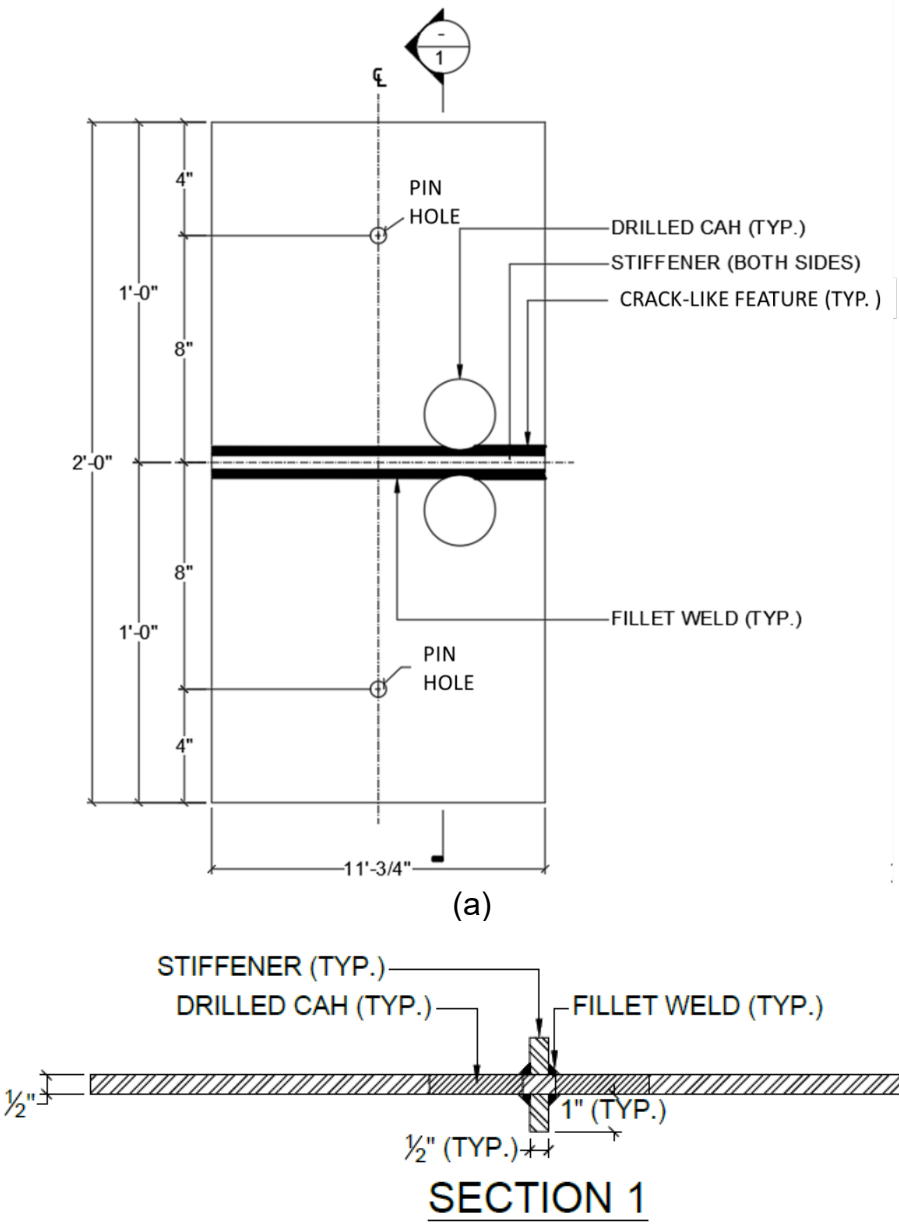

Figure 24. Fatigue test specimen (a) elevation view; (b) section view.

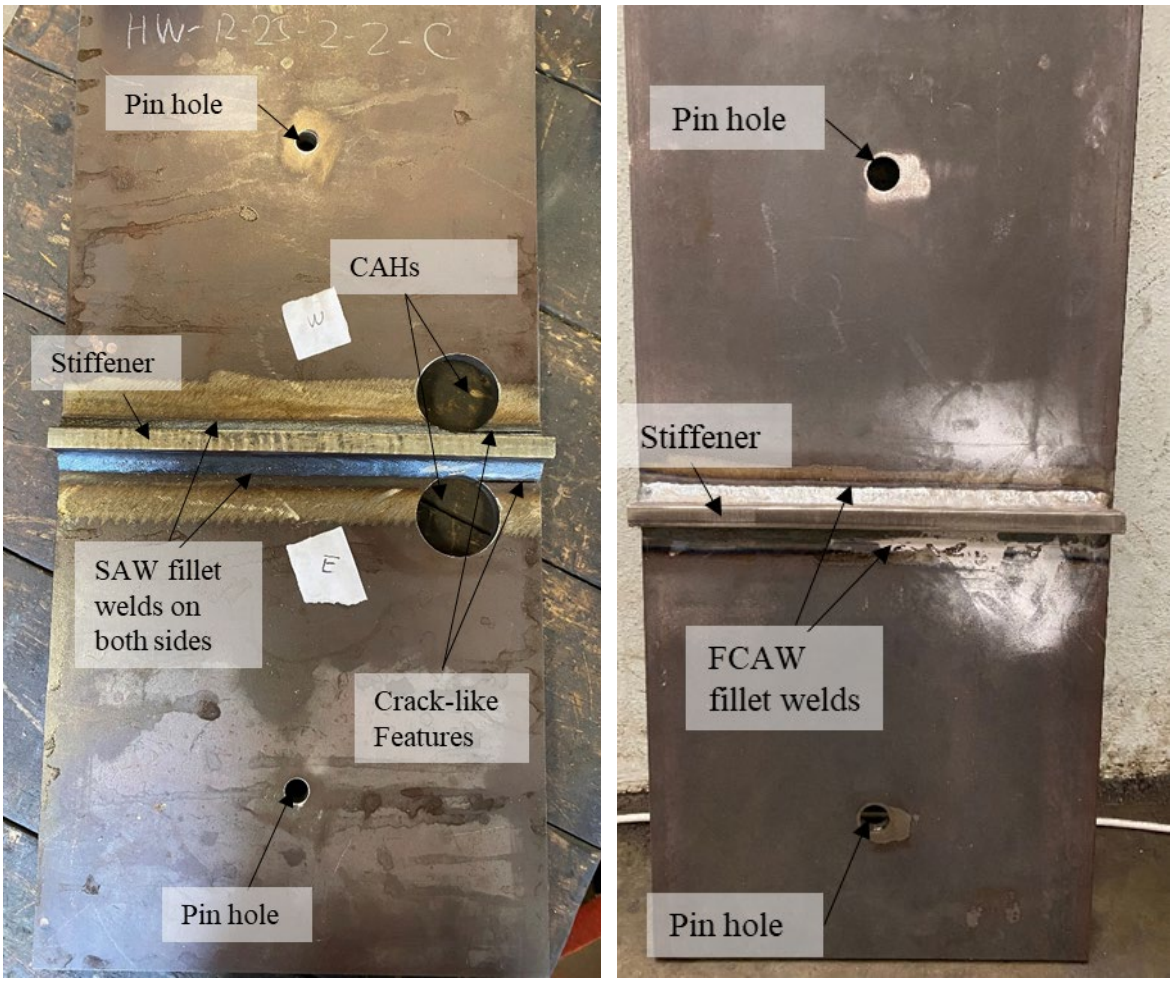

Figure 25. Photo of (a) Test Specimen; (b) Spare Specimen.

Test Setup

The fatigue tests used the setup in the Multi-Directional Experimental Laboratory at the ATLSS Engineering Research Center depicted in Figure 26. Two specimens were tested simultaneously in this test setup which was located near the southwest corner of the laboratory on the strong floor. Loads were applied using a 12 kip MTS hydraulic actuator (model 204.23), which was mounted to a test fixture and included a reaction beam that spanned between two W12xt190 reaction columns. The reaction beam was comprised of two W12x190 stacked flange-to-flange and bolted together, and supported on stiffened brackets bolted to the reaction columns. Lateral bracing was installed between the reaction columns and the laboratory strong wall.

As shown in Figure 27 and Figure 28, a load cell was mounted to the end of the actuator. The load cell was connected to a clevis that was bolted to a spreader beam, which equally divided the load between the two test specimens. The spreader beam was comprised of two L3x3x1/2 angles and was pinned to loading tees at each end which loaded the stiffeners of the specimens over a transverse length of 3 inches. The tees were notched to match the stiffener thickness of the specimens, maintaining the position of the loading tee with respect to the test specimen. Two layers of rosin paper were inserted in the notches between the specimens and loading tees to help evenly distribute the applied load.

The specimens were centered between steel bearings. A fixed bearing was located at one end and a rocker bearing was located at the other end. At each bearing, the rotation of the specimen about the bearing axis is intended to be unrestrained. A 1/2 inch diameter vertical pin was installed at each bearing, to prevent movement of the specimens during cyclic loading, and these pins passed through the 9/16 inch pin holes in the test specimens. The bearings were bolted to a test fixture that included steel pedestals clamped to the strong floor. To ensure the specimens remained in contact with the bearings during cyclic loading, several layers of rosin paper were inserted in gaps between the specimens and bearings when required.

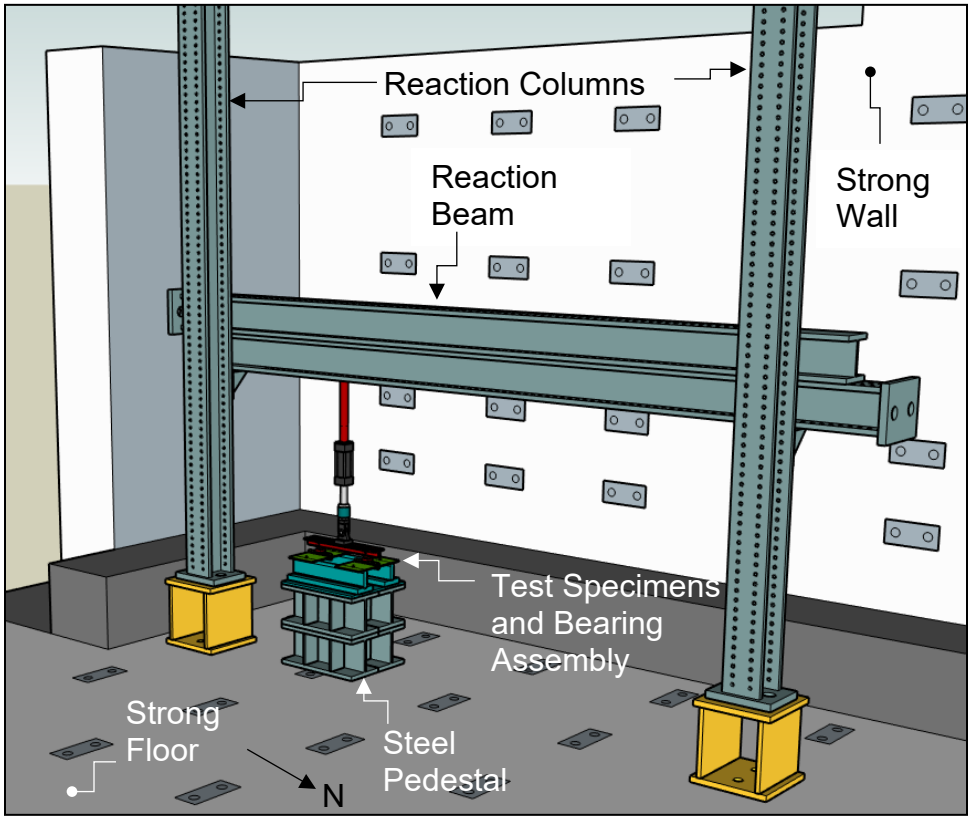

Figure 26. Overview of test setup used for fatigue tests near southwest corner of Multi-Directional Experimental Laboratory strong floor.

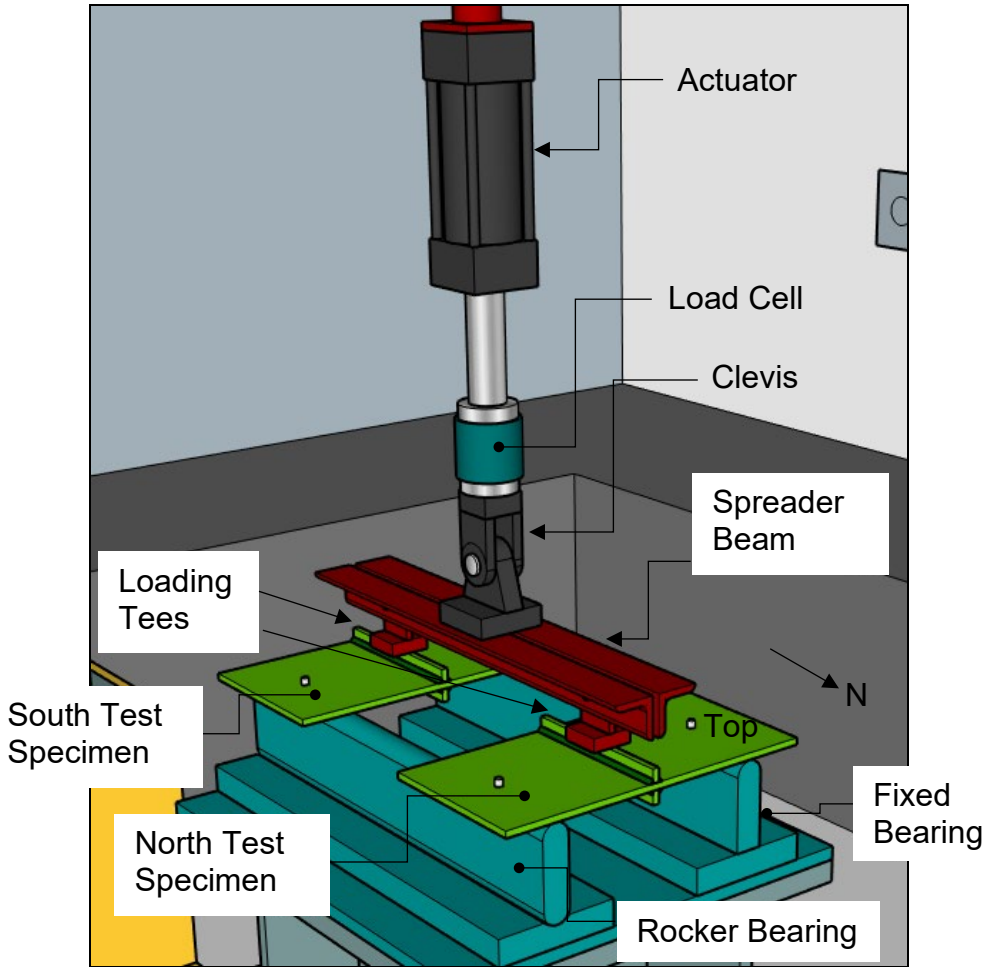

Figure 27. Test setup with specimens for cyclic loading laboratory fatigue tests.

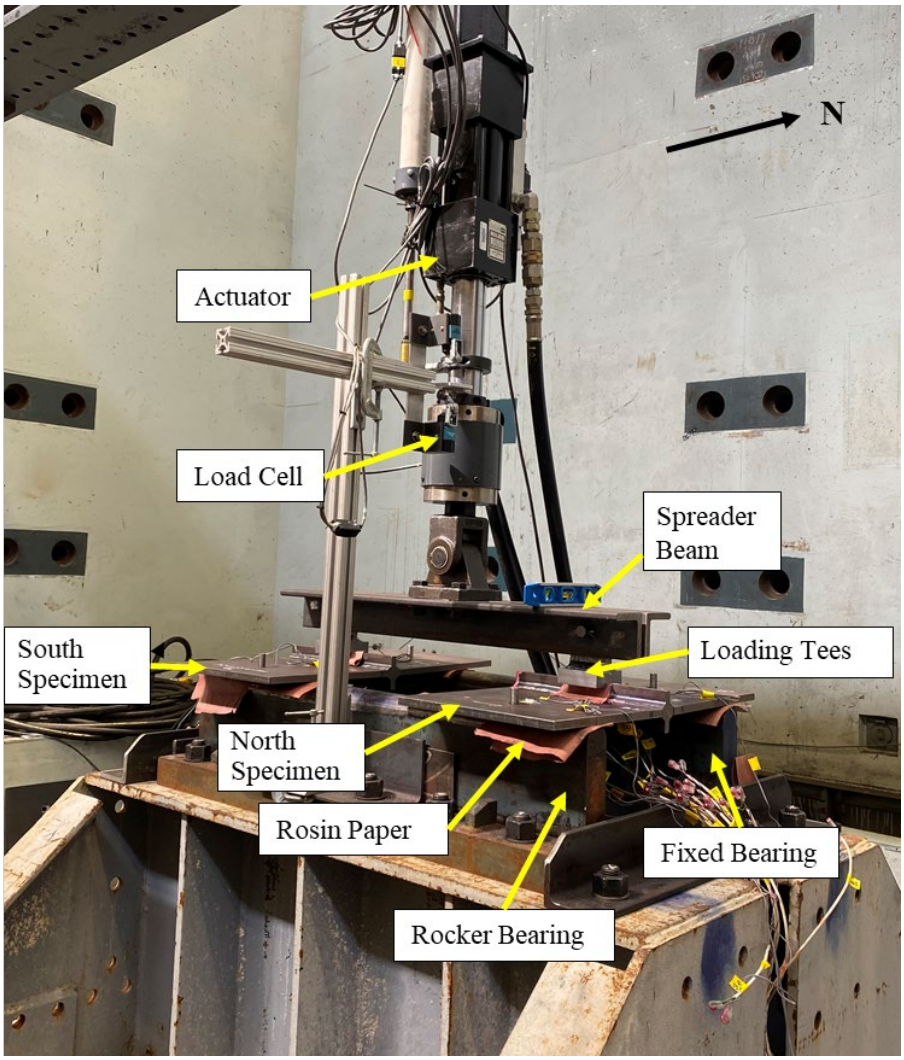

Figure 28. Photo of test setup during fatigue tests.

Control System and Loading Protocol

Loads were applied to the test specimens using a hydraulic actuator controlled with an MTS FlexTest servo-hydraulic control system (see Figure 29). The actuator was operated in "force control" using a sinusoidal time-varying force profile. An initial force P_{min} (i.e., the "minimum load") was applied by the actuator to ensure that the specimens remain in firm contact with the bearings. A second force P_R (i.e., the "load range") was applied cyclically by the actuator using the sinusoidal time-varying force profile. P_{min} and P_R were determined via FEA and adjusted during the tests to generate the target LSS range at the toe of each fillet weld. Note that the largest principal stress at the weld toe of the test specimen, determined by FEA from the sum of P_{min} and P_R, was maintained to be less than 50 ksi which is the yield stress for the grade 50 steel primary plate of the test specimen. The magnitudes of the adjusted P_{min} and P_R used during the cyclic loading fatigue tests for each test specimen are shown in Table 9. As shown in Table 9, the magnitude of P_R depends on the crack-like feature length and the target LSS range.

The hydraulic control system was programmed with error limits for the force and stroke displacement of the actuator. If either of the force or displacement error limits was exceeded (indicating a problem with the test specimen, test setup, or hydraulic loading system), the control system was programmed to immediately

stop the test. In addition, two physical emergency stop switches were placed near the test setup to enable a test to be stopped manually. Cycle counting during the cyclic loading was performed by the control system. The cyclic loading frequency was 6 Hz when the tests were run during the daytime and 4 Hz when the tests were run overnight.

Figure 29. MTS FlexTest control system.

Table 9. Cyclic loading protocol used for laboratory fatigue tests.

Test Specimen Name	Crack-like Feature Length (inch)	Target LSS Range (ksi)	Minimum Force, P_{min} (kips)	Force Range, P_R (kips)
SAW-12-25-2-2.5-Z	2.0	25	0.4	2.4
SAW-12-25-4-2.5-Z	4.0	25	0.4	1.7
SAW-12-25-2-2-Z	2.0	25	0.4	2.4
SAW-12-25-4-2-Z	4.0	25	0.4	1.7
SAW-12-30-2-2.5-Z	2.0	30	0.4	2.8
SAW-12-30-4-2-Z	4.0	30	0.4	2.0
SAW-12-40-2-2-Z	2.0	40	0.4	3.6
SAW-12-40-4-2.5-Z	4.0	40	0.4	2.6

Inspection Protocol and Data Acquisition System

During the fatigue tests, regular inspection of the test specimens, test fixtures, and hydraulic actuator/loading system was performed to identify fatigue cracks in the test specimens and unintended response of the test setup. The inspections were performed every 50,000 cycles (+/- 10,000 cycles). Inspection logs were maintained to record the date, time, cycle number, inspector(s), control system force and displacement, and observations at each inspection. A paper copy of the log was kept in the laboratory, and a digital copy of the log was also maintained.

The toes of the fillet welds that were subjected to tensile stresses are on the bottom face of the primary plate of the test specimen, which was not readily accessible for unassisted visual inspection. Multiple inspection tools were used during the visual inspections as shown in Figure 30. Visual inspections used an inspection mirror and bright lighting from portable lights with flexible goose-neck mounts. When necessary, an aerosol degreaser was sprayed on a suspected crack location to more easily observe evidence of crack opening and closing under cyclic loading. One live camera was installed underneath each specimen to monitor specimens during cyclic loading, however, fatigue crack identification relied on visual inspections and strain gage data (discussed later), since the resolution of the live cameras was not sufficient to enable weld toe cracks to be observed.

Two Campbell Scientific CR9000 data loggers were used to record strains gage data, displacement data, and applied forces during the cyclic loading fatigue tests (see Figure 31). One data logger was assigned to each of the two test specimens being tested simultaneously. The data logger assigned to the north test specimen was configured with one CR9050 analog input card and three CR9052 filter cards for a total of 16 channels. The data logger assigned to the south test specimen was configured with one CR9050 analog input card and two CR9052 filter cards for a total of 14 channels. The CR9050 analog card was used to record force/ displacement data from the hydraulic control system, and the CR9052 filter card was used to record measured strains from the strain gages on the test specimens. The strain gages were utilized in a quarter Wheatstone-bridge configuration.

The data loggers were programmed to record a 60 second time-history of measured data every hour on the hour at a sampling rate of 200 Hz during each cyclic loading fatigue test. In addition, strain-range spectra were calculated for each strain gage during each fatigue test via the rainflow cycle-counting algorithm (Downing & Socie, 1982) every 15 minutes using the 200 Hz time-history data from the previous 15 minute period. The recorded hourly strain time-history data and the rainflow strain-range spectra data were used to monitor the fatigue response of the test specimens. As described later, reductions in the measured strain ranges near the weld toes were used as an early indication of fatigue cracking, before the fatigue cracks could be observed visually.

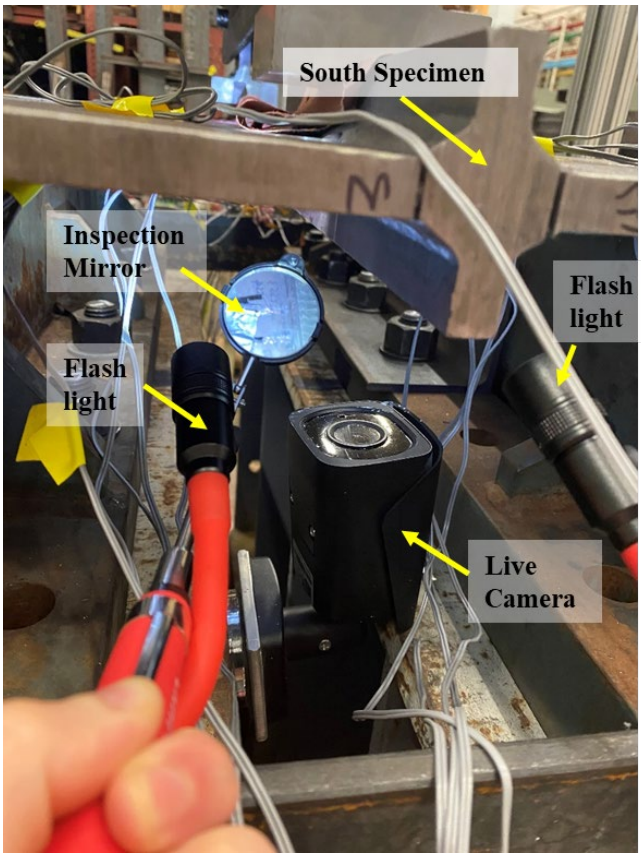

Figure 30. Inspection tools.

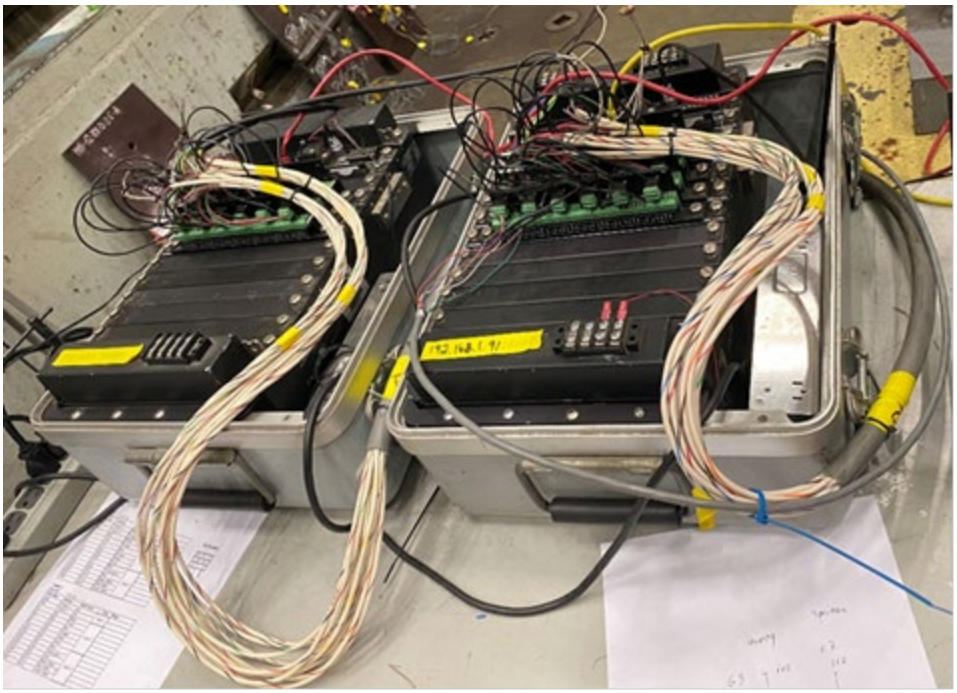

Figure 31. Campbell Scientific CR9000 data acquisition systems.

Instrumentation

Based on FEA results, an instrumentation plan was developed to measure strains and estimate the stress response of the test specimens. Strain gages were installed on the primary plate surfaces as shown in Figure 32 to measure strains used to estimate the stresses needed to calculate the LSS at the fillet weld toes using the linear extrapolation method. These gages were bondable uniaxial gages manufactured by Tokyo Measuring Instruments Laboratory, Co. Ltd., with 1 mm (model FLA1-11) gage lengths. In addition, 6 mm long uniaxial gages (Tokyo Measuring Instruments Laboratory, Co. Ltd., model FLA-6-11) were installed in a "back-to-back" configuration on opposite faces of the plate to measure relative contributions of membrane and bending strains at locations away from the weld toes. Additional 1 mm long strain gages were used to measure strains on the CAH edges.

The locations and names for the strain gages are shown in Figure 32. Strain gage names in parenthesis denote gages installed on the primary plate face subjected to a compressive stress range (on the top face of the specimen as installed in the test setup), which is opposite to the face shown in the figure. The four 6 mm gages on the plate surface are identified as G1 through G4. These gages were installed mid-width and 6 inches from the ends of the test specimens. The gages normal to the fillet weld toe are identified as LSS1 through LSS8. These 1 mm long gages were installed on the primary plate face subjected to tensile stress ranges (bottom face of the specimen as installed in the test setup). The LSS gages were installed at distances from the fillet weld toe that are consistent with the linear extrapolation LSS method. The first gage nearest to the weld toe was located 0.4t (nominally 0.2 inches) from the weld toe, and a second gage was located 1.0t (nominally 0.5 inch) from the weld toe. Gages LSS1, LSS2, LSS5 and LSS6 were installed a distance away from the edge of the CAH similar to $L_{Max\text{-}LSS}$ determined from the FEA of the test specimen. $L_{Max\text{-}LSS}$ from the FEA and the nominal location of these gages are given in Table 10 for each test specimen. Gages LSS3, LSS4, LSS7 and LSS8 were installed an additional 1 inch farther from the edge of the CAH.

Additional 1 mm gages, identified as Edge1 and Edge2 were installed at the edges of the two CAHs for 7 selected specimens. These edge gages were positioned at the side of CAH away from the crack-like feature as shown in Figure 32a, where the MMPS occurs in FEA results for the test specimen. The edge gages were installed on the CAH edge as close as possible to the face of the primary plate which is in tension. A photo showing the CAH edge gage and its location is presented in Figure 33. Table 11 gives the distance from the center of the edge gage to the corner where the CAH edge meets the tension face of the primary plate as measured with a caliper, for each specimen with edge gages.

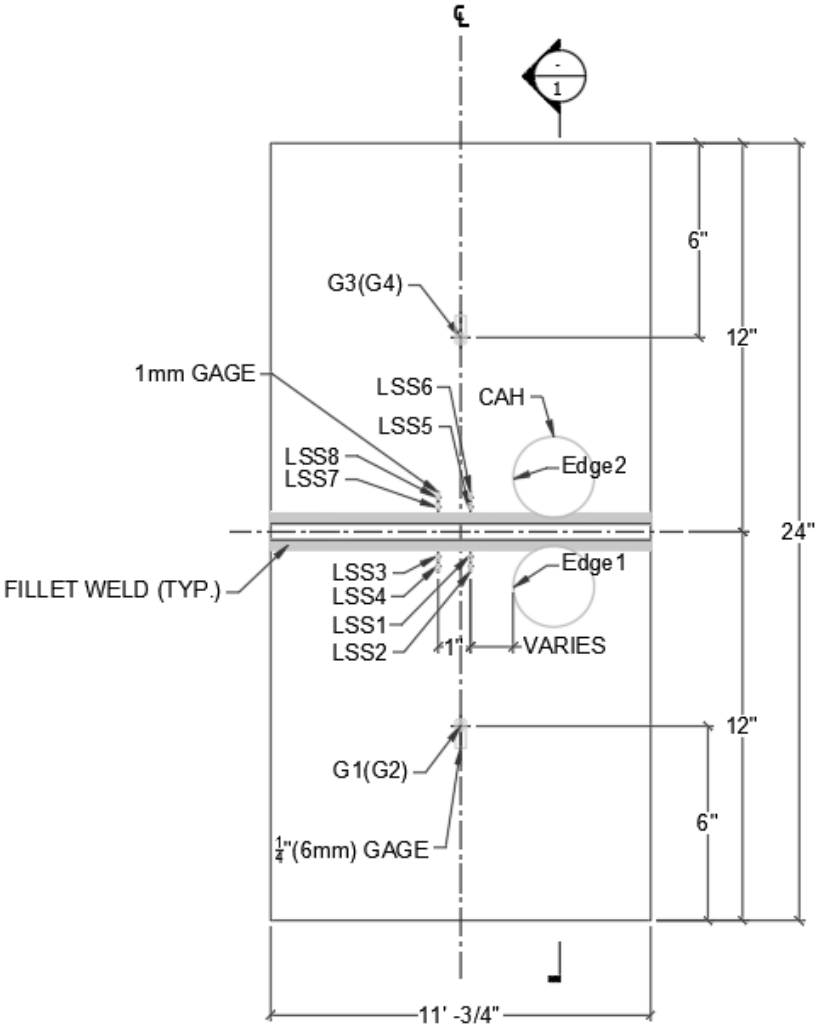

(a)

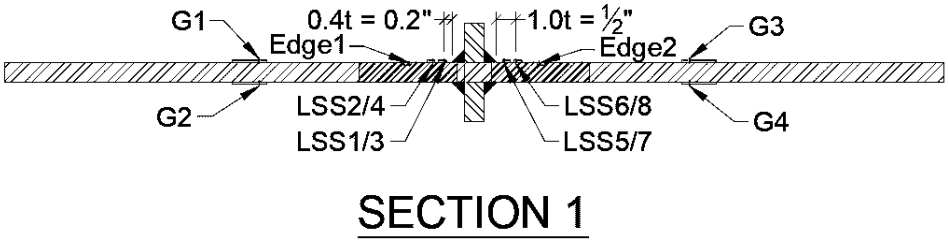

(b)

Figure 32. (a) Strain gage names; (b) Section view with LSS gage dimensions.

Table 10. Nominal gage locations for gages LSS1, LSS2, LSS5, and LSS6.

Test Specimen Name	$L_{Max\text{-}LSS}$ from FEA (inch)	Nominal Gage Location from Edge of CAH (inch)
SAW-12-25-2-2.5-Z	1.53	1.5
SAW-12-25-4-2.5-Z	0.97	1.0
SAW-12-25-2-2-Z	1.38	1.375
SAW-12-25-4-2-Z	0.99	1.0
SAW-12-30-2-2.5-Z	1.53	1.5
SAW-12-30-4-2-Z	0.99	1.0
SAW-12-40-2-2-Z	1.38	1.375
SAW-12-40-4-2.5-Z	0.97	1.0

Figure 33. Edge of east CAH with edge gage installed for specimen SAW-12-25-4-2-N.

Table 11. Measured edge gage locations for various specimens.

Test Specimen Name	Gage Name	Gage Location Relative to Stiffener	Gage Location from Corner of CAH (inch)
SAW-12-25-4-2.5-S	Edge1	West	0.058
SAW-12-25-4-2.5-S	Edge2	East	0.067
SAW-12-25-2-2-N	Edge1	West	0.092
SAW-12-25-2-2-N	Edge2	East	0.080
SAW-12-25-4-2-N	Edge1	West	0.049
SAW-12-25-4-2-N	Edge2	East	0.048
SAW-12-30-2-2.5-N	Edge1	West	0.066
SAW-12-30-2-2.5-N	Edge2	East	0.076
SAW-12-30-4-2-N	Edge1	West	0.074
SAW-12-30-4-2-N	Edge2	East	0.065
SAW-12-40-2-2-N	Edge1	West	0.048
SAW-12-40-4-2.5-N	Edge1	West	0.074
SAW-12-40-4-2.5-N	Edge2	East	0.084

Measurement of Strain and Estimation of Stress Ranges

As mentioned above, a 60 second time-history of measured strain data was recorded every hour during the cyclic loading fatigue tests. From this data, for each hour of cyclic loading, a stress range was determined for each strain gage as follows.

An hourly average measured strain range was calculated by subtracting the average minimum strain from the average maximum strain for the 60 second time-history of data. The 60 second time-history includes 360 cycles during daytime loading at 6 Hz and 240 cycles during overnight loading at 4 Hz. Then these hourly average measured strain range values were averaged to determine the average measured strain range for the test.

The stress range for a test was estimated from the average measured strain range for each strain gage assuming a plane stress condition (i.e., the through-thickness stress is zero). An element in axial tension with transverse deformation restraint (or with an applied transverse stress) is in a biaxial stress state. In this case, the axial stress is a function of the axial strain, the transverse strain, Poisson's ratio, and the elastic modulus. For the test specimens subjected to plate bending, the axial tension stress varies through the primary plate thickness. Uniaxial strain gages on the primary plate surface measured only axial strains (i.e., in the direction of the strain gage) during the fatigue tests. So, FEA results were used to estimate the ratio of the axial to transverse strain at the location of uniaxial strain measurements (Hobbacher, 2016). The stress range was estimated as follows: (1) obtain the ratio of axial to transverse strain at the strain gage location from the corresponding FEA results; (2) correct the measured axial strain for the effects of transverse sensitivity using strain gage manufacturer data; (3) estimate the axial stress range using elastic theory and assuming plane stress conditions.

CHAPTER 5

Fatigue Test Results

Constant-amplitude cyclic loading fatigue tests of the 16 test specimens were performed as described earlier. The 16 test specimens include four specimens for each combination of crack-like feature length and CAH diameter. In the tests, the force range, P_R was adjusted to obtain the target LSS range at the fillet weld toe. As noted earlier, the target LSS range was either 25 ksi, 30 ksi, or 40 ksi, depending on the test specimen, where the LSS range during each test was calculated from the stress ranges estimated from the average measured strain ranges for the LSS gages. The estimated stress ranges and LSS ranges from the cyclic loading laboratory fatigue tests were compared with FEA results. The stress-life (S-N) data for the test specimens from the constant-amplitude cyclic loading fatigue tests was compared with the finite-life fatigue resistance of AASHTO Fatigue Category C.

ESTIMATED STRESS RANGES

To generate the target LSS ranges at the fillet weld toe, the force ranges (P_R) shown in Table 9 were used. The estimated stress range for each strain gage was determined from the average measured strain range using the stress estimation process described earlier.

Table 12 through Table 19 show the estimated stress ranges for the G1 through G4 gages in the back-to-back configuration on the primary plate of each test specimen. In these tables, negative stress range values indicate the stresses ranges are in compression. The estimated stress ranges for each test specimen are compared with the corresponding FEA stress ranges for a test specimen with the given crack-like feature length and CAH diameter. The difference between the estimated stress range and the FEA stress range was determined at each strain gage location for each specimen. A negative difference indicates the estimated stress range from the cyclic loading fatigue test is smaller in magnitude than the FEA stress range. Generally, the estimated stress ranges are close to the FEA stress ranges for gages G1 through G4, with an average absolute difference of 6.5% over all test specimens, indicating the global bending behavior of the test specimens was in good agreement with the FEA results.

Table 20 through Table 27 show the estimated stress ranges for the LSS1 through LSS8 gages, which are located perpendicular to the fillet weld toes. For the test specimens with the target LSS range of 25 ksi, the estimated stress ranges for the LSS gages at 0.4t from the weld toe vary from 19.6 ksi to 26.8 ksi. The estimated stress ranges for the LSS gages at 1.0t from the weld toe vary from 16.1 ksi to 25.4 ksi. For the target LSS range of 30 ksi, the estimated stress ranges for the LSS gages vary from 24.5 ksi to 30.8 ksi at 0.4t from the weld toe; and vary from 21.5 ksi to 28.5 ksi at 1.0t from the weld toe. For the target LSS range of 40 ksi, the estimated stress ranges for the LSS gages vary from 33.0 ksi to 37.5 ksi at 0.4t from the weld toe; and vary from 31.6 ksi to 38.8 ksi at 1.0t from the weld toe.

At all LSS1 through LSS8 gages, the estimated stress ranges were smaller than the FEA stress ranges, even for the specimens with large estimated stress ranges at the back-to-back gages (e.g. SAW-12-25-2-2.5-N and SAW-12-30-2-2.5-N). The differences between the estimated stress ranges and the FEA stress ranges for the LSS gages at 0.4t from the weld toe vary from 0% to -31%, with a mean of -12.1%. The differences between the estimated stress ranges and the FEA stress ranges for the LSS gages at 1.0t vary from -2% to -

43%, with a mean of -13.5%. These results show that the FEA tends to overestimate the local stresses near the weld toe.

Table 21 shows the estimated stress ranges for the Edge1 and Edge2 gages for selected specimens. The differences between the estimated stress ranges and the FEA stress ranges for the Edge1 and Edge2 gages varies from 5% to -18%, with an average absolute difference of 11.0%. The differences in the stresses for the edge gages are likely due to strain averaging and actual locations of the strain gages that deviate from the locations of the highly-localized FEA stress. Through the thickness of the primary plate at the edge of the CAH, the principal stress from FEA changes from over 30 ksi in tension to a similar magnitude in compression, resulting in a stress change of approximately 60 ksi over 0.5 inch. Thus, a small difference in the strain gage position during installation can cause a significant difference in the strain measurement.

In addition to unintended differences in the strain gage locations, various other reasons can introduce differences between the estimated stress range for the cyclic loading fatigue tests and the FEA stress range. Slight misalignment of the test specimen, loading fixtures (e.g., the spreader beam), or bearings, variations in the specimen dimensions, and noise during data acquisition could be potential sources of these differences. For example, the average measured primary plate thickness for all specimens is 0.511 inch, which is 0.011 inch thicker than the primary plate in the FEA model, which results in approximately 4% reduction in stress at all gage locations relative to the FEA results.

Table 12. Comparison of FEA stress range to estimated stress range at gages G1-G4 for specimens SAW-12-25-2-2.5-N and SAW-12-25-2-2.5-S.

Gage Name	Location on Plate Surface	Location from Stiffener	FEA Stress Range (ksi)	SAW-12-25-2-2.5-N		SAW-12-25-2-2.5-S	
				Stress Range (ksi)	Difference (%)	Stress Range (ksi)	Difference (%)
G1	Bottom	West	4.9	5.5	12	4.9	0
G2	Top	West	-4.9	-5.3	8	-4.9	0
G3	Bottom	East	4.8	5.2	8	5.2	8
G4	Top	East	-4.9	-5.6	14	-4.9	0

Table 13. Comparison of FEA stress range to estimated stress range at gages G1-G4 for specimens SAW-12-25-4-2.5-N and SAW-12-25-4-2.5-S.

Gage Name	Location on Plate Surface	Location from Stiffener	FEA Stress Range (ksi)	SAW-12-25-4-2.5-N		SAW-12-25-4-2.5-S	
				Stress Range (ksi)	Difference (%)	Stress Range (ksi)	Difference (%)
G1	Bottom	West	3.4	3.7	9	3.2	-6
G2	Top	West	-3.4	-3.6	6	-3.1	-9
G3	Bottom	East	3.2	3.2	0	3.4	6
G4	Top	East	-3.4	-3.4	0	-3.4	0

Table 14. Comparison of FEA stress range to estimated stress range at gages G1-G4 for specimens SAW-12-25-2-2-N and SAW-12-25-2-2-S.

Gage Name	Location on Plate Surface	Location from Stiffener	FEA Stress Range (ksi)	SAW-12-25-2-2-N		SAW-12-25-2-2-S	
				Stress Range (ksi)	Difference (%)	Stress Range (ksi)	Difference (%)
G1	Bottom	West	4.9	5.0	2	4.6	-6
G2	Top	West	-4.9	-5.0	2	-4.7	-4
G3	Bottom	East	4.9	4.9	0	4.5	-8
G4	Top	East	-4.9	-4.8	-2	-4.6	-6

Table 15. Comparison of FEA stress range to estimated stress range at gages G1-G4 for specimens SAW-12-25-4-2-N and SAW-12-25-4-2-S.

Gage Name	Location on Plate Surface	Location from Stiffener	FEA Stress Range (ksi)	SAW-12-25-4-2-N		SAW-12-25-4-2-S	
				Stress Range (ksi)	Difference (%)	Stress Range (ksi)	Difference (%)
G1	Bottom	West	3.3	3.2	3	2.8	-15
G2	Top	West	-3.4	-2.9	-15	-2.7	-21
G3	Bottom	East	3.4	2.4	-29	3.2	-6
G4	Top	East	-3.4	-2.8	-18	-3.0	-12

Table 16. Comparison of FEA stress range to estimated stress range at gages G1-G4 for specimens SAW-12-30-2-2.5-N and SAW-12-30-2-2.5-S.

Gage Name	Location on Plate Surface	Location from Stiffener	FEA Stress Range (ksi)	SAW-12-30-2-2.5-N		SAW-12-30-2-2.5-S	
				Stress Range (ksi)	Difference (%)	Stress Range (ksi)	Difference (%)
G1	Bottom	West	5.9	6.2	5	n.a.	n.a.
G2	Top	West	-5.9	-6.9	17	-5.9	0
G3	Bottom	East	5.9	5.9	0	5.9	0
G4	Top	East	-5.9	-5.6	-5	-5.8	-2

Table 17. Comparison of FEA stress range to estimated stress range at gages G1-G4 for specimens SAW-12-30-4-2-N and SAW-12-30-4-2-S.

Gage Name	Location on Plate Surface	Location from Stiffener	FEA Stress Range (ksi)	SAW-12-30-4-2-N		SAW-12-30-4-2-S	
				Stress Range (ksi)	Difference (%)	Stress Range (ksi)	Difference (%)
G1	Bottom	West	3.9	3.9	0	3.7	-5
G2	Top	West	-4.1	-3.9	-5	-3.9	-5
G3	Bottom	East	4.1	3.9	-5	3.9	-5
G4	Top	East	-4.1	-4.0	-2	-4.0	-2

Table 18. Comparison of FEA stress range to estimated stress range at gages G1-G4 for specimens SAW-12-40-2-2-N and SAW-12-40-2-2-S.

Gage Name	Location on Plate Surface	Location from Stiffener	FEA Stress Range (ksi)	SAW-12-40-2-2-N		SAW-12-40-2-2-S	
				Stress Range (ksi)	Difference (%)	Stress Range (ksi)	Difference (%)
G1	Bottom	West	7.5	7.1	-5	7.0	-7
G2	Top	West	-7.5	-7.1	-5	-7.0	-7
G3	Bottom	East	7.4	7.1	-4	6.8	-8
G4	Top	East	-7.5	-7.5	0	-7.3	-3

Table 19. Comparison of FEA stress range to estimated stress range at gages G1-G4 for specimens SAW-12-40-4-2.5-N and SAW-12-40-4-2.5-S.

Gage Name	Location on Plate Surface	Location from Stiffener	FEA Stress Range (ksi)	SAW-12-40-4-2.5-N		SAW-12-40-4-2.5-S	
				Stress Range (ksi)	Difference (%)	Stress Range (ksi)	Difference (%)
G1	Bottom	West	5.3	5.2	-2	3.3	-38
G2	Top	West	-5.3	-5.0	-6	-4.7	-11
G3	Bottom	East	5.1	4.6	-10	5.0	-2
G4	Top	East	-5.3	-4.7	-11	-5.3	0

Table 20. Comparison of FEA stress range to estimated stress range at gages LSS1-LSS8 for specimens SAW-12-25-2-2.5-N and specimens SAW-12-25-2-2.5-S.

Gage Name	Distance from Weld Toe	Location from Stiffener	FEA Stress Range (ksi)	SAW-12-25-2-2.5-N		SAW-12-25-2-2.5-S	
				Stress Range (ksi)	Difference (%)	Stress Range (ksi)	Difference (%)
LSS 1	0.4t	West	27.0	26.8	-1	24.0	-13
LSS 2	1.0t	West	25.9	25.4	-2	23.0	-12
LSS 3	0.4t	West	26.4	25.9	-2	24.1	-9
LSS 4	1.0t	West	25.1	24.6	-5	22.8	-11
LSS 5	0.4t	East	27.0	25.6	-6	24.2	-12
LSS 6	1.0t	East	25.9	23.3	-11	23.3	-11
LSS 7	0.4t	East	26.4	25.5	-4	25.2	-5
LSS 8	1.0t	East	25.1	22.9	-9	22.9	-10

Table 21. Comparison of FEA stress range to estimated stress range at gages LSS1-LSS8 for specimens SAW-12-25-4-2.5-N and SAW-12-25-4-2.5-S

Gage Name	Distance from Weld Toe	Location from Stiffener	FEA Stress Range (ksi)	SAW-12-25-4-2.5-N		SAW-12-25-4-2.5-S	
				Stress Range (ksi)	Difference (%)	Stress Range (ksi)	Difference (%)
LSS 1	0.4t	West	26.6	22.2	-17	24.2	-9
LSS 2	1.0t	West	25.7	22.0	-14	20.5	-20
LSS 3	0.4t	West	24.8	22.9	-8	22.8	-8
LSS 4	1.0t	West	23.6	21.2	-10	21.8	-8
LSS 5	0.4t	East	26.6	22.5	-16	23.5	-12
LSS 6	1.0t	East	25.7	21.8	-15	23.7	-8
LSS 7	0.4t	East	24.8	22.8	-8	23.8	-4
LSS 8	1.0t	East	23.6	20.9	-11	22.2	-6

Table 22. Comparison of FEA stress range to estimated stress range at gages LSS1-LSS8 for specimens SAW-12-25-2-2-N and SAW-12-25-2-2-S.

Gage Name	Distance from Weld Toe	Location from Stiffener	FEA Stress Range (ksi)	SAW-12-25-2-2-N		SAW-12-25-2-2-S	
				Stress Range (ksi)	Difference (%)	Stress Range (ksi)	Difference (%)
LSS 1	0.4t	West	26.7	24.9	-7	23.2	-14
LSS 2	1.0t	West	26.0	23.6	-10	22.0	-17
LSS 3	0.4t	West	26.2	24.8	-6	21.9	-20
LSS 4	1.0t	West	24.9	23.0	-8	20.4	-22
LSS 5	0.4t	East	26.7	26.7	0	24.3	-10
LSS 6	1.0t	East	26.0	20.2	-29	22.9	-14
LSS 7	0.4t	East	26.2	24.7	-6	22.9	-15
LSS 8	1.0t	East	24.9	23.1	-8	21.8	-14

Table 23. Comparison of FEA stress range to estimated stress range at gages LSS1-LSS8 for specimens SAW-12-25-4-2-N. and SAW-12-25-4-2-S.

Gage Name	Distance from Weld Toe	Location from Stiffener	FEA Stress Range (ksi)	SAW-12-25-4-2-N		SAW-12-25-4-2-S	
				Stress Range (ksi)	Difference (%)	Stress Range (ksi)	Difference (%)
LSS 1	0.4t	West	26.4	22.2	-19	24.2	-10
LSS 2	1.0t	West	25.4	21.5	-18	20.6	-22
LSS 3	0.4t	West	24.3	19.6	-24	22.1	-10
LSS 4	1.0t	West	23.0	16.1	-43	20.1	-15
LSS 5	0.4t	East	26.4	20.2	-31	22.7	-16
LSS 6	1.0t	East	25.4	21.5	-18	21.9	-16
LSS 7	0.4t	East	24.3	21.3	-14	20.9	-16
LSS 8	1.0t	East	23.0	19.9	-16	18.5	-24

Table 24. Comparison of FEA stress range to estimated stress range at gages LSS1-LSS8 for specimens SAW-12-30-2-2.5-N and specimens SAW-12-30-2-2.5-S.

Gage Name	Distance from Weld Toe	Location from Stiffener	FEA Stress Range (ksi)	SAW-12-30-2-2.5-N		SAW-12-30-2-2.5-S	
				Stress Range (ksi)	Difference (%)	Stress Range (ksi)	Difference (%)
LSS 1	0.4t	West	32.8	28.7	-13	28.1	-14
LSS 2	1.0t	West	31.3	27.8	-11	28.4	-9
LSS 3	0.4t	West	31.7	29.2	-8	27.3	-14
LSS 4	1.0t	West	30.1	28.5	-5	26.7	-11
LSS 5	0.4t	East	32.8	28.2	-14	26.6	-19
LSS 6	1.0t	East	31.3	27.4	-12	28.3	-10
LSS 7	0.4t	East	32.0	30.8	-4	28.9	-10
LSS 8	1.0t	East	30.4	25.7	-15	26.4	-13

Table 25. Comparison of FEA stress range to estimated stress range at gages LSS1-LSS8 for specimens SAW-12-30-4-2-N and SAW-12-30-4-2-S

Gage Name	Distance from Weld Toe	Location from Stiffener	FEA Stress Range (ksi)	SAW-12-30-4-2-N		SAW-12-30-4-2-S	
				Stress Range (ksi)	Difference (%)	Stress Range (ksi)	Difference (%)
LSS 1	0.4t	West	31.7	27.9	-12	26.0	-18
LSS 2	1.0t	West	30.5	26.6	-13	27.1	-11
LSS 3	0.4t	West	29.1	25.4	-13	26.2	-10
LSS 4	1.0t	West	27.6	25.2	-9	25.4	-8
LSS 5	0.4t	East	31.7	29.1	-8	27.2	-14
LSS 6	1.0t	East	30.5	27.2	-11	25.9	-15
LSS 7	0.4t	East	29.1	27.4	-6	24.5	-16
LSS 8	1.0t	East	27.6	25.1	-9	21.5	-22

Table 26. Comparison of FEA stress range to estimated stress range at gages LSS1-LSS8 for specimens SAW-12-40-2-2-N and SAW-12-40-2-2-S.

Gage Name	Distance from Weld Toe	Location from Stiffener	FEA Stress Range (ksi)	SAW-12-40-2-2-N		SAW-12-40-2-2-S	
				Stress Range (ksi)	Difference (%)	Stress Range (ksi)	Difference (%)
LSS 1	0.4t	West	41.5	35.8	-14	35.4	-15
LSS 2	1.0t	West	40.4	34.7	-14	38.8	-4
LSS 3	0.4t	West	40.7	35.8	-12	35.7	-12
LSS 4	1.0t	West	38.6	33.5	-13	32.0	-17
LSS 5	0.4t	East	41.5	35.1	-15	37.5	-10
LSS 6	1.0t	East	40.4	34.6	-14	35.4	-12
LSS 7	0.4t	East	40.7	35.0	-14	34.6	-15
LSS 8	1.0t	East	38.6	33.8	-12	32.9	-15

Table 27. Comparison of FEA stress range to estimated stress range at gages LSS1-LSS8 for specimens SAW-12-25-4-2-N. and SAW-12-25-4-2-S.

Gage Name	Distance from Weld Toe	Location from Stiffener	FEA Stress Range (ksi)	SAW-12-25-2-2.5-N		SAW-12-25-2-2.5-S	
				Stress Range (ksi)	Difference (%)	Stress Range (ksi)	Difference (%)
LSS 1	0.4t	West	41.9	37.4	-11	34.3	-18
LSS 2	1.0t	West	40.5	34.9	-14	32.6	-20
LSS 3	0.4t	West	39.1	35.7	-9	33.3	-15
LSS 4	1.0t	West	37.2	32.0	-14	32.5	-13
LSS 5	0.4t	East	42.0	33.5	-20	35.2	-16
LSS 6	1.0t	East	40.5	34.9	-14	34.0	-16
LSS 7	0.4t	East	39.1	33.0	-16	33.5	-14
LSS 8	1.0t	East	37.2	31.8	-15	31.6	-15

Table 28. Comparison of FEA stress range to estimated stress range at gages Edge1 and Edge2 for selected specimens.

Gage Name	Specimen Name	Location from Stiffener	Location from Corner of CAH (inch)	FEA Stress Range (ksi)	Stress Range (ksi)	Difference (%)
Edge1	SAW-12-25-4-2.5-S	West	0.058	24.7	21.6	-13
Edge2	SAW-12-25-4-2.5-S	East	0.067	25.8	21.3	-17
Edge1	SAW-12-25-2-2-N	West	0.092	24.9	26.1	5
Edge2	SAW-12-25-2-2-N	East	0.080	23.2	23.3	0
Edge1	SAW-12-25-4-2-N	West	0.049	28.6	23.5	-18
Edge2	SAW-12-25-4-2-N	East	0.048	28.6	24.2	-15
Edge1	SAW-12-30-2-2.5-N	West	0.066	30.8	27.6	-10
Edge2	SAW-12-30-2-2.5-N	East	0.076	29.2	26.6	-9
Edge1	SAW-12-30-4-2-N	West	0.074	30.7	26.8	-13
Edge2	SAW-12-30-4-2-N	East	0.065	32.2	30.2	-6
Edge1	SAW-12-40-2-2-N	West	0.048	45.1	40.1	-11
Edge1	SAW-12-40-4-2.5-N	West	0.074	37.3	33.5	-10
Edge2	SAW-12-40-4-2.5-N	East	0.084	35.3	29.8	-16

LINEARLY EXTRAPOLATED LSS RANGES

The estimated stress ranges for each pair of LSS gages perpendicular to the weld toe and the corresponding linearly extrapolated LSS ranges are plotted for the face of the primary plate under tension in Figure 34 through Figure 41. The corresponding LSS ranges from FEA are plotted in each figure for comparison. As discussed previously, two sets of LSS gages were installed perpendicular to the weld toe. Gages LSS1, LSS2, LSS5 and LSS6 were installed $L_{Max\text{-}LSS}$ from the CAH edge; and Gages LSS3, LSS4, LSS7 and LSS8 were installed an additional 1 inch farther from the CAH edge. Accordingly, two LSS ranges were determined for each fillet weld toe. In each figure, the estimated stress ranges and LSS ranges at $L_{Max\text{-}LSS}$ are given in part (a) of the figure, and the estimated stress ranges and LSS ranges at $L_{Max\text{-}LSS}$ + 1.0 inch from the CAH edge are given in part (b).

In Figure 34 through Figure 41, the FEA results show that the stress ranges are expected to gradually increase in the direction perpendicular to (toward) the weld toe. The average stress gradient toward the weld toe from the FEA results is 3.7 ksi/inch, 4.5 ksi/inch, and 5.9 ksi/inch for the various test specimens with various crack-like feature lengths and CAH diameters with 25 ksi, 30 ksi, and 40 ksi target LSS ranges, respectively. For the 16 test specimens, with LSS gages for both the east and west fillet welds and with the LSS gages located at $L_{Max\text{-}LSS}$ and at $L_{Max\text{-}LSS}$ + 1.0 inch from the CAH edge, a total of 64 LSS ranges are estimated from the LSS gages, as shown in Figure 34 through Figure 41. As shown in the figures, most of the stress gradients (i.e., slopes) used for the LSS extrapolation from the LSS gage data are similar to those from the FEA results; however, nine of the 64 stress gradients are considered to be too large, more than 3 times the stress gradient from the FEA results for that specific specimen type, or are negative. Data for these sets of LSS gages are shown in grey in Figure 34 through Figure 41. The stress gradients from these LSS gages are considered to be outliers, and the LSS ranges from these sets of LSS gages are considered to be invalid. Eight of these nine sets of LSS gages are located at $L_{Max\text{-}LSS}$ from the CAH edge. These invalid LSS ranges are identified in Table 29, which presents the LSS ranges.

Excluding the invalid LSS ranges, the difference in LSS ranges between the specimens with the same crack-like feature length and CAH diameter at both $L_{Max\text{-}LSS}$ and $L_{Max\text{-}LSS}$ +1.0 inch from the CAH edge are relatively small. The largest difference in LSS ranges appears at $L_{Max\text{-}LSS}$ +1.0 inch on the pair of specimens with the 4.0 inch long crack-like feature and 2.5 inch diameter CAH subjected to 40 ksi target LSS range, where the LSS ranges vary from 33.8 ksi (S-E) to 38.1 ksi (N-W), a difference of 4.3 ksi as shown in Figure 41b.

Although the LSS range from FEA at $L_{Max\text{-}LSS}$ is larger than at $L_{Max\text{-}LSS}$ +1.0 inch, by approximately 2% for the specimens with the 2.0 inch long crack-like feature and approximately 6% for the specimens with the 4.0 inch long crack-like feature, the LSS ranges from the cyclic loading fatigue tests are not as consistent. For some specimens (and east or west fillet welds) the LSS ranges are slightly larger at $L_{Max\text{-}LSS}$, and for others the LSS ranges are slightly larger at $L_{Max\text{-}LSS}$ +1.0 inch from the CAH edge. The largest difference between the LSS ranges at the two locations is 3.4 ksi at the west fillet weld of specimen SAW-12-30-4-2-N, where the LSS range is 29.2 ksi at $L_{Max\text{-}LSS}$ and 25.8 ksi at $L_{Max\text{-}LSS}$ +1.0 inch.

Overall, most of the LSS ranges from the cyclic loading fatigue tests are comparable to the target LSS ranges. The average absolute difference between the test results and the FEA results over all the valid LSS ranges for the 16 test specimens is 10.6%. The valid LSS ranges, estimated from the LSS gage data during the fatigue tests, are used to assess the fatigue performance of the fillet weld toes on the face of the primary plate. The assessment of fatigue performance is presented later.

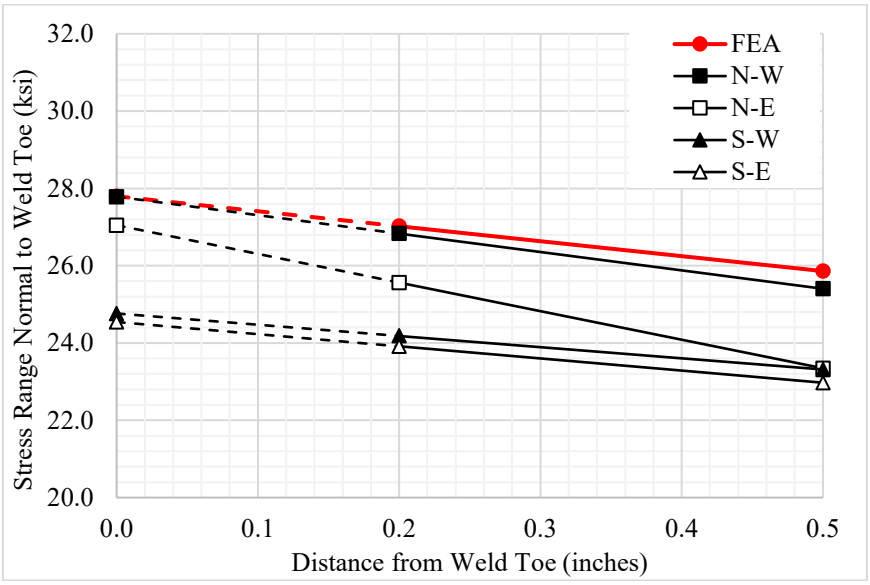

(a)

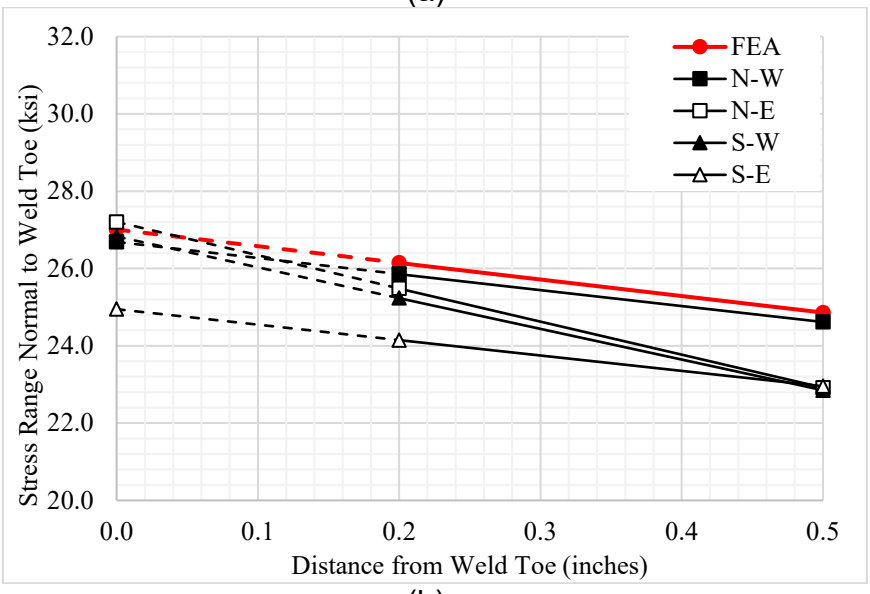

(b)

Figure 34. Comparison of FEA (red) to estimated stress range perpendicular to weld toe versus distance from weld toe with LSS linear extrapolation (dashed) for specimens SAW-12-25-2-2.5-N and SAW-12-25-2-2.5-S at (a) $L_{Max\text{-}LSS}$ from CAH edge, and (b) $L_{Max\text{-}LSS}$ +1.0 inch from CAH edge.

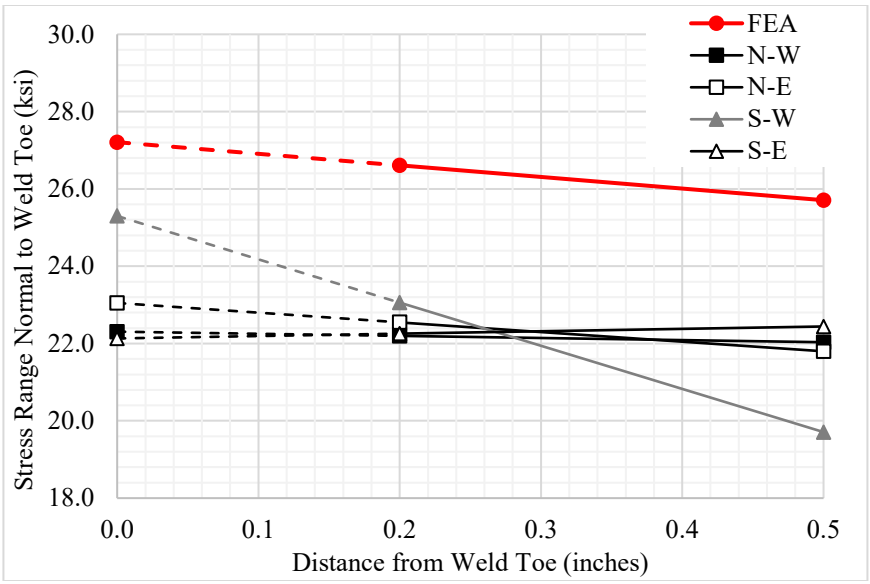

(a)

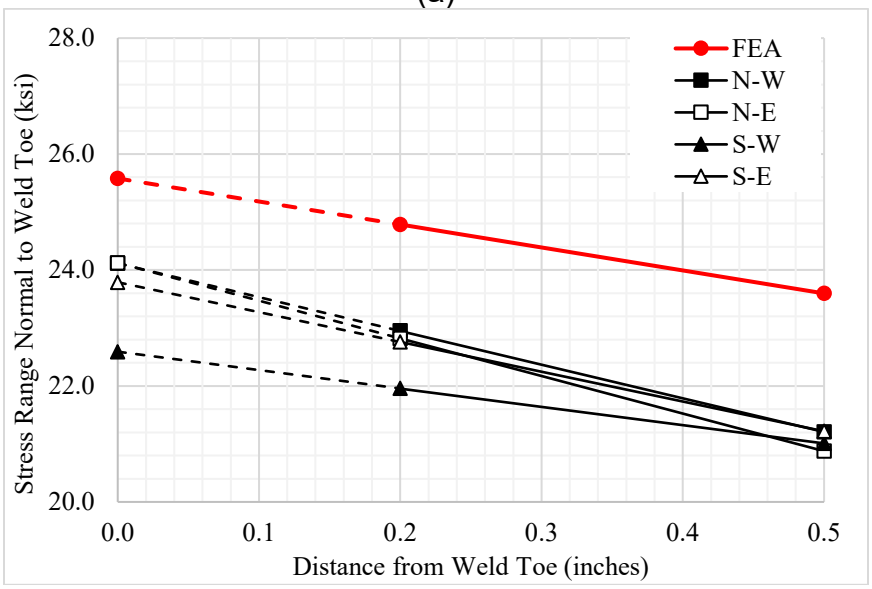

(b)

Figure 35. Comparison of FEA (red) to estimated stress range perpendicular to weld toe versus distance from weld toe with LSS linear extrapolation (dashed) for specimens SAW-12-25-4-2.5-N and SAW-12-25-4-2.5-S at (a) $L_{Max\text{-}LSS}$ from CAH edge, and (b) $L_{Max\text{-}LSS}$ +1.0 inch from CAH edge.

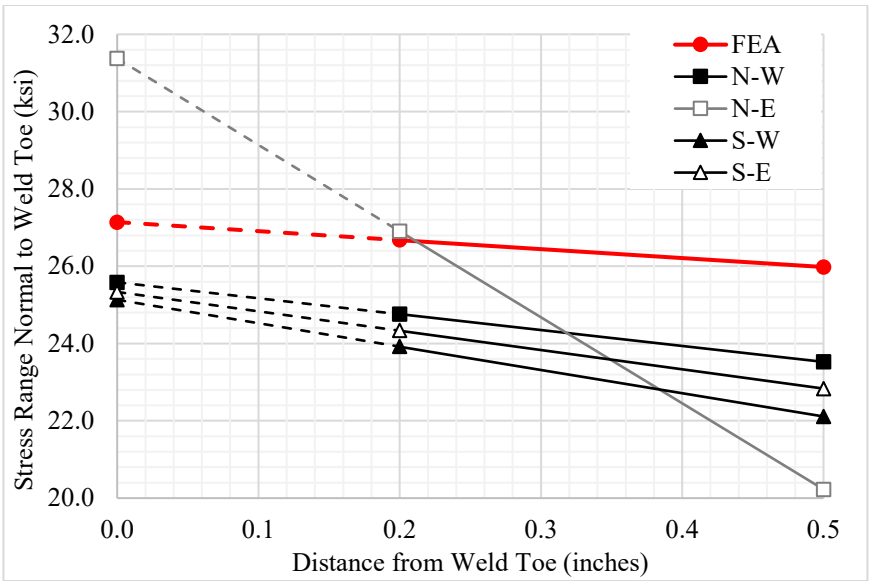

(a)

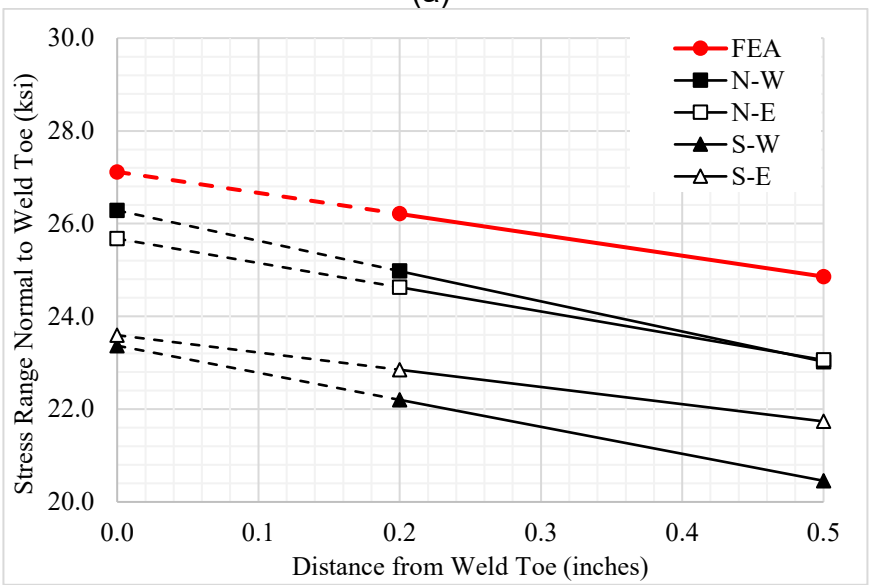

(b)

Figure 36. Comparison of FEA (red) to estimated stress range perpendicular to weld toe versus distance from weld toe with LSS linear extrapolation (dashed) for specimens SAW-12-25-2-2-N and SAW-12-25-2-2-S at (a) $L_{Max\text{-}LSS}$ from CAH edge, and (b) $L_{Max\text{-}LSS}$ +1.0 inch from CAH edge.

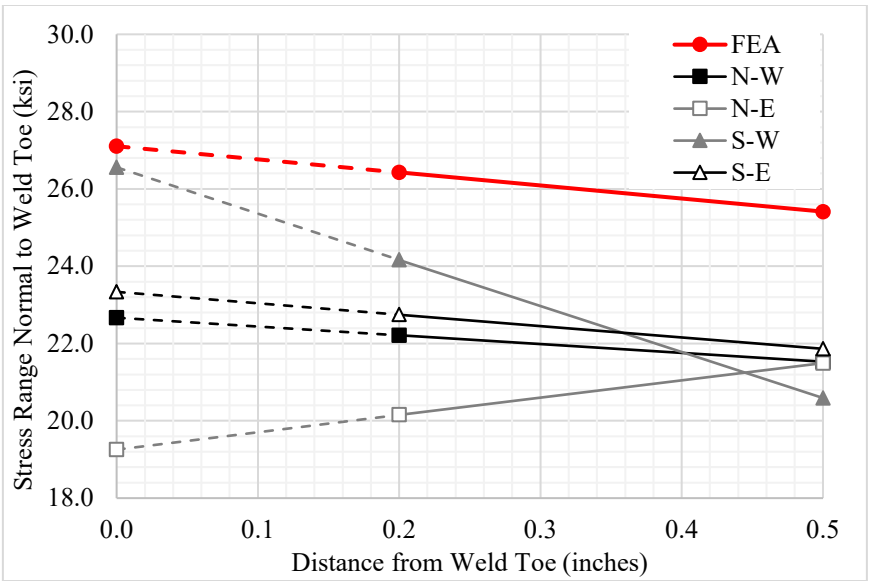

(a)

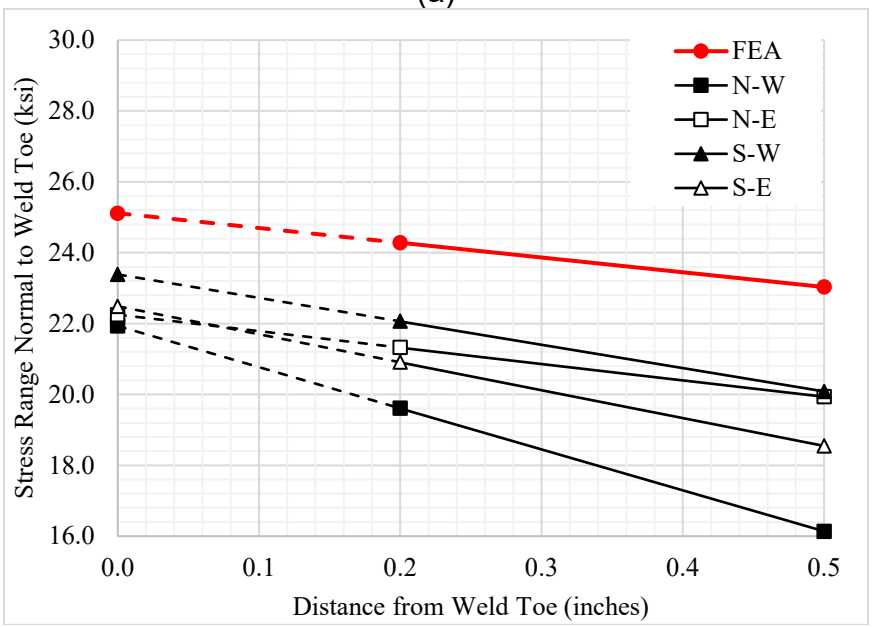

(b)

Figure 37. Comparison of FEA (red) to estimated stress range perpendicular to weld toe versus distance from weld toe with LSS linear extrapolation (dashed) for specimens SAW-12-25-4-2-N and SAW-12-25-4-2-S at (a) $L_{Max\text{-}LSS}$ from CAH edge, and (b) $L_{Max\text{-}LSS}$ +1.0 inch from CAH edge.

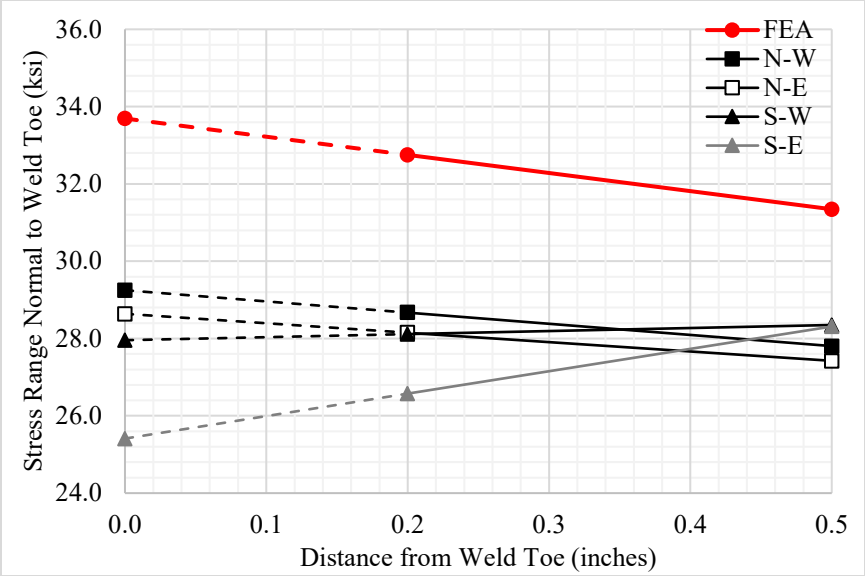

(a)

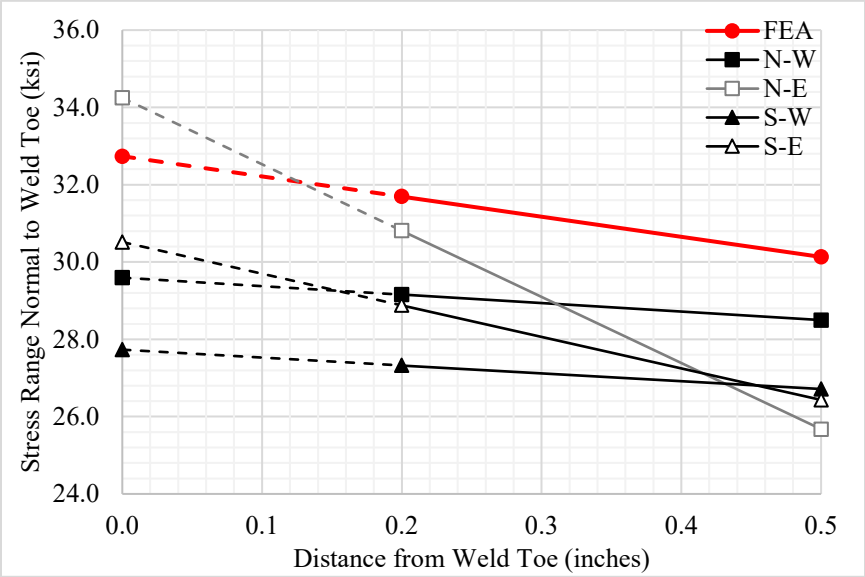

(b)

Figure 38. Comparison of FEA (red) to estimated stress range perpendicular to weld toe versus distance from weld toe with LSS linear extrapolation (dashed) for specimens SAW-12-30-2-2.5-N and SAW-12-30-2-2.5-S at (a) $L_{Max\text{-}LSS}$ from CAH edge, and (b) $L_{Max\text{-}LSS}$ +1.0 inch from CAH edge.

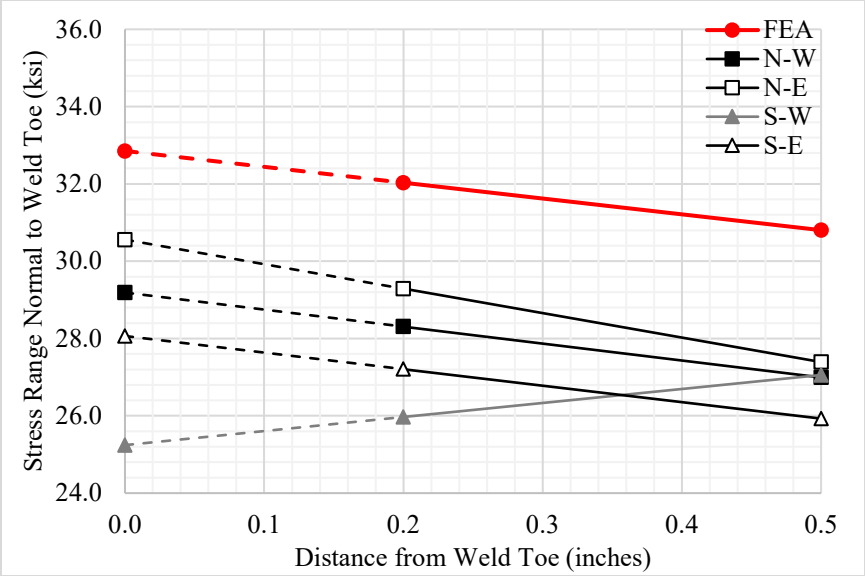

(a)

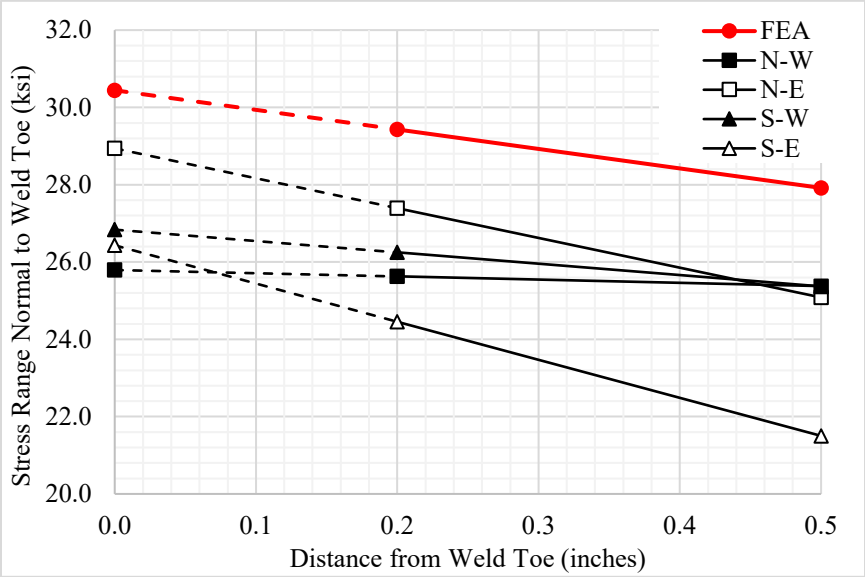

(b)

Figure 39. Comparison of FEA (red) to estimated stress range perpendicular to weld toe versus distance from weld toe with LSS linear extrapolation (dashed) for specimens SAW-12-30-4-2-N and SAW-12-30-4-2-S at (a) $L_{Max\text{-}LSS}$ from CAH edge, and (b) $L_{Max\text{-}LSS}$ +1.0 inch from CAH edge.

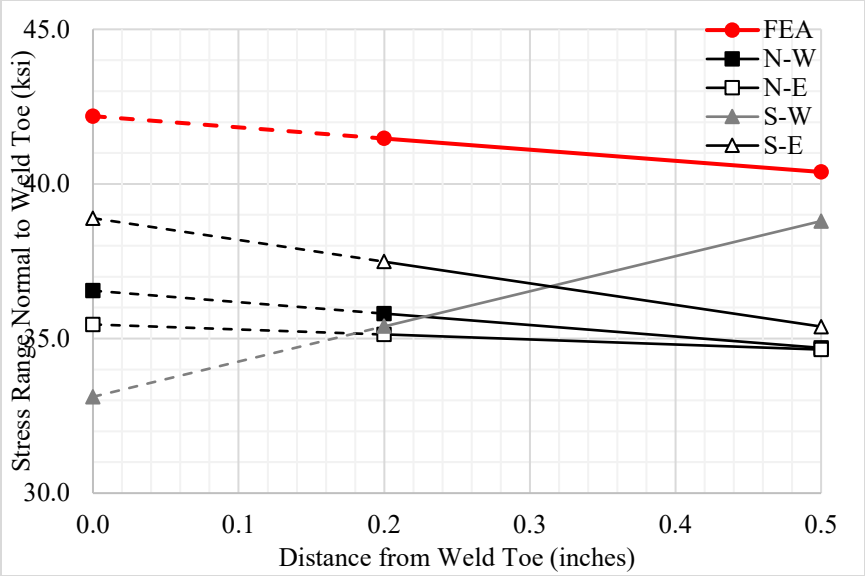

(a)

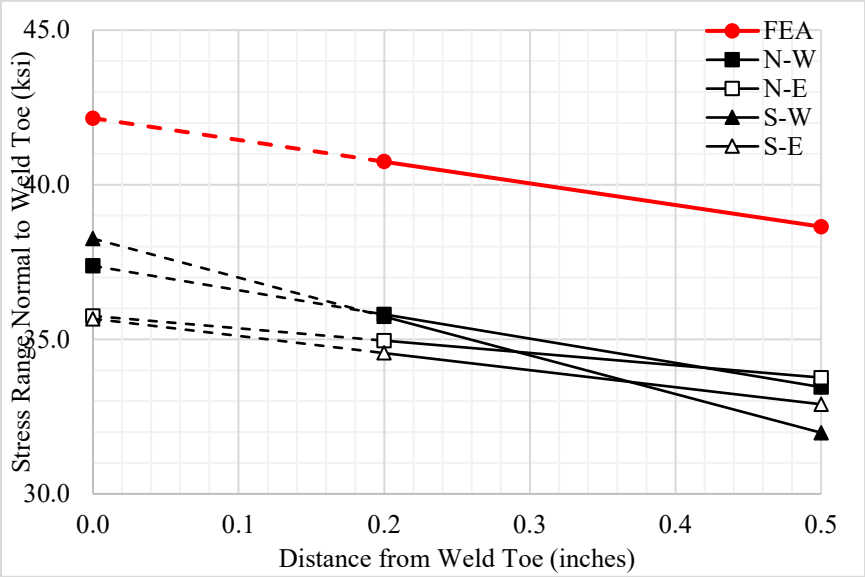

(b)

Figure 40. Comparison of FEA (red) to estimated stress range perpendicular to weld toe versus distance from weld toe with LSS linear extrapolation (dashed) for specimens SAW-12-40-2-2-N and SAW-12-40-2-2-S at (a) $L_{Max\text{-}LSS}$ from CAH edge, and (b) $L_{Max\text{-}LSS}$ +1.0 inch from CAH edge.

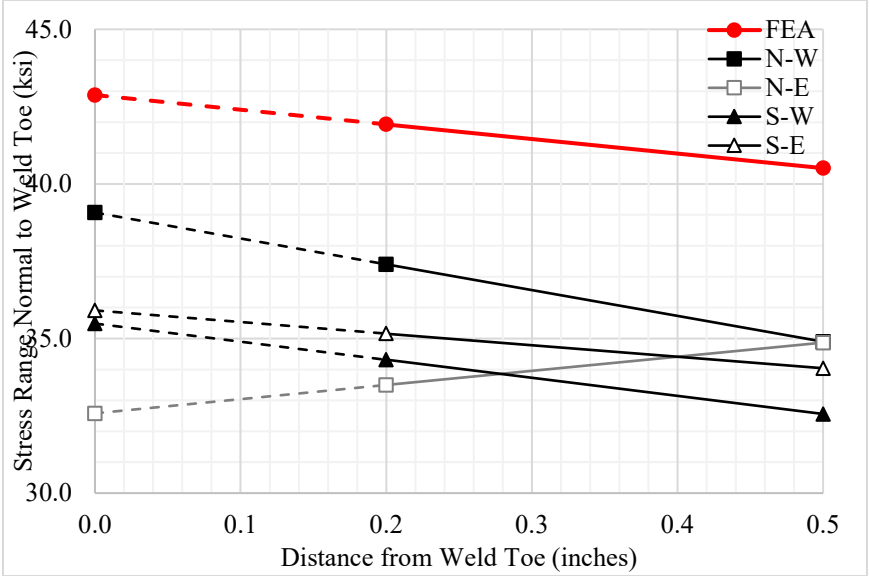

(a)

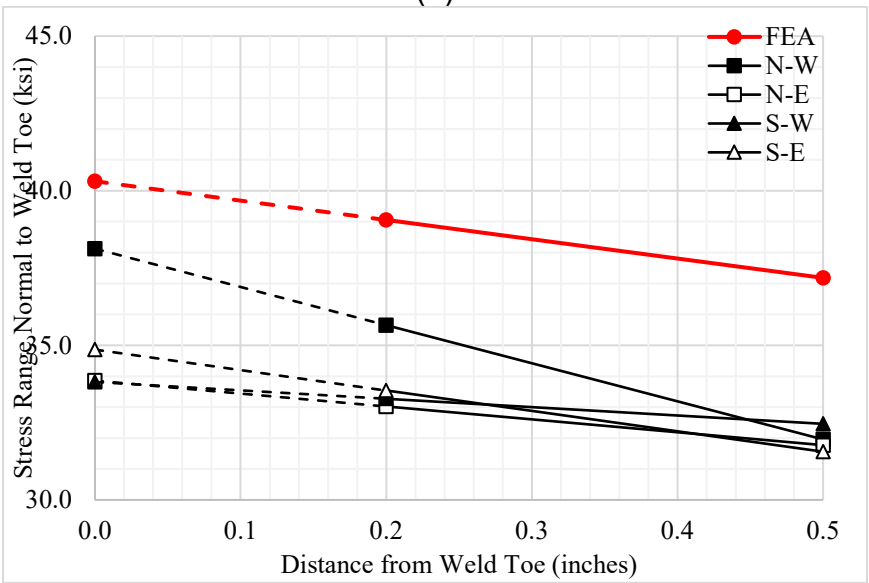

(b)

Figure 41. Comparison of FEA (red) to estimated stress range perpendicular to weld toe versus distance from weld toe with LSS linear extrapolation (dashed) for specimens SAW-12-40-4-2.5-N and SAW-12-40-4-2.5-S at (a) $L_{Max\text{-}LSS}$ from CAH edge, and (b) $L_{Max\text{-}LSS}$ +1.0 inch from CAH edge.

INSPECTION FINDINGS

During the fatigue tests, regular unaided visual inspections were performed to identify fatigue cracks in the test specimens. Cracks were observed at the fillet weld toes near LMax-LSS from the CAH edge where the FEA stress results were large. Cracks were not observed to initiate at the edge of the CAH in any of the 16 test specimens.

During the cyclic loading fatigue tests, before the weld toe fatigue cracks could be observed in an unaided visual inspection, the estimated stress ranges from some of the LSS gages located 0.4t from the weld toe was observed to decrease steadily under cyclic loading, as shown in Figure 42. The figure shows the estimated stress range for a typical LSS gage at 0.4t plotted versus the number of loading cycles. This LSS gage is located at $L_{Max\text{-}LSS}$+1.0 inch from the CAH edge at 0.4t from of the west fillet weld toe of specimen SAW-12-25-4-2-S. As shown in Figure 42, the estimated stress range was approximately 22.1 ksi for approximately 700,000 cycles, and then the estimated stress range decreased by 20% to 17.7 ksi at 1,316,000 cycles. The rate of decrease gradually increased with the number of cycles and the estimated stress range decreased by another 50% (of the original 22.1 ksi) to 6.5 ksi at 2,000,000 cycles. The variation of the estimated stress range for the LSS gage at 0.4t versus the number of cycles for other fillet weld toe locations that developed fatigue cracks was similar to that shown in Figure 42. Typically, a large number of cycles were needed for the estimated stress range to decrease, indicating relatively slow crack propagation.

To define the fatigue life for these test specimens, which simulate the condition of a CAH installed to retrofit an original fatigue crack propagating vertically (downward) along the weld toe from the top edge of the connection plate-to-web weld under out-of-plane bending of the web plate, a conservative approach was used. The fatigue life is defined to be the number of loading cycles until a new weld toe fatigue crack is first observed (at a location below) the CAH, which is a location where the weld toe stress ranges were insignificant before the CAH was installed (as shown in Chapter 3). As discussed below, when a 20% decrease in the estimated stress range at an LSS gage located 0.4t from the weld toe was observed, the dye penetration test performed on the test specimen often revealed single or multiple fatigue cracks that were not observed during unaided visual inspection. Therefore, the number of loading cycles when a 20% decrease in the estimated stress range for an LSS gage at 0.4t from the weld toe is first observed, denoted "N20" is selected as the fatigue life. This number of loading cycles, N20, is a conservative estimate of the fatigue life, because these fatigue cracks grow slowly as suggested by Figure 42 and discussed further below.

The first observation of a 20% decrease in the estimated stress range at 0.4t from the fillet weld toe was observed at either of the two LSS gage set locations, at $L_{Max\text{-}LSS}$ or $L_{Max\text{-}LSS}$ + 1.0 inch from the CAH edge, with about the same frequency. The difference in LSS range at these two locations (within 3.4 ksi) in the test specimens did not have a clear effect on the location where the 20% decrease in the estimated stress range at an LSS gage at 0.4t was first observed and where a fatigue crack was subsequently observed using a dye penetration test, demonstrating the randomness of fatigue crack initiation. After the estimated stress range decreased by 20% for the LSS gage at 0.4t at one location, a decrease in the estimated stress range was typically observed at the LSS gage at 0.4t adjacent to this gage, indicating the weld toe crack propagated along the fillet weld to the location of the adjacent LSS gage, or another crack initiated near the adjacent LSS gage. Also, a decrease in the estimated stress range for the LSS gage at 1.0t from the weld toe was typically observed at N20.

To study the initiation and propagation of the weld toe fatigue cracks, dye penetration tests were performed at N20 for specimen SAW-12-25-4-2.5-N at the N-E location, specimen SAW-12-25-2-2-N at the N-W location, specimen SAW-12-25-2-2-S at the S-W location, specimen SAW-12-25-4-2-N at the N-W location, specimen SAW-12-30-2-2.5-S at the S-E location, and specimen SAW-12-40-2-2-S at the S-E location. Dye penetration tests were performed near the fillet weld toes for the entire width of the test specimens. Figure 43 shows the west fillet weld of specimen SAW-12-25-2-2-S, after 521,000 loading

cycles (i.e., after N20 = 521,000). The figure also shows: (1) the LSS results from FEA along the weld toe; (2) a photo of the dye penetration test results; and (3) the contour plot of stress from FEA in the direction perpendicular to the weld toe with the locations of the LSS strain gages included. At N20, the estimated stress range had decreased from 23.2 ksi to 18.0 ksi at the 0.4t LSS gage located at $L_{Max\text{-}LSS}$ from the CAH edge. Each part of Figure 43 is aligned and scaled to enable a direct comparison. The LSS ranges determined from the estimated stress ranges during the test are 25.1 ksi at $L_{Max\text{-}LSS}$ (1.375 inches), and 23.4 ksi at $L_{Max\text{-}LSS}$ + 1.0 inch (2.375 inches) from the CAH edge. As shown in the figure, two short weld toe fatigue cracks (with lengths of 1.5 inches and 1.75 inches) were indicated by the thin and discontinuous red lines (dye indications) from the dye penetration test. The cracks were located a short distance from the edge of the CAH, and not at the intersection between the CAH edge and fillet weld toe, as expected from the FEA results and from the findings of (Liu, et al., 2018). The two fatigue cracks are located along the weld toe where the FEA stress results were large. The location of the left crack in the figure coincides with $L_{Max\text{-}LSS}$ determined from FEA, which is the location of one set of LSS gages. The observation of these cracks in these locations provides support for the use of FEA and the LSS approach to assess fatigue at the fillet weld toe near a CAH retrofit of an original fatigue crack propagating along a connection plate-to-web weld toe under out-of-plane bending of the web plate.

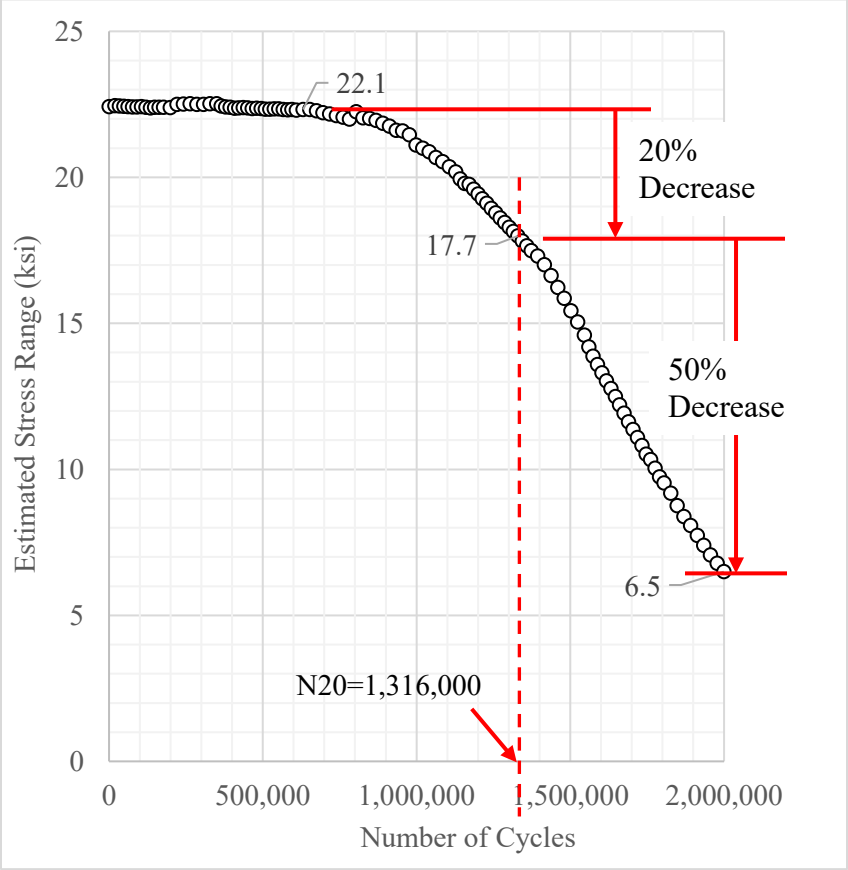

Figure 42. Variation of estimated stress range for LSS gage at 0.4t, $L_{Max\text{-}LSS}$ +1.0 inch from CAH edge for west fillet weld of specimen SAW-12-25-4-2-S.

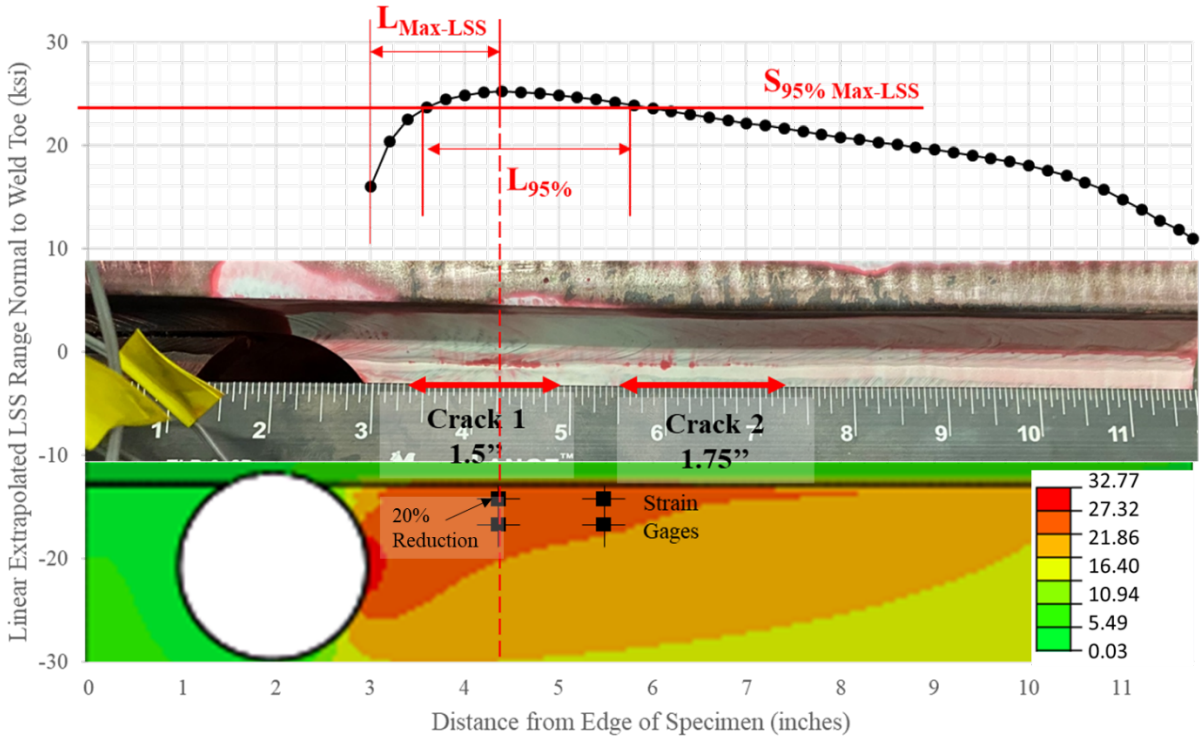

Figure 43. Comparison between FEA linear extrapolated LSS along weld toe (top), dye penetration test result (center), and FEA contour of stress normal to weld toe (bottom) for specimen SAW-12-25-2-2-S, west weld at 521,000 cycles after 20% decrease in estimated stress range for LSS gage at 0.4t, $L_{Max\text{-}LSS}$ from CAH edge.

After weld toe fatigue cracks were observed in a test specimen during the cyclic loading fatigue test, the test of the cracked specimen continued until the hydraulic control system load error exceeded the load error limit. When the load error limit was exceeded, the weld toe fatigue cracks could be detected with unaided visual inspection under cyclic loading at a frequency of 1 Hz. Cracks were not observed to initiate at the edge of the CAH in any of the test specimens. For most of the test specimens, the estimated stress ranges from the LSS gages at 0.4t decreased by more than 65% when the load error limit was reached. The number of cycles corresponding to a 65% decrease in the estimated stress range at the LSS gage at 0.4t is N65. A photo of the dye penetration test result for the east fillet weld of specimen SAW-12-25-2-2.5-S after 1,333,000 loading cycles is shown in Figure 44. The fatigue crack propagated to a length of over 6.0 inches along the weld toe, but did not propagate all the way to the intersection of the CAH edge and the fillet weld toe. Compared to the dye penetration test result shown in Figure 43, the darker red line in the dye penetration test result shown in Figure 44 indicates a deeper fatigue crack at the weld toe. This comparison suggests that after the initial stage of fatigue cracking at N20, the fatigue crack(s) propagated both along the weld toe and into the primary plate thickness, though it is unlikely that the crack(s) propagate through the primary plate thickness into regions of compression stress since the test specimens were subjected to bending only.

Approximately 500,000 loading cycles were applied to grow the fatigue crack(s) from the lengths shown in Figure 43, corresponding to N20 to lengths shown in Figure 44 corresponding to N65. Similar observations have been made during out-of-plane loading fatigue tests of steel bridge girders with connection plates welded to the girder web by (Liu, et al., 2018) and (Fisher, et al., 1990). (Liu, et al., 2018) found weld toe fatigue cracking using a dye penetration test after 450,000 out-of-plane loading cycles of a steel girder with connection plate specimen (with a CAH retrofit). The cracks propagated another 3.0 inches

at 805,000 cycles, after an additional 355,000 cycles. Fatigue test results presented by (Fisher, et al., 1990) showed that at the ends of connection plate-to-web welds in test girders subjected to out-of-plane loading, fatigue cracks propagated an additional 1 to 2 inches from 10 to 17 million loading cycles after the cracks were first identified.

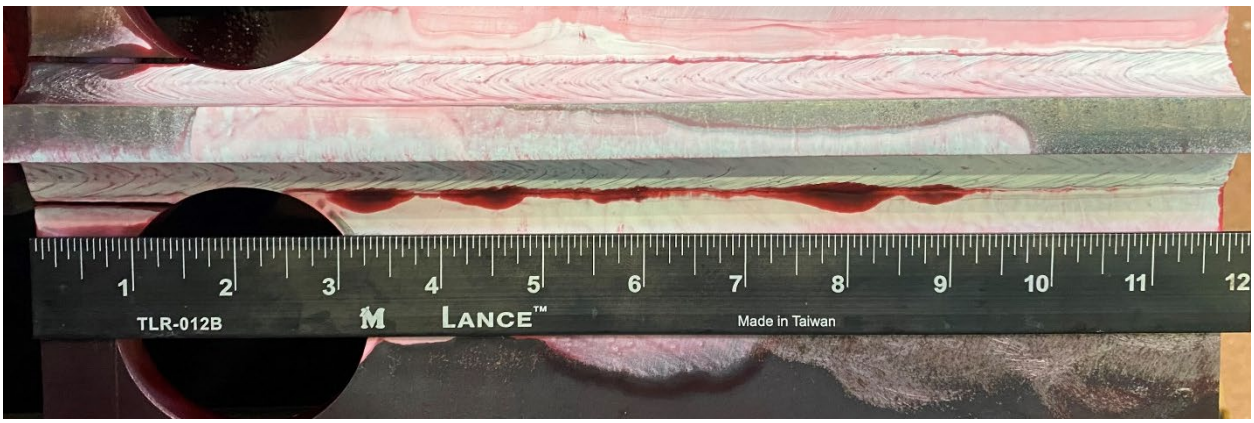

Figure 44. Photo of dye penetration result for specimen SAW-12-25-2-2.5-S east weld after 1,333,000 cycles of cyclic loading fatigue testing.

ASSESSMENT OF FATIGUE PERFORMANCE

The stress-life (S-N) data for a test specimens is defined as the weld toe linearly extrapolated LSS range (before a decrease is observed), S, and the number of loading cycles, N, when a 20% decrease in the estimated stress range for an LSS gage at 0.4t from the weld toe is first observed (i.e., N = N20). This S-N data is compared to the fatigue resistance for cracks initiating from the geometrical discontinuity at a fillet weld toe specified in (AASHTO, 2018) and (ECCS, TC6, 2018) to make a fatigue performance assessment for weld toe cracking after a CAH retrofit.

Each of the 16 test specimens included two (east and west) fillet welds on the bottom face of the primary plate that were subjected to tensile stress ranges during the cyclic loading fatigue tests. The relevant S-N data for the corresponding 32 fillet welds are shown in Table 29. The table lists the location of the LSS gage at 0.4t for which a 20% decrease in the estimated stress range was first observed, the LSS ranges at $L_{Max\text{-}LSS}$ from the CAH edge and at $L_{Max\text{-}LSS}$ +1.0 inch from the CAH edge, and the value of N20.

The weld toe LSS ranges used for the stress-life data are from the location from the CAH edge (either $L_{Max\text{-}LSS}$ or $L_{Max\text{-}LSS}$ +1.0 inch) where the 20% decrease in the estimated stress range was first observed, except when the LSS range is invalid because of an unusually large or negative stress gradient, as discussed earlier. For the eight locations with invalid LSS ranges at $L_{Max\text{-}LSS}$, the LSS ranges at $L_{Max\text{-}LSS}$ +1.0 inch from the CAH edge were used as the stress range for the stress-life data. The FEA results show that the LSS range at $L_{Max\text{-}LSS}$ is expected to be larger than at $L_{Max\text{-}LSS}$ +1.0 inch from the CAH edge, and using a smaller LSS range for the stress-life data is conservative. The LSS ranges used for the stress-life data of the test specimens are shown in bold in Table 29.

For eight of the fillet welds of the test specimens, a fatigue life was not determined from the cyclic loading fatigue tests since a 20% decrease in the estimated stress range for an LSS gage at 0.4t from the weld toe was not observed before the test was concluded. For these fillet welds, the value of N20 is noted as N.A. (not available) in Table 29. Two of these eight fillet welds were tested beyond the upper bound fatigue resistance of AASHTO Fatigue Category C (described below) with no cracking observed, and, therefore, these fillet welds are identified as “runouts”. The other six fillet welds were not tested beyond the upper bound fatigue resistance of AASHTO Fatigue Category C (not runouts), but the tests were terminated because of a long fatigue crack in the other fillet weld in the test specimen. The smaller of the two LSS

ranges (at either $L_{Max\text{-}LSS}$ or $L_{Max\text{-}LSS}$ +1.0 inch from the CAH edge) was used in the stress-life data for these eight fillet welds.

Table 29. S-N data from test specimen fillet welds.

Specimen Name	Location from Stiffener	Location of LSS Gage with 20% Decrease	$L_{Max\text{-}LSS}$ LSS Range (ksi)	$L_{Max\text{-}LSS}$ +1.0 LSS Range (ksi)	N20
SAW-12-25-2-2.5-N	West	$L_{Max\text{-}LSS}$+1.0	27.8	**26.7**	694,000
SAW-12-25-2-2.5-N	East	N.A.	**27.0**	27.2	785,000[T]
SAW-12-25-2-2.5-S	West	$L_{Max\text{-}LSS}$	**24.8**	26.8	785,000
SAW-12-25-2-2.5-S	East	N.A.	**24.5**	24.9	1,333,000[T]
SAW-12-25-4-2.5-N	West	N.A.	**22.3**	24.1	849,000[T]
SAW-12-25-4-2.5-N	East	$L_{Max\text{-}LSS}$	**23.0**	24.1	849,000
SAW-12-25-4-2.5-S	West	N.A.	25.3*	**22.6**	3,248,000[R]
SAW-12-25-4-2.5-S	East	N.A.	**22.1**	23.8	3,248,000[R]
SAW-12-25-2-2-N	West	$L_{Max\text{-}LSS}$+1.0	25.6	**26.3**	755,000
SAW-12-25-2-2-N	East	$L_{Max\text{-}LSS}$	31.4*	**25.7**	661,000
SAW-12-25-2-2-S	West	$L_{Max\text{-}LSS}$	**25.1**	23.4	521,000
SAW-12-25-2-2-S	East	N.A.	25.3	**23.6**	521,000[T]
SAW-12-25-4-2-N	West	$L_{Max\text{-}LSS}$	**22.7**	21.9	1,043,000
SAW-12-25-4-2-N	East	$L_{Max\text{-}LSS}$	19.3*	**22.3**	515,000
SAW-12-25-4-2-S	West	$L_{Max\text{-}LSS}$+1.0	26.6*	**23.4**	1,316,000
SAW-12-25-4-2-S	East	$L_{Max\text{-}LSS}$	23.3	**22.5**	2,003,000[T]
SAW-12-30-2-2.5-N	West	$L_{Max\text{-}LSS}$+1.0	29.3	**29.6**	568,000
SAW-12-30-2-2.5-N	East	N.A.	**28.6**	34.2*	601,000 [T]
SAW-12-30-2-2.5-S	West	$L_{Max\text{-}LSS}$+1.0	28	**27.7**	585,000
SAW-12-30-2-2.5-S	East	$L_{Max\text{-}LSS}$+1.0	25.4*	**30.5**	601,000
SAW-12-30-4-2-N	West	$L_{Max\text{-}LSS}$+1.0	28.8	**25.6**	898,000
SAW-12-30-4-2-N	East	$L_{Max\text{-}LSS}$+1.0	30.4	**29.0**	791,000
SAW-12-30-4-2-S	West	$L_{Max\text{-}LSS}$+1.0	25.2*	**26.8**	854,000
SAW-12-30-4-2-S	East	$L_{Max\text{-}LSS}$+1.0	28.1	**26.4**	1,032,000
SAW-12-40-2-2-N	West	$L_{Max\text{-}LSS}$+1.0	36.5	**37.4**	345,000
SAW-12-40-2-2-N	East	$L_{Max\text{-}LSS}$+1.0	35.5	**35.8**	321,000
SAW-12-40-2-2-S	West	$L_{Max\text{-}LSS}$+1.0	33.1*	**38.3**	312,000
SAW-12-40-2-2-S	East	$L_{Max\text{-}LSS}$+1.0	38.9	**35.7**	352,000
SAW-12-40-4-2.5-N	West	$L_{Max\text{-}LSS}$+1.0	39.1	**38.1**	237,000
SAW-12-40-4-2.5-N	East	$L_{Max\text{-}LSS}$+1.0	32.6*	**33.9**	208,000
SAW-12-40-4-2.5-S	West	$L_{Max\text{-}LSS}$+1.0	35.5	**33.8**	244,000
SAW-12-40-4-2.5-S	East	$L_{Max\text{-}LSS}$	**35.9**	34.9	266,000

Note:
1. Invalid LSS range*.
2. LSS range used for stress-life data are in **bold.**
3. N.A. not applicable as 20% decrease in estimated stress range was not observed before test was concluded.
4. Runout[R].
5. Test terminated due to fatigue cracking on opposite side weld toe[T].

The 32 S-N (stress-life) data points from Table 29 are plotted in Figure 45 along with the design, mean, and upper bound finite-life fatigue resistance curves (i.e., S-N curves) for AASHTO Fatigue Category C. The design S-N curve from (AASHTO 2018) for a given fatigue category was established (*for design*) by fitting a probability distribution to fatigue test data, and establishing a lower bound that is two standard deviations below the mean to provide 97.5% probability and 95% confidence that fatigue failure would not occur for a given stress range (S) and corresponding number of loading cycles (N). Therefore, each AASHTO design S-N curve provides a lower bound to the finite-life fatigue resistance (in terms of number of loading cycles to failure). For a given AASHTO fatigue category and stress range, the mean number of cycles to failure (i.e., the mean fatigue life), as well as an upper bound that is two standard deviations above the mean (with 97.5% probability and 95% confidence that fatigue failure would occur) can be determined from the statistics used to establish the design S-N curve (Keating & Fisher, 1986) (Moses, et al., 1987).

Figure 45 shows that the S-N data from the test specimens are located to the right of the design S-N curve for AASHTO Fatigue Category C, and most of the S-N data are also located to the right of the mean S-N curve, even though the value of N used for the S-N data from the tests was relatively conservative (i.e., N = N20) when the fatigue cracks were difficult to identify and not observable using unaided visual inspection. Therefore, an important finding from the cyclic loading fatigue tests is that using FEA and the LSS approach to determine the stress range S for the fillet weld toe near a CAH retrofit of a connection plate-to-web weld under web plate bending, and then using this value of S with the finite-life fatigue resistance for AASHTO Fatigue Category C will result in a conservative estimate of the fatigue life (i.e., the number of cycles before a fatigue crack is observed, N) for the weld toe near the CAH.

Although the finite-life fatigue performance of the connection plate-to-web weld toe was the focus of the fatigue tests, the infinite-life fatigue resistance (CAFL) for AASHTO Fatigue Category C of 10 ksi is also shown Figure 45. As shown, the LSS ranges (S) of the S-N data from the test specimens, even for the runouts, are well above the 10 ksi CAFL.

Note that the test specimens were made using the submerged-arc-welding (SAW) process, which was commonly used for floor beam connection plate-to-web welds in typical two-girder bridges constructed in the 1960's and 1970's that are likely to be damaged by distortion-induced fatigue cracking. Floor beam connection plate-to-web welds in two-girder bridge systems were also made using the shielded-metal-arc-welding (SMAW) process in the 1960's and 1970's. Therefore, it is important to consider whether the finding from Figure 45 that AASHTO Fatigue Category C provides a significantly conservative estimate of fatigue life would be applicable if the test specimens had been made using the SMAW process.

The European Convention for Structural Steelwork (ECCS) (ECCS, TC6, 2018) provides comparative S-N curves for weld toe fatigue cracking of test specimens fabricated using the two different welding processes, SAW and SMAW. This S-N data was part of the basis for fatigue design according to Eurocode 3 (Eurocode, 2006). Figure 46 shows the S-N data for the test specimens of the present study plotted with the mean S-N curves for SAW and SMAW test specimens from ECCS (ECCS, TC6, 2018), as well as the design and mean S-N curves for AASHTO Fatigue Category C. The figure shows that the S-N data for the test specimens of the present study (welded using the SAW process) are close to the mean S-N curve for SAW from ECCS (ECCS, TC6, 2018), while the mean S-N curve for AASHTO Fatigue Category C is close to the mean S-N curve for SMAW from ECCS (ECCS, TC6, 2018). Therefore, although using AASHTO Fatigue Category C for the finite-life fatigue resistance appears quite conservative for the floor beam connection plate-to-web weld conditions considered in the present study, AASHTO Fatigue Category C may not be as conservative if the welds of the test specimens had been made using the SMAW process; although Figure 46 suggests that using AASHTO Fatigue Category C is sufficiently conservative and is therefore applicable for floor beam connection plate-to-web welds made using the SMAW process.

Finally, no significant difference in the S-N data for the test specimens is observed as the lengths of the crack-like features and the diameters of the CAH are varied. Therefore, FEA and the LSS approach presented earlier are appropriate for determining the stress range S needed to assess the fatigue performance

of the fillet weld near the CAH retrofit of a connection plate-to-web weld under web plate bending, since FEA and the LSS approach account for the effects of the length of the original fatigue crack and the diameter of the CAH on the fatigue stress demand.

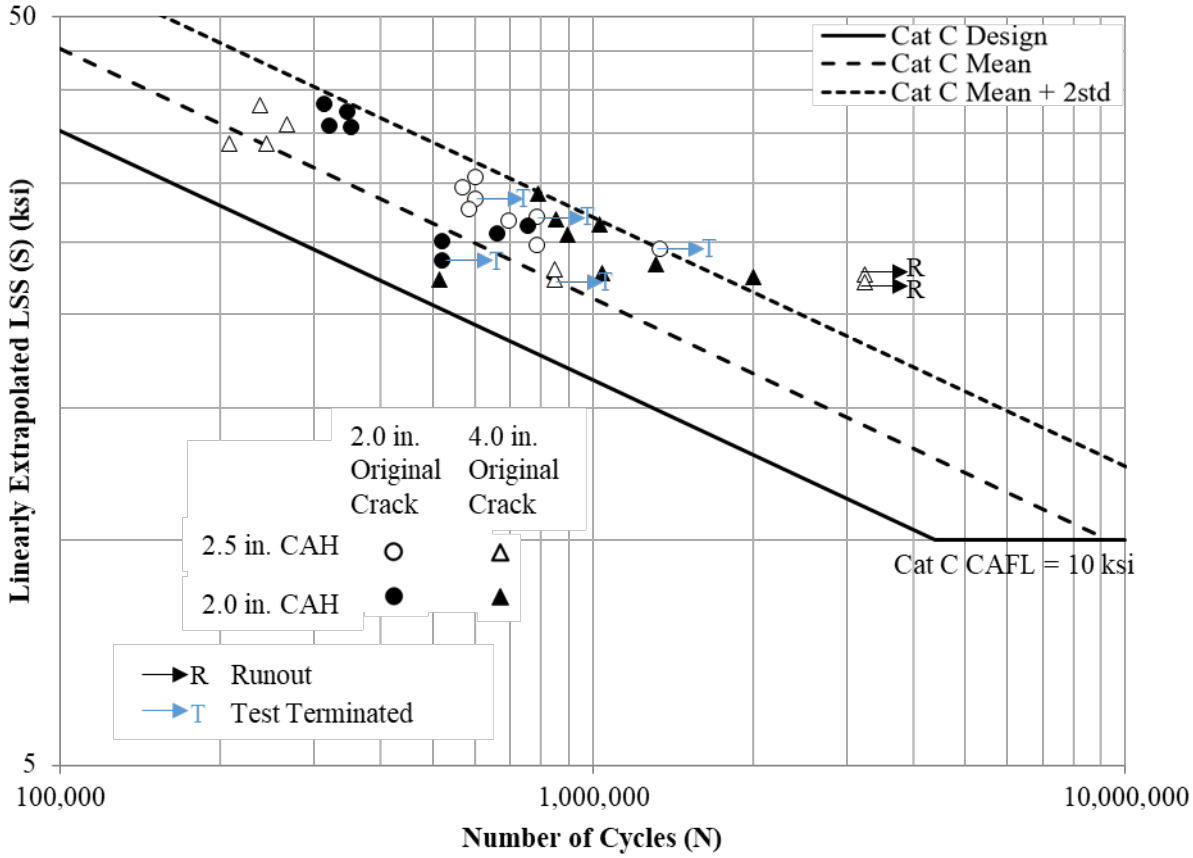

Figure 45. S-N data for test specimens and design, mean, and upper bound S-N curves for AASHTO Fatigue Category C.

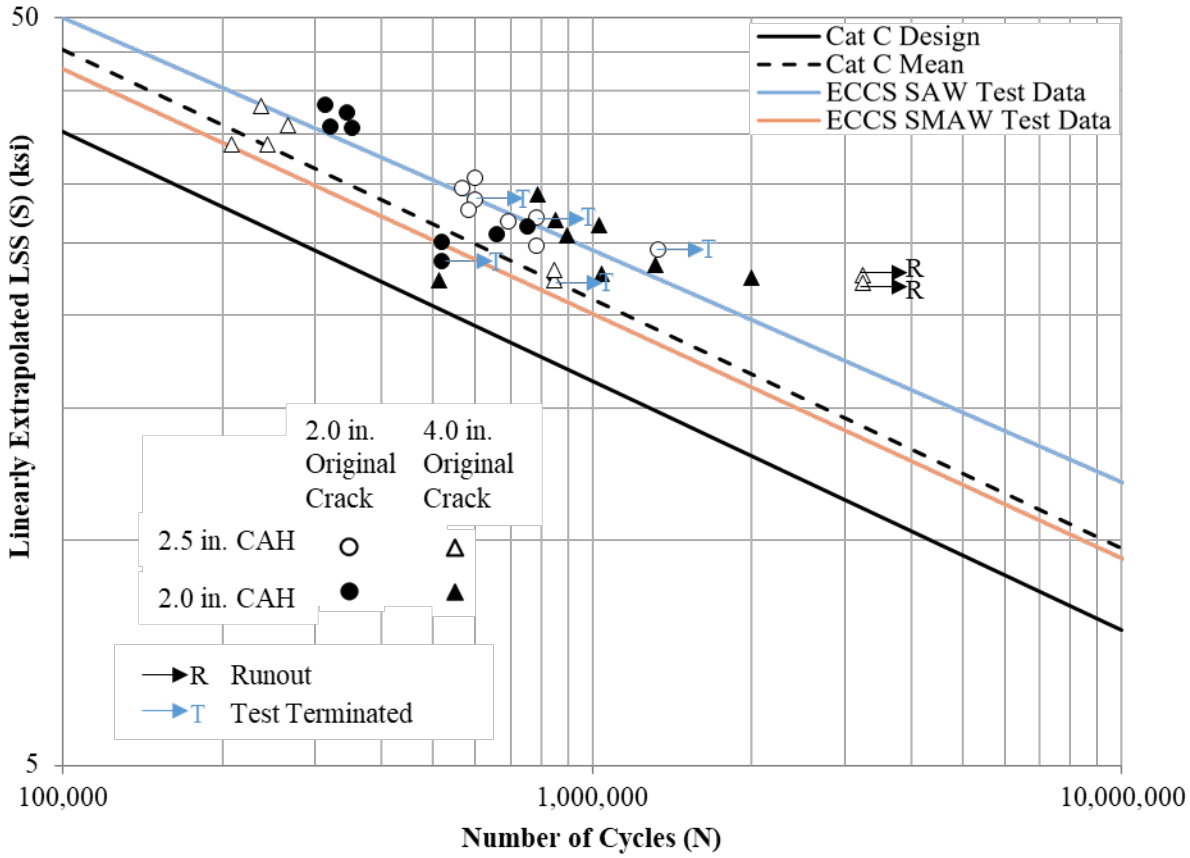

Figure 46. S-N data for test specimens, design and mean S-N curves for AASHTO Fatigue Category C, and mean S-N curves for ECCS SAW test data and ECCS SMAW test data.

CHAPTER 6

CAH Design Approach

Based on the work presented in the previous chapters, this chapter presents an approach for design of an effective crack-arrest hole (CAH) to retrofit a distortion-induced fatigue crack in a steel bridge girder that initiated in a web gap and has propagated vertically along a transverse member connection plate-to-web weld. The objectives for the CAH installation are: (1) to remove the tip of the original distortion-induced fatigue crack propagating along the connection plate-to-web weld toe; and (2) to avoid producing a stress condition at the weld toe beyond the CAH (i.e., away from the original fatigue crack) or on the CAH edge that could lead to future fatigue cracking.

DETAILS OF CAH DESIGN APPROACH

The CAH design approach assumes that the original fatigue crack in the bridge girder web gap region is propagating along a transverse member connection plate-to-web weld, and that the CAH retrofit is intended to eliminate the potential for further propagation of this crack. The approach uses 3D finite element analysis (FEA) to determine stresses in the web gap region. The approach uses the linearly extrapolated local structural stress (LSS) range at critical weld toe locations and the maximum magnitude principal stress (MMPS) range on the CAH edge to assess the fatigue performance. The design approach is as follows:

- Create a 3D global FEA model of the steel girder bridge with distortion-induced fatigue damage in the web gap region. The global FEA model should include the effects of bridge spans on either side of the transverse member (e.g., floor beam) of interest. A finer mesh of the region near the connection of this transverse member to the bridge girder web is recommended and a coarser mesh away from this transverse member connection can be used to reduce the model size. Shell elements or solid elements should be used for the global model. Secondary bridge components which could contribute to the global response of the bridge girder should be included in the global model, including floor beam brackets, lateral bracing, concrete bridge deck, sidewalks, median, and parapets. Models of welds, fatigue cracks, or CAHs in the global model are not needed. Models of these features should be included in finer mesh submodels, as described below.
- Select an appropriate live load model. The Fatigue I or the Fatigue II live load model from (AASHTO, 2018) may be used. Fatigue II is appropriate for finite-life fatigue design, and Fatigue I is appropriate for infinite-life fatigue design.
- Perform FEA using the 3D global FEA model while varying the positions of the live load model to produce the largest out-of-plane bending stress range in the girder web near (and within) the web gap region where the CAH will be installed.
- From the most recent bridge inspection report, determine the length(s) of the original fatigue crack(s) propagating along the connection plate-to-web weld toe(s). In the work presented in this report, two cracks with the same length were assumed to be propagating vertically along the toes

of the two fillet welds on either side of the connection plate. The lengths of such cracks in a given bridge may vary, and the model(s) for the original fatigue crack(s) should reflect the actual crack lengths.

- Select a trial CAH diameter in the range of 2.0 to 3.0 inches, based on FEA results given earlier and recommendations in (Dexter & Ocel, 2013).
- Create a detailed submodel of the connection plate-to-web connection region surrounding the web gap region, which is consistent with Sub Model B presented earlier in the report. The submodel should be made with solid elements with a 0.4t x 0.4t mesh, as shown earlier. The submodel should include the web gap, fillet welds, and CAH(s) with the trial diameter. The original connection plate-to-web weld toe fatigue crack(s) should be included in the model as a "seam" discontinuity in the element mesh. The CAH should be at the end of the original fatigue crack and penetrate the fillet weld (e.g., by 1/8 inch) as shown earlier.
- Perform FEA of the submodel of the connection plate-to-web region. The FEA of the submodel should be driven (loaded) by boundary displacements from FEA of the global model with the live load model positioned to produce the largest out-of-plane bending stress range in the girder web where the CAH(s) will be installed. Note that two levels of submodels may be used, as in the FEA work presented in this report, to reduce the level of submodeling effort and computational time.
- Assess the connection plate-to-web weld toe using stress results from FEA of the submodel. For the weld toe, the linearly extrapolated LSS should be used. The weld toe LSS range should be determined at many points along the weld toe, starting from the intersection of the edge of the CAH with the weld toe, and moving away from the CAH until the LSS range clearly decreases. The linear extrapolation method is recommended to determine the LSS range at each point. The largest weld toe LSS range should be used to assess the CAH design, by comparing it with AASHTO Fatigue Category C.
- Assess the edge of the CAH using stress results from FEA of the submodel. For the edge of the CAH, the MMPS range on the CAH edge should be used. The MMPS range should be determined at many points around the circumference of the CAH. The largest MMPS range should be used to assess the CAH design, by comparing it with AASHTO Fatigue Category A.
- Assessing the LSS range at the connection plate-to-web weld toe and the MMPS range on the CAH edge by comparing with AASHTO Fatigue Category C and Fatigue Category A, respectively, should use either an infinite-life approach or a finite-life approach, consistent with the live load model applied to the global FEA model. When the Fatigue I live load model (i.e., the Fatigue I live load factor) is used, the stress ranges should be compared with the constant amplitude fatigue limit (CAFL) for the appropriate fatigue category, and if the stress range is below the CAFL, infinite life is expected. When the Fatigue II live load model is used, the stress ranges should be compared with the finite-life fatigue resistance for the appropriate fatigue category to determine the design life (number of cycles, N) of the connection plate-to-web weld toe and the CAH edge. The minimum design life between the connection plate-to-web weld toe and the CAH edge should be used.
- If the fatigue performance assessment indicates infinite life (Fatigue I) or an acceptable design life (Fatigue II), then the CAH design is acceptable. Otherwise, the CAH design should be modified by increasing the CAH diameter, and the fatigue assessment process should be repeated, beginning by creating a new detailed submodel.

For situations when adequate fatigue design life or infinite life cannot be obtained for the connection plate-to-web weld toe, regardless of the CAH diameter, weld toe fatigue life improvement, for example by peening, can be considered.

Finally, when the CAH(s) are installed, each CAH should penetrate the fillet weld to capture the weld toe (e.g., by 1/8 inch) as shown earlier. Although the weld toe may make it difficult to properly identify the original fatigue crack geometry (especially, the crack tip), the CAH must be installed to contain or intercept the crack tip to prevent the original crack from continuing to grow. The edge and corners of the CAH should be surface finished after drilling, following recommendations in (Dexter & Ocel, 2013).

APPLICATION OF CAH DESIGN APPROACH

The CAH design approach is applied to the example two-girder bridge with the deck supported by floor beams and stringers, and with a history of distortion-induced fatigue cracking at the floor beam connection plate-to-web fillet welds. This bridge was summarized in Chapter 2, where the 3D global FEA model and FEA submodels were presented.

The global FEA model was loaded with the Fatigue I load model. For the FEA submodel, 2.0 inch long original fatigue cracks were assumed, one at each of the toes of the floor beam connection plate-to-web welds. A 2.0 inch diameter CAH was selected, with one CAH centered on the crack tip of each of the original fatigue cracks.

The FEA results show that under the Fatigue I load model, the largest LSS range normal to the connection plate-to-web weld toe occurs at 1.1 inch from the intersection of the CAH edge with the weld toe, with a value of 6.1 ksi. This largest LSS range is less than the 10 ksi CAFL for the AASHTO Fatigue Category C. Therefore, infinite fatigue life is expected at the connection-plate-to-web weld toe after the CAH is installed. Similarly, the FEA results show that under the Fatigue I load, the largest MMPS range on the CAH edge has a value of 5.0 ksi. This largest MMPS range is less than the 24 ksi CAFL for the AASHTO Fatigue Category A and infinite fatigue life is expected for the CAH edge. Thus, the infinite-life assessment indicates the 2.0 inch diameter CAH design is acceptable.

The (alternate) finite-life approach can also be considered to assess the CAH design. The finite-life fatigue assessment may be used if the CAH design does not provide infinite life (i.e., the stress range is greater than the CAFL), or if there is concern about comparing infinite-life fatigue resistance (i.e., the CAFL) with the LSS range calculated using the International Institute of Welding (IIW) (Hobbacher, 2016) approach, since this comparison (for infinite life) is not as well-established in the research literature and engineering practice as the comparison of finite-life fatigue resistance with the LSS range, which is well-established.

For fatigue assessment of the CAH design using the finite-life approach, the largest LSS range normal to the connection plate-to-web weld toe is considered. Since the fatigue load factor for the Fatigue I load model is 2.2 times the load factor for the Fatigue II load model (AASHTO 2018), and the FEA and LSS range calculations are completely linear, the largest LSS range for finite life (i.e., based on the Fatigue II load model) can be determined from the largest LSS range for infinite life (i.e., based on the Fatigue I load model) as (6.1 ksi)/2.2 = 2.8 ksi. Using this largest LSS range of 2.8 ksi with the design S-N curve for AASHTO Fatigue Category C, the remaining fatigue life is 200 million cycles. With an $(ADTT)_{SL}$ (single-lane average daily truck traffic) equal to 3,000 over the CAH design life, and with each truck passage producing 1.5 stress range cycles (since the connection plate is near an interior support of a continuous girder, according to (AASHTO, 2018)), the remaining fatigue life is 122 years, which is sufficiently long for the CAH design to be acceptable. A similar finite-life assessment can be made for the CAH edge.

Note that for both the infinite-life and the finite-life fatigue assessment, the potential for prior fatigue damage to the connection plate-to-web weld toe from the fatigue loading cycles before the CAH is installed is not included in the example. For each CAH design, however, some consideration of prior fatigue damage should be given. Recall that the FEA results presented in Chapter 3 (see Figure 9 and Table 1) show that

the LSS *before and after* the original crack is present and *before the CAH* is installed is small (well below the CAFL for AASHTO Fatigue Category C) at the *location of the largest LSS range* along the weld toe *after the CAH* is installed; this location of the largest LSS range along the weld toe after the CAH is installed tends to be at a significant distance from the original crack tip. Therefore, potential fatigue damage to the connection plate-to-web weld toe from the fatigue loading cycles before the CAH is installed are not included in the example application of the CAH design approach.

CHAPTER 7

Conclusions and Recommendations

Distortion-induced fatigue cracking in the web gap region near a transverse member (e.g., floor beam) connection plate is relatively common for steel girder bridges constructed in the 1960's and 1970's. Retrofit of a distortion-induced fatigue crack that runs along the transverse member connection plate-to-web weld with a crack-arrest hole (CAH) is also relatively common. However, fatigue cracking, in which a fatigue crack appears to reinitiate beyond the CAH, has been observed after a CAH retrofit. This research considers two reasons why a fatigue crack may appear to reinitiate: (1) the CAH was not properly designed, or (2) the original fatigue crack geometry was not properly identified, so that the CAH did not intercept the tip of the crack. This report specifically addresses the first reason.

Given that distortion-induced web gap fatigue cracking is relatively common, and that CAHs are often used to retrofit cracks that run along a connection plate-to-web weld toe, the objective of this report is to present a design approach for these CAHs. Since the initiation of a fatigue crack along the connection plate-to-web weld toe after the CAH is installed would indicate that that the CAH is ineffective (i.e., improperly designed), this research focuses on the stress conditions that could cause fatigue cracking at the connection plate-to-web weld toe after the CAH is installed, or could cause fatigue cracking from the CAH edge. The original fatigue crack, propagating from the web gap along the connection plate-to-web weld toe, is assumed to have been properly identified and the CAH is assumed to intercept the tip of the original fatigue crack.

Detailed three-dimensional (3D) finite element analyses (FEA) of an example two-girder bridge with floor beams and stringers, and constructed in the late 1960s, were used to study distortion-induced fatigue stress response in the web gap region of the bridge girders. A global FEA model and detailed submodels were used, where fillet welds, original fatigue cracks, and CAHs were explicitly modeled in the submodels. The sensitivity of the FEA results to different levels of element mesh refinement and different mesh configurations was assessed. Parametric FEA studies were performed, in which the length of the original fatigue crack along the connection plate-to-web weld toe and the diameter of the CAH are varied. Several different estimates of the fillet weld toe local structural stress (LSS) (Hobbacher, 2016) (DNV, 2011) were considered, and a linear extrapolation method to determine the LSS was selected for the remaining work.

A CAH design approach and recommended CAH dimensions were presented, which are expected to provide good fatigue performance by avoiding fatigue cracking after CAHs are installed. In the design approach, the linearly-extrapolated LSS range at a critical connection plate-to-web weld toe location and the maximum magnitude principal stress range on the CAH edge were used to assess the fatigue performance of a CAH design. In this fatigue performance assessment, these stress results, obtained from FEA and LSS methods, are compared with standard fatigue resistance from (AASHTO, 2018).

Fatigue tests of small-size test specimens with full-scale welds, simulated cracks, and CAHs were performed to validate the fatigue performance assessment used in the CAH design approach. Stresses from FEA and measured stresses were used to assess the potential for fatigue cracking in the test specimens. The test specimens were studied under out-of-plane plate bending to simulate the controlling mechanism in the web gap region surrounding a connection plate-to-web weld in a steel bridge girder subjected to distortion-induced fatigue cracking. FEA was used to design the test specimens and the FEA stress ranges were compared to the stress range results (calculated from measured strains) from the fatigue testing. The FEA

results for the test specimens (and the example 2-girder bridge), as well as the subsequent test results, show that the l*ocation of largest LSS* in the web gap region after a CAH is installed to retrofit a connection plate-to-web weld toe fatigue crack, is not at the intersection between the edge of the CAH and the weld toe, but is a short distance (approximately 1 inch) away from this intersection. This finding, that the location of the largest LSS is a short distance away from this intersection, is consistent with FEA results from (Liu, et al., 2018).

During the cyclic loading fatigue tests of the test specimens, a 20% decrease in the stress range at a strain gage located 0.4t (where t is the test specimen primary plate thickness) from the weld toe was observed before cracks were observed by unaided visual inspection. When the 20% decrease in stress range was seen, a subsequent dye penetration test often revealed single or multiple fatigue cracks at the weld toe at a short distance away from the CAH, and within (or near) the length of weld toe with elevated LSS caused by the presence of the CAH. Based on this observation and using the linearly extrapolated LSS, the stress-life (S-N) data for a test specimen was defined as the weld toe LSS range (before a decrease is observed), S, and the number of loading cycles, N, when a 20% decrease in the estimated stress range for a strain gage at 0.4t from the weld toe is first observed (i.e., N = N20). This S-N data was compared to the fatigue resistance for AASHTO Fatigue Category C (AASHTO, 2018) to make a fatigue performance assessment for weld toe cracking after a CAH retrofit.

CONCLUSIONS FROM FEA RESULTS

Based on the FEA results presented in this report, the following conclusions are made:

1. The fatigue stresses generated in the web gap region are dominated by out-of-plane bending of the girder web, and fatigue stresses due to primary (in-plane) bending of the girder web are insignificant.
2. Installation of a CAH at the connection plate-to-web weld toe can eliminate the tip of an original crack from distortion-induced fatigue; however, a short distance (approximately 1 inch) away from the intersection of the CAH with the connection plate-to-web weld toe, the weld toe stresses are increased due to a stress concentration from the CAH combined with the geometric effect of the connection plate and weld.
3. Increasing the CAH diameter reduces the fatigue stresses on the CAH edge and the fatigue stresses at the connection plate-to-web weld toe within a short distance from the CAH. The recommended CAH diameter is in the range of 2.0 to 3.0 inches, providing efficiency in reducing the fatigue stresses. There is little benefit to using a CAH with a diameter larger than 3.0 inches.
4. When *constant amplitude deformation* is assumed to drive the distortion-induced fatigue, for example, when the relative rotation between the floor beam end and the plane of the girder web in a typical two-girder bridge remains constant as the original distortion-induced fatigue crack grows or when CAHs are installed, then a longer original fatigue crack results in smaller stresses on the CAH edge and at the connection plate-to-web weld toe as a result of increased flexibility of the web gap region.
5. The LSS at the fillet weld toe near a CAH based on linear extrapolation converges using a FEA mesh of solid elements with edge lengths of 0.4t x 0.4t (i.e., Mesh 3), where t is the thickness of the part where the surface stress is being determined. This mesh meets the requirements for a relatively fine mesh of 0.4t x1.0t specified in (Hobbacher, 2016) and requires less modeling effort.
6. The LSS from linear extrapolation and the single-point LSS method converge and provide comparable stress results when Mesh 3 is used.

7. When a sufficiently-refined mesh, such as Mesh 3 (i.e., 0.4t x 0.4t), is used in the FEA, the stresses on the CAH edge and the LSS at the connection plate-to-web weld toe are not sensitive to the mesh configuration (e.g., a skewed mesh versus a uniform mesh).

CONCLUSIONS FROM FATIGUE TESTS

Based on the fatigue test results presented in this report, the following conclusions are made:

1. When a CAH is installed to retrofit an original distortion-induced fatigue crack propagating along a connection plate-to-web weld toe, additional (i.e., new) weld toe fatigue cracking may occur at a short distance (approximately 1 inch) away from the CAH; the approximate length of the weld toe where this new fatigue cracking may occur can be predicted using the linearly extrapolated LSS based on FEA results from a sufficiently-refined FEA submodel.
2. The LSS ranges determined from cyclic loading fatigue tests on the test specimens are generally in good agreement with the LSS ranges determined from FEA results. The average absolute difference between the test results and FEA results for the 16 test specimens is 10.6%. The FEA results were generally larger than the results from the fatigue tests.
3. Propagation of weld toe cracks from cyclic plate bending stress is relatively slow. In some test specimens, the fatigue crack lengths increased by approximately 3 inches over 500,000 cycles, which is similar to observations made by others (Liu, et al., 2018; Fisher, et al., 1990).
4. The S-N stress-life data from the fatigue tests was defined as the linearly extrapolated LSS range at the weld toe, S, and the number of loading cycles, N, when a weld toe crack is first observed from a 20% decrease in stress range adjacent to the weld toe (i.e., N = N20); this stress-life data consistently exceeded the design S-N curve and typically exceeded the mean S-N curve for AASHTO Fatigue Category C; therefore, AASHTO Fatigue Category C is a reasonable and conservative fatigue resistance for assessing the potential for new weld toe fatigue cracking at a short distance (approximately 1 inch) away from a CAH.
5. No significant difference in the S-N stress-life data from the test specimens was observed as the lengths of the crack-like features and CAH diameters were varied, which validates the use of the linearly extrapolated LSS to quantify the stress range for fatigue resistance as these geometric parameters are varied.
6. Since the test specimens included variations in the lengths of the crack-like features and CAH diameters, and the results from FEA, including the linearly extrapolated LSS, are relatively consistent with the test results, the use of FEA and the linearly extrapolated LSS to account for the original fatigue crack length and CAH diameter in the fatigue assessment of a CAH retrofit is validated.
7. No fatigue cracks were observed to initiate at the CAH edge in any of the test specimens after the fatigue tests were complete.

RECOMMENDATIONS

1. Chapter 6 of this report presents an approach to design a CAH for a distortion-induced fatigue crack in a steel bridge girder web that initiated in a web gap and has propagated vertically along a transverse member connection plate-to-web weld; this CAH design approach is recommended, including the specific recommendations in Chapter 6 for the CAH diameter, FEA models, and fatigue assessment approaches.

2. Each CAH designed and installed to retrofit a weld toe fatigue crack should penetrate the fillet weld to capture the weld toe, and the CAH must be installed to contain or intercept the crack tip to prevent the original crack from continuing to grow.
3. The edge and corners of the CAH should be surface finished after drilling, following recommendations in (Dexter & Ocel, 2013) .

FUTURE WORK

As mentioned earlier, retrofit of a distortion-induced fatigue crack that runs along a connection plate-to-web weld using a CAH is relatively common, and fatigue cracking beyond the CAH after the retrofit has been observed. This research has considered two reasons why a fatigue crack may appear to reinitiate: (1) the CAH was not properly designed, or (2) the original fatigue crack geometry was not properly identified, so that the CAH did not intercept the tip of the crack. This report specifically addressed the first reason, and in the research reported herein, the original fatigue crack is assumed to have been properly identified and the CAH is assumed to intercept the tip of the original fatigue crack.

Reliably identifying a fatigue crack along the weld toe, and especially locating the crack tip when the crack is driven by out-of-plane bending deformation of the plate at the weld toe, is quite challenging. Inspections of the fatigue test specimens in this research showed that these weld toe fatigue cracks were not detectable with unaided visible inspection until they reached a length of 3.5 inches (and this length was measurable by a dye penetration test, not by unaided visual inspection). A similar fatigue crack would be even more challenging to accurately identify in a bridge under field conditions with a painted and possibly corroded steel girder web. Therefore, future research should address reliable field inspection methods for identifying a fatigue crack along a weld toe that is driven by out-of-plane bending of the plate at the weld toe, and for locating the crack tip; these inspection methods are needed to enable reliable CAH retrofit of such cracks.

Also, as mentioned in Chapter 5, the weld process used to make a connection plate-to-web weld may influence the weld toe fatigue resistance. The difference in two S-N curves from ECCS (ECCS, TC6, 2018) for test specimens fatigue-tested in tension indicates that the fatigue resistance for welds made using the shielded-metal-arc-welding (SMAW) process may be less than the fatigue resistance for welds made using the submerged-arc-welding (SAW) process. The test specimens in the present research were made using the SAW process, which was commonly used for connection plate-to-web welds in typical two-girder bridges constructed in the 1960's and 1970's. Connection plate-to-web welds in two-girder bridges were also made using the SMAW process in the 1960's and 1970's. Future research should consider fabricating additional specimens with SMAW welds (that are otherwise similar to those used in the present research) and testing these specimens under cyclic loading plate bending fatigue testing, to understand any potential sensitivity of the fatigue resistance to the welding process.

REFERENCES

AASHO, 1949. *Standard Specifications for Highway Bridges, 5th Edition.* Washington, D.C.: American Association of State Highway Officials.

AASHTO, 2016. *AASHTO LRFD Bridge Design Specifications 7th edition,* Washington, DC: American Association of State Highway and Transportation Officials.

AASHTO, 2018. *AASHTO LRFD Bridge Design Specifications 8th Edition,* Washington, DC: American Association of State Highway and Transportation Officials.

Bowman, M. et al., 2012. *Fatigue Evaluation of Steel Bridges,* s.l.: Transportation Research Board.

Campbell, L. E., Connor, R. J., Whitehead, J. M. & Washer, G. A., 2019. Benchmark for Evaluating Performance in Visual Inspection of Fatigue Cracking in Steel Bridges. *Journal of Bridge Engineering,* 25(1).

Dassault Systemes Simulia Corp., 2016. *ABAQUS/Standard Documentation, Version 16,* Providence, RI: Dassault Systemes, Inc..

Demers, C. E. & Fisher, J. W., 1989. *Fatigue Cracking of Steel Bridge Structures, Volume 1: A Survey of Localized Cracking in Steel Bridges - 1981 to 1988, Report No. FHWA-RD-89-166,* s.l.: Federal Highway Adminstration.

Dexter, R. J. & Ocel, J. M., 2013. *Manual for Repair and Retrofit of Fatigue Cracks in Steel Bridges, Report No. FHWA-IF-13-020,* s.l.: Federal Highway Adminstration.

DNV, 2011. *Fatigue Design of Offshort Stuctures, DNV-RP-C203,* s.l.: s.n.

Downing, S. D. & Socie, D. F., 1982. Simple Rainflow Counting Algortithms. *International Journal of Fatigue,* pp. 31-40.

ECCS, TC6, 2018. *Background Information on Fatigue Design Rules - Statistical Evaluation, 2nd Edition,* s.l.: ECCS.

Eurocode, 2006. *Eurocode 3: Design of Steel Structures - Part 2: Steel Bridges,* Brussels: European Committee for Standardization.

Fisher, J. W. et al., 1974. *Fatigue Strength of Steel Beams with Welded Stiffeners and Attachments,* s.l.: National Coorperative Highway Research Program.

Fisher, J. W., Jin, J., Wagner, D. & Yen, B., 1990. *NCHRP Report 336, Distortion-Induced Fatigue Cracking in Steel Bridges,* Washington, D.C.: TRB, National Research Council.

Hobbacher, A. F., 2016. *Recommendations for Fatigue Design of Welded Joints and Components,* Switzerland: Springer.

Keating, P. B. & Fisher, J. W., 1986. *Review of Fatigue Tests and Design Criteria on Welded Details, Final Report,* Bethlehem, PA: Fritz Laboratory.

Liu, H. et al., 2018. Effectiveness of Crack-Arrest Holes under Distortion-Induced. *Journal of Bridge Engineering,* p. 23.2.

Moses, F., Schilling, C. & Raju, K., 1987. *NCHRP Report 299, Fatigue evaluation procedures for steel bridges,* Washington, D.C.: TRB, National Research Council.

Saunders, J., 2021. *Fatigue Assessment of Steel Plate Cut-outs using a Local Nominal Stress with Application to Slit RFB Connections,* s.l.: Doctoral dissertation, Lehigh University.